UNIVERSITY OF OKLAHOMA

GRADUATE COLLEGE

CATALYTIC DEHYDRATION OF POLY(VINYL ALCOHOL-CO-ETHYLENE) WITH HETEROGENEOUS ACID CATALYSTS

A THESIS

SUBMITTED TO THE GRADUATE FACULTY

in partial fulfillment of the requirements for the

Degree of

MASTER OF SCIENCE

BY

Luis Mario Trevisi

Norman, Oklahoma

2023

CATALYTIC DEHYDRATION OF POLY(VINYL ALCOHOL-CO-ETHYLENE) WITH HETEROGENEOUS ACID CATALYSTS

A THESIS APPROVED FOR THE

SCHOOL OF SUSTAINABLE CHEMICAL, BIOLOGICAL AND MATERIALS ENGINEERING

BY THE COMMITTEE CONSISTING OF

Dr. Lance Lobban, Chair

Dr. Steven Crossley

Dr. Bin Wang

Table of Contents

Acknowledgements

First of all, I would like to thank Dr. Lance Lobban for all his unconditional support throughout these couple of years. His willingness to support all of the people in his group with clever ideas and even hands-on work was indispensable for our success. I want to also thank him for pushing me to accomplish more than what I thought possible, listening to my explanations and theories and giving me his honest and supportive opinion throughout this project, even when the experiments did not go as expected.

I want to thank Dr. Steven Crossley and Dr. Bin Wang for always been willing to hear my results, inside or outside our regular meetings. I want to also thank them for all their clever and insightful suggestions which always gave me a new useful angle to elucidate the meaning behind the experiments and to figure out the future steps that needed to be taken. I also want to thank them for their cheerful and supporting environment that they always created in the lab. I want to also thank Dr. Keisha Walters and Dr. Liangzhong (Shawn) Xiang who taught me how to me so much during my undergraduate and prepared me for this opportunity.

None of this could have happened without the support from my senior graduate student colleagues which supported me throughout all my master's. I want to specially thank Han Chau and Ana Jerdy who introduced me to the marvels of catalysis and were always willing to give me a hand in any experiment. I want to also thank Pratik Samant and Brandon Abbot who were always patient and supportive with me in my initial stages in the lab. I want to also give a big thanks to Dai-Phat Bui and Thomas Salas whose unconditional support, cleaver ideas and friendship was crucial in this stage of my life. I also want to thank Yokly Leng and Lucas Condes

for been such good friends throughout the years, always willing to support me whenever I needed help. I would also like to thank Cesar Marquez, Lorena Salguedo, Maria Grisel Morillo, Claudia Caballini, Javier Chavez and all of my friends for creating such a supportive community, which without I wouldn't have made it.

I would like to thank the United World Scholar Program, and the scholarship donors for financially supporting me throughout my time here at OU. Without their help, I wouldn't be able to reach where I am now. Also I will like to thanks Andrew D'Amico for all his support during maintenance and troubleshooting the lab equipment.

Finally, I would like to thank my Parents, Antonio Trevisi and Daniella Ramirez, my sister Alejandra Trevisi, my wife Antonieta Hernandez and my grandparents for always been there for me when I needed them. Giving me their unconditional love no matter the distance. Because as we know, we are all under the same sky and as such we may never be truly alone. Thanks for everything.

Abstract

This study investigates the role of acid site density, pore size, and solvent selection in the catalytic dehydration of Poly (vinyl alcohol-co-ethylene) (EVOH) using zeolite catalysts. The first set of experiments reveals that catalysts with lower acid site densities and larger pores exhibit higher maximum rates and better activity retention after deactivation, attributed to enhanced mass transfer through additional available pores. Conversely, zeolites with higher acid site densities demonstrate consistently higher maximum rates overall, but lower acid site density zeolites outperform them when normalized, emphasizing the significance of larger pores and the mass transfer limited nature of this reaction. External active sites are found to play a crucial role in the polymer dehydration reaction, as their removal leads to reduced maximum rates and faster catalyst deactivation.

The investigation of solvents shows that use of DMSO results in limited reactivity with zeolite catalysts, potentially due to competition for acid sites or inhibition of certain transition steps. In contrast, a water-propanol mixture proves effective in dissolving EVOH while reducing the degree of competition compared to DMSO. Thus, this solvent offers better activity while also enabling additional chemistry like alcohol-induced ether formation. However, the ratio of water to 1-propanol significantly impacts catalyst performance, with a 12.5% water loading resulting in optimum rates possibly due to a combination of water competing for the active sites and the degree of solvation of the polymer.

However, challenges in analyzing results with NMR due to sampling inconsistencies make inviable a detailed study of the underlying mechanism and rates for this reaction under solvated

environment. Cryomilling was used to improve random sampling, but heterogeneities in the final polymer sample persisted, accentuating the difficulties of characterization. DSC and FTIR analyses confirm these heterogeneities and highlight the need to find techniques that analyze representative samples to achieve accurate measurements.

Table of Figures

Chapter 1: Introduction and Literature Review

1.1 Polyvinyl alcohol (PVA) and its co-polymers

PVA is one of the most highly produced water-soluble polymers in the world, in the range of one hundred kilotonnes per year[1]. However, its production does not follow the typical scheme where the monomer units are polymerized by chain or step growth. This is due to the monomer (vinyl alcohol) being highly unstable thus leading to uncontrolled and spontaneous degradation of the monomer to enols by a thermodynamic drive. To circumvent this issue, polyvinyl acetate is used as a parent homopolymer due to its higher stability and better control during polymerization[1,2]. This parent homopolymer is synthesized by a free radical polymerization of the monomer vinyl acetate in alcoholic solution or suspension depending on the application. Once the polyvinyl acetate is obtained, a saponification reaction is carried out to hydrolyze the acetate units to PVA (Figure 1). Thus, the polyvinyl alcohol commonly found in industry is actually a co-polymer due to the processing and production steps which can leave a certain degree of non-hydrolyzed acetate units. The degree of hydrolysis for this polymer ranges between 70 to 99% and depends on the processing conditions, such as time, temperature, catalyst used, etc[1].

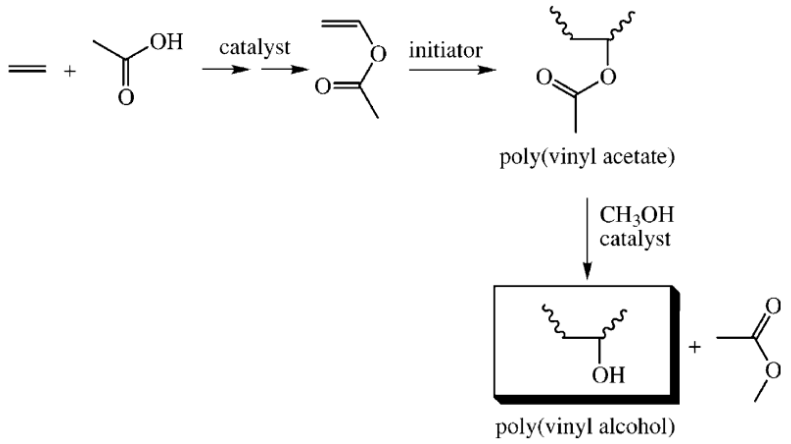

Figure 1: Polymerization of Polyvinyl Acetate and saponification[1]

The main functional group for PVA is a hydroxyl group which is responsible for several of its properties and characteristics. The hydroxyl group is responsible for the water solubility of the polymer as it will interact favorably with the water molecules through hydrogen bond interactions. Furthermore, the presence of this neutral functional group helps the formation of crystalline structures through the mutual interaction of the hydroxyl group (hydrogen bond) which tends to be one of the key factors that determined the natural arrangement of the polymer strands[3]. Consequently, the high crystallinity derived from the functional group gives polyvinyl alcohol a great range of functionalities such as low gas permeation due to the lower free volume available for the gas molecules to diffuse, higher strength, stiffness and hardness due to the higher degree of bonding, but at the same time the higher crystallinity decreases the toughness of the material and makes it opaque as visible light cannot easily pass through the densely packed crystals[3].

Nevertheless, every polymer possesses its own set of characteristic properties which could be advantageous or detrimental to certain applications. Thus, finding the specific pure polymer that can achieve the ideal combination of properties for a certain application while

keeping it economical can be truly challenging if not outright impossible. To tackle this issue, co-polymerization techniques have been developed which allows the use of two or more monomers in the polymerization reaction to achieve a combination of properties from its pure original polymers. These co-polymerization techniques can be divided in several subsections depending on the stage at which the process is apply and the control given on the position of each monomer on the polymer chain (Table 1).

Table 1: Copolymer terminology and types

	Short Sequences	
Unspecified	*–co–*	poly(*A–co–B*)
Statistical	*–stat–*	poly(*A–stat–B*)
Random	*–ran–*	poly(*A–ran–B*)
Alternating	*–alt–*	poly(*A–alt–B*)
Periodic	*–per–*	poly(*A–per–B–per–C*)
	Long Sequences	
Block	*–block–*	poly *A–block–*poly *B*
Graft	*–graft–*	poly *A–graft–*poly *B*
Star	*–star–*	*star–*poly *A*
Blend	*–blend–*	poly *A–blend–*poly *B*
Starblock	*–star– . . . –block–*	*star–*poly *A–block–*poly *B*
	Networks	
Cross-linked	*–net–*	*net–*poly *A*
Interpenetrating	*–inter–*	*cross*-poly *A–inter–net–*poly *B*
AB-cross–linked	*–net–*	poly *A–net–*poly B

In the case of polyvinyl alcohol, the use of copolymerization is crucial for many applications[4,5]. One of the most common examples is its use as a gas barrier. As was explained previously, polyvinyl alcohol has shown great properties as a gas barrier due to its high crystallinity. However, its solubility in water can be highly detrimental as the humidity in the environment can work as a plasticizer which will severely affect the crystallinity and consequently

the gas permeation properties of the polymer[3,4]. To tackle this issue, vinyl acetate is usually copolymerized with ethylene units and then hydrolyzed (Figure 2) to achieve a combination of the gas barrier properties from polyvinyl alcohol and the water resistance properties of polyethylene. Thus, its combination achieves improved properties as a gas barrier, improves processibility and decreases moisture sensitivity[4].

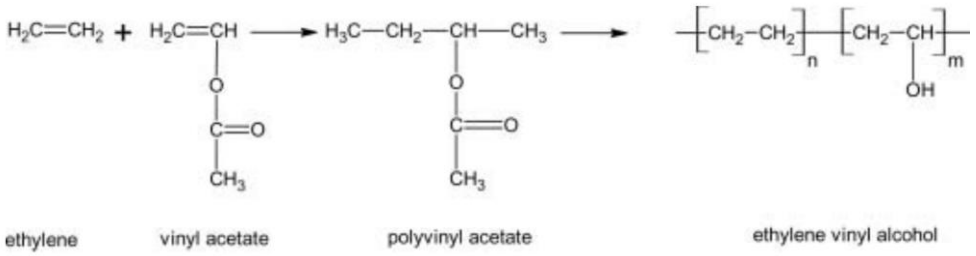

Figure 2: Copolymerization scheme for Poly(vinyl alcohol-co-ethylene)[4]

It is important to highlight that the composition of the monomer mixture will affect the final properties of the polymer. Usually, the final product characteristics will resemble the properties shown by the pure polymer of the most abundant monomer. This can be seen in Figure 3, where the water permeation decreases with an increment in ethylene monomer proportion while the oxygen permeation decreases with an increase in vinyl alcohol monomer proportion which agrees with the characteristics of each pure polymer.

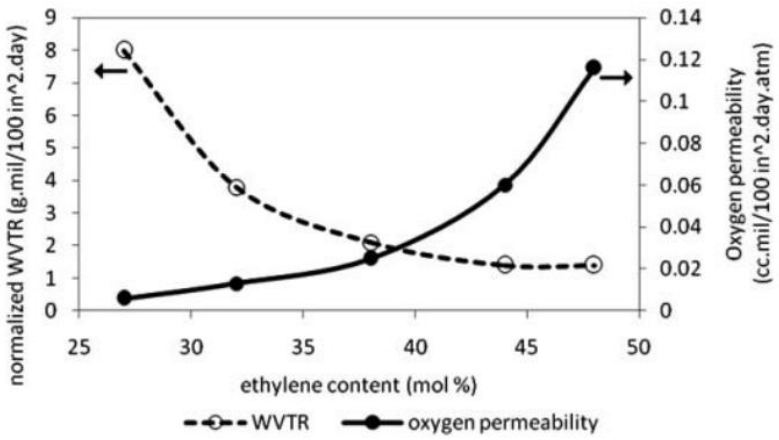

Figure 3: Oxygen permeability and thickness normalized water vapor transmission (WVTR) as a function of ethylene content for EVOH copolymers[4]

While the co-polymerization technique helps to fine tune the properties for a given application, it still requires some degree of compromise. As we can see for polyvinyl alcohol-co ethylene, as the fraction of ethylene units increases, the polymer becomes more resistant to water but at the expense of lowering its oxygen barrier capabilities. To overcome such limitations, industry has developed multilayer plastics in which different types of plastic are combined by layering to compensate and reinforce the desirable characteristics that each provides. In this case, to protect the polyvinyl alcohol from exposure to water, two layers of polyethylene are allocated to each side, which will not only protect the polyvinyl alcohol from getting affected by water and thus reducing its oxygen barrier properties but also providing a humidity barrier which could be highly beneficial for certain applications such as food storage and transportation (Figure 4).

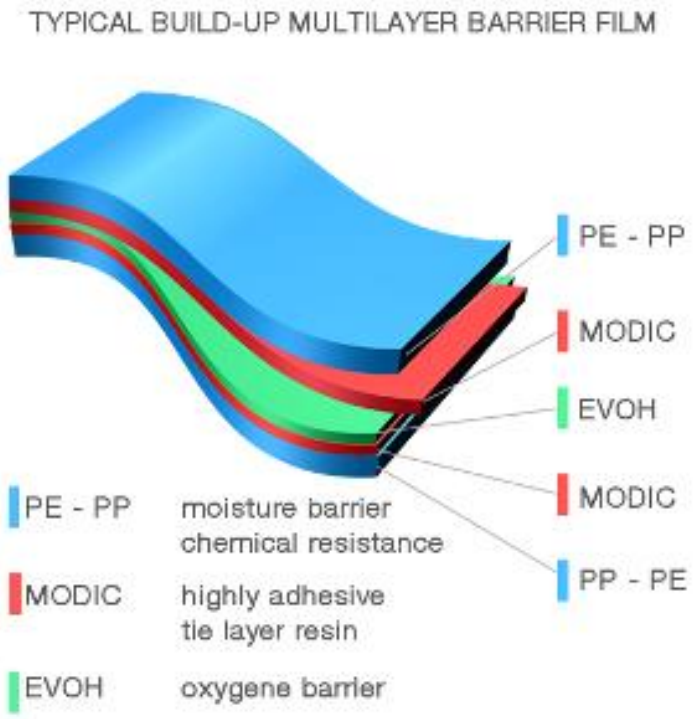

Figure 4: Multilayer Plastics[6]

While combining plastics provides the best option in terms of property versatility and fine-tuning, it comes at the expense of elevated difficulty for reuse and recycling at disposal facilities. This is because most recycling is currently done by mechanical methods, which make handling complex streams challenging as formation of different polymeric phases while in the molten state will detrimentally affect the final properties of a mechanically recycled plastic mixture. This issue is particularly apparent in the European annual report, which showcases how complex polymer streams are more likely to be landfilled or incinerated compared to pure or single type polymer feeds[7].

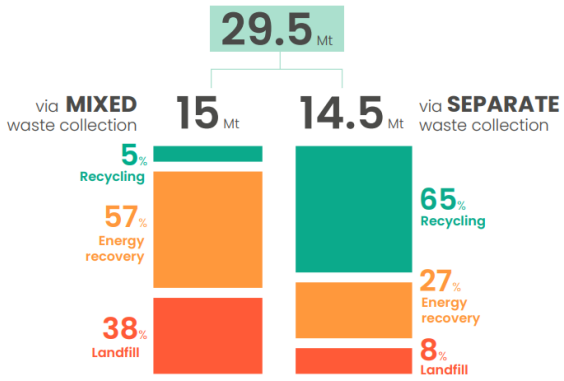

Figure 5: Final destination of plastic in the European Union by the type of stream[7]

While these challenges are particularly relevant with the rise of awareness of the detrimental impacts of plastics on wildlife and even human health[8–11], complete eradication of plastics and especially multilayered plastics seems to be practically inviable as they have found an almost unshakable spot in our modern life with few alternatives[11,12]. This is especially so in the food industry as multilayer plastic films allows prolonging the shelf life and reduces the possible contamination of the organic goods, reducing consequential loss of resources from growing, processing and transporting in case of food spoiling [2,13]. As such, alternative solutions to handle waste plastic streams and especially complex multi-plastic mixtures in an efficient and economical way need to be developed to tackle the environmental crises caused by end-of-life plastic disposal while limiting societal consequences of removing this versatile material from society.

1.2 Current recycling methodologies and research advances

As plastic problems keep showing relevance in every aspect of society, the need to develop recycling techniques that transition into a circular economy becomes more prominent. This is especially so considering the fact that recycling will not only prevent the disposal of such

materials into the environment, but recycling will also save billions of dollars in the raw materials and energy usually required for the production of such commodities[14]. As such, researchers have started to look for new technologies that allow them to tackle plastic waste treatment with a special emphasis on commingled plastic waste as current methodologies do not permit the recycling of multiple types of plastic at the same time due to reductions of the properties from the creation of several phases when the polymers are melted. This inability to process mixed polymer streams is especially relevant as it makes the different recycling companies unable to process plastic products that contain more than one polymer such as multilayer plastics, pushing them to perform expensive and complex pre-sorting procedures that would inevitably impact the profitability of the industry[14].

Currently, the most common and well established recycling methodology is known as mechanical recycling. This methodology takes advantage of thermoplastic ability to melt and flow at high temperature to reshape and mix polymer waste product while retaining their properties so long as no contamination from other type of polymers is included. Nevertheless, though this method allows effective recycling of certain polymers such as Polyethylene terephthalate and Polyethylene, other types of polymers such as thermosets, composites and temperature sensitive plastics won't be able to be processed using this technology. Thus, only allowing us to effectively recycle about 46% of the annual production of plastic in the best-case scenario[14]. While the current mechanical recycling technology only allows us to recycle pure polymer streams, researchers have been actively trying to change this situation. Recently, it has been proposed that by adding block co-polymers, the detrimental effects of the polymeric impurities could be mitigated[15]. Nevertheless, this solution would require a thorough understanding of the type of

polymers present on the mixed stream and its implementation would need to be further researched in case more than one polymer is present in the mixture, limiting its current application to certain scenarios.

The other popular method currently used for dealing with waste plastic is incineration. This is a particularly convenient method as it does not require a pre-sorting procedure before the plastic is burnt to produce heat or electricity. Nevertheless, this method does not allow the recovery of the material once it is burnt which detrimentally affects the energy balance making it less competitive with recycling in this aspect, while at the same time it releases CO_2. Furthermore, with current regulations, many scrubbers need to be implemented to ensure that no dangerous pollutants are released to the environment, reducing the economic viability of incineration[16].

Lastly, pyrolysis, which is considered a type of chemical recycling, may also be used to recycle some types of polymers. This technique relies on the thermal degradation of the polymers to produce monomers, fuels and waxes which can be used for several applications in industry[17]. Furthermore, this technology has the advantage of been able to use different types of catalysts which could improve the control of the product distribution while reducing the required energy to accomplish this type of recycling[18–20], making it competitive with other current methodologies. Nevertheless, even with the use of catalyst, current mainstream pyrolysis techniques usually require high temperature[19] while at the same time the energy previously expended for polymerization would be wasted which makes this method especifically energy demanding, affecting the sustainability and profitability of this approach. To tackle this issue, some researchers have developed new methodologies that take advantage of catalysts properties to

drastically reduce the temperature requirement and consequently the energy consumption of breaking polyethylene, one of the most used polymers, while keeping good selectivity towards alkanes in the waxes and fuel ranges which are the most economically relevant[21–23]. Nevertheless, handling of complex streams and other types of polymers still requires further exploration, as each type of the stream will affect the product distribution[24], accentuating the need for methodologies that can handle more than one polymer at a time.

One recent innovative method that is able to handle more than one plastic at a time implements target solvents to separate each polymer type through a multistep and multi-solvent process. This technique is known as STRAP, and may be able to separate polyethylene, polyvinyl alcohol, and polyethylene terephthalate with the use of DMSO, acetone, Toluene, GVL and water as solvents and antisolvents[25]. This methodology may be applied to other more complex polymeric mixtures by identifying selective solvents for each specific polymer in a mixture. This process comes at the expense of being solvent intensive which could be expensive and thus economically unviable without extensive optimization and efficient solvent recovery methodologies.

1.3 Heterogeneous Catalysis

Heterogeneous catalysis is the field that implements solid materials with specific surface and structural properties to facilitate the transformation of a reactant into products while not being consumed during the process[26,27]. In this way, the catalyst's main function is to provide an energetically favorable pathway for a desired product by stabilizing the transition state that leads to this targeted product[28]. Thus, the introduction of a catalyst permits us to have more control

over the reaction selectivity while reducing the energetic requirements to convert the reactants into products.

One of the most commonly used classes of heterogeneous catalysts are oxides, especially zeolites which are aluminosilicate crystalline oxides. These crystal structures consist of SiO_4 and AlO_4^- in the tetrahedral position interlinked by common oxygens which induce a charge imbalance that needs to be compensated by a cation such as an alkali metal or H^+, the latter giving rise to Brønsted acid sites[29]. These crystal structures are highly ordered, thermally resilient and contain micropores with different sizes and shapes depending on the type of template that was used during synthesis[30,31]. In this way, the active sites for zeolites can be considered to have two degrees of depth, the first one being the Brønsted acid site itself coupled with the pocket that surrounds it within the micropores which in tandem could significantly impact the stability of certain transition states and intermediates through acidic and confinement effects, and in this manner, affect the selectivity and rate of the final products for a given reaction (Figure 6)[32].

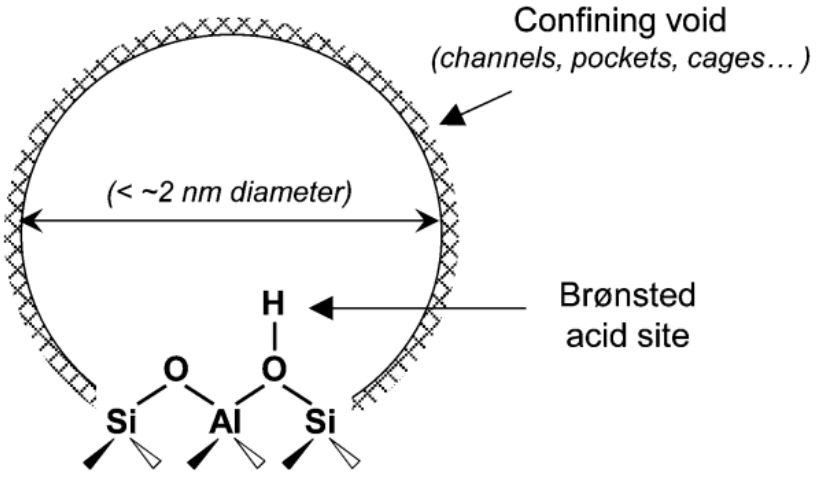

Figure 6: Two-dimensional representation of a zeolitic active site, comprised of Brønsted acid sites that are similar in acid strength and of confining void environments that vary in size and topology[32].

The Brønsted acid sites are the main contributor for the catalytic activity of zeolites for many reactions. One of such benefited reactions is the dehydration of alcohol, which is a reaction well known for being possible in the presence of an acidic environment. The mechanism in which dehydration process is accomplished consists of an initial protonation of hydroxyl group in the alcohol, converting the poor leaving hydroxide group into water, which is a good leaving group. As such, the reaction can proceed through the elimination of the water and deprotonation of the chain, forming alkenes and water as can be seen in Figure 7[33]. Nevertheless, it is important to highlight that this dehydration reaction exist in an equilibrium, as the formed alkene can be hydrated by protonating the double bond using the acidic proton, creating a carbocation which will allow a nucleophilic attack from a nearby water followed by a deprotonation of the generated oxonium ion, thus recovering the initial alcohol[33].

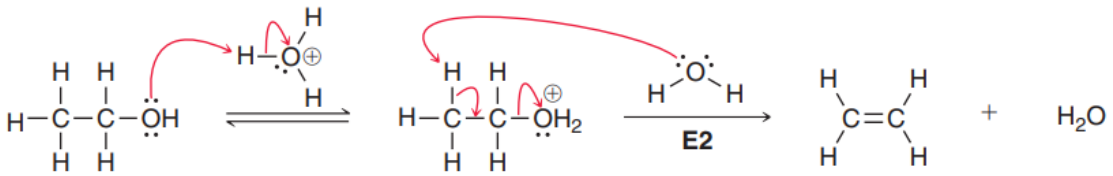

Figure 7: Acid catalyzed dehydration[33]

The ability to dehydrate different types of alcohol using acid sites coupled with high thermal stability has permitted the use of zeolites in the valorization of different types of biomasses. This is especially important in the production of biofuels as the presence of oxygen functionalities detrimentally affects the fuel properties[34]. An example of such valorization is the production of hydroxymethylfurfural from starchy and sugary biomass, where zeolites benefits

from it confinement effects to reduce undesirable secondary reactions such as polymerization and fragmentation while at the same time being able perform efficiently given appropriate conditions[35]. Nevertheless, the same confinement effects that bring an increase in selectivity come at the expense of a reduction in rates compare to other catalysts due to mass transfer limitations, which would become more relevant as the size of the reactant increases[35,36].

Another important issue that zeolites have with this type of reaction is their sensitivity to water[35–37]. It has been well known that the presence of steam will dealuminate the zeolite, which would consequently generate mesoporous structures, reduce crystallinity, and reduce the number of Brønsted acid site while increasing hydrothermal stability depending on conditions[38–41]. Thus, zeolites implemented for hydrothermal processes usually undergo an ultra-stabilization step in which the catalyst is steamed to increase its resilient to humid reaction conditions. However, the previously explored behavior of zeolites and water interaction in the gas phase do not apply in the liquid phase [37]. It has been shown that under hot water conditions, zeolites show a similar sensitivity to water in which a decrease in crystallinity, pore structure and activity in different reactions are present, however, the mechanism in which this occurs is different which can be appreciated by how the ultra-stabilization step which previous increased the stability of the zeolites becomes detrimental under hot water conditions[35–37]. This change in water sensitivity behavior can be attributed to a new dominant destabilization mechanism in which the silanol-terminated defects provide a hydrophilic patch where water can wet and nucleate making the hydrolysis, and thus the destruction of the zeolite, easier[37]. This mechanism, in tandem, shows that using almost structural defect free zeolites or functionalizing the zeolite with hydrophobic groups to limit the access to the hydrophilic patches would allow the preservation

of the crystallinity and integrity of the zeolites, improving the preservation of the catalyst activity and providing better recyclability capability and improving life span[37,42].

While water does have some negative effects on the zeolite structure itself, the presence of it is not entirely detrimental during reactions as it allows for the delocalization of the proton from the active site, forming hydronium ions, which could modify rates by changing the acid strength, confining environment, stability of transition states, solubility of reactants, among other properties[43–45]. Nevertheless, water can also compete for the active site, which detrimentally affects the rate of the reaction[43,45]. As such, water can play many roles in the reaction, and careful study of it in the reaction procedure should be applied when expected to be present.

Another relevant issue for today's society is the plastic industry, especially the low ability to recycle that the industry currently has for several polymer and polymer mixtures. As such, recent emphasis has been placed on finding methods to alleviate this concern, one of the most prominent being the use of catalysts to convert the different waste materials into economical relevant commodities. Thankfully, due to the similarities between biomass processing and polymer recycling, many of the findings and ideas can be translated into this new emerging field which give a pivotal point to improve the research efficiency and approaches to target this issue[46]. However, there are still some key differences between these two systems, mainly the reactant size and viscosity which will prove to be particularly problematic due to limited mass transport capabilities of the polymer strands into the pore channels of commonly use catalysts and the distribution of the catalyst particles within the polymer itself. The viscosity issue, which is correlated with diffusion, could be particularly exacerbated within the pore structure as the

confinement effects would lead to a change in diffusion dynamics from reptation and Rouse type to entropic barrier regimes which would lead to an apparent increase in viscosity and thus reduction of diffusion rates[47]. Furthermore, once the polymer chains move inside the pore, they would have a particularly difficult time to be released and thus exiting the pore which could present an additional layer of difficulties for mass transfer within molten polymer systems at low temperatures due to strong dispersion interactions[48]. This highlights the need to carefully study the pore size effects to properly equilibrate selectivity benefits with reaction rates. The other major factor to consider is the catalyst selectivity towards a certain phase. Elias et al. explore the migration dynamics of nanosilica particles in a polypropylene and poly(ethylene -co-vinyl acetate) blend in which the polymers differ by polarity attributes. In this case, the hydrophilic nanosilica particles had a tendency to migrate towards the polar poly(ethylene -co-vinyl acetate) and remain in this phase. Nevertheless, due to high viscosity, Brownian motion was particularly limiting, requiring external stirring for the particles to reach their preferred phase[49]. This highlights the need for proper stirring to achieve good dispersion of the particles within the polymer itself and also assure a proper phase selectivity in the case that polarity difference be taken advantage of to target a certain phase.

1.4 Motivation and study goal

The goal of this study is to develop a methodology and general kinetic understanding on how to handle complex polymer streams in an efficient, reliable, and economical way using heterogeneous catalysts. This would be accomplished by using heterogeneous catalysts, specifically zeolites, which are not only easier to separate compared to homogeneous catalyst but also provides surface and reactive environment tunability which allows to vary the selectivity

and consequently exert better control on the compatibilization of different polymers. As proof of concept, selective dehydration coupled with etherization of polyvinyl alcohol with different alcohols feeds will be studied. This may allow us to control the properties of the polymer by not only removing the major hydroxyl functional group, forming a double bond but also allow us to carry out etherization of the hydroxyl group with different alcohol structures to better homogenize the plastic mixture, thus preventing the formation of different phases and consequently reducing the properties loss of the material when recycling. This ability to selectively substitute for the polymer functional groups of an already made polymer through etherization of the hydroxyl groups with an alcohol could be beneficial for recycling and even potentially upcycling of the polymer.

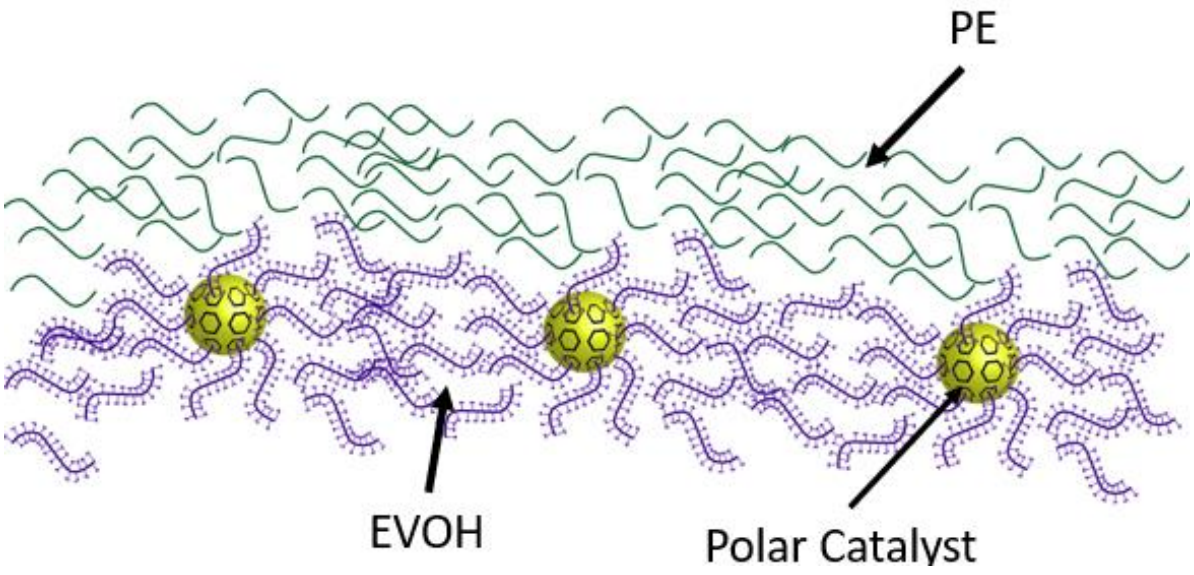

Figure 8: Complex Polymer stream to be recycle using polar heterogeneous catalysts.

Chapter 2: Catalytic dehydration of polyvinyl alcohol in molten state

2.1 Abstract

This section presents an investigation into the influence of acid site density and pore size on the catalytic performance of different zeolite frameworks in the dehydration of polymers. Two sets of experiments were conducted to analyze the effects of acid site density and pore size independently. In the first set, the acid site density was kept constant while varying the total available pores (mass loadings), and in the second set, the catalyst mass was set constant while altering the acid site density. Zeolite frameworks MFI, BEA, and FAU, with different pore sizes, were used to explore the impact of these factors on the reaction rates.

The results showed that in the experiments with varying acid site density, higher maximum rates were achieved with catalysts having lower acid site density. The degree of difference in maximum rates was correlated to the difference between acid sites of the explored zeolites, showing higher suppression of the rate when the acid site density was higher. Moreover, zeolites with low acid site density and large pores demonstrated greater final rates after deactivation compared to high acid site density zeolites. These results were supported by the experiments with constant catalyst mass where the catalyst with low acid site density had higher turnover frequency compared to their high acid site counterparts. Additionally, the study investigated the influence of external active sites by comparing a normal MFI zeolite with an MFI zeolite having a silica shell that removed all external active sites. The results demonstrated a significant decrease in maximum achievable rate and faster deactivation when external active

sites were removed, emphasizing the crucial role of external active sites and mass transfer in this reaction.

Overall, this research highlights the interplay between acid site density, pore size, and catalytic performance in different zeolite for polymeric dehydration. The findings contribute to a better understanding of the factors influencing reaction rates and provide insights for optimizing catalyst design in polymeric transformations.

2.2 Introduction

The thermal degradation of polyvinyl alcohol has been extensively investigated[50–60]. It has been shown that the thermal decomposition of polyvinyl alcohol and its co-polymer comprises two steps or mechanisms: Dehydration of the hydroxy functional group and cracking[52,54,57,58,60]. It has been shown that thermal dehydration starts around 195 °C[53,57], but the rate does not become significant until a temperature of about 247 °C has been reached[54]. Cracking, on the other hand, does not occur at significant rates until about 396 °C.

Several mechanisms for the thermal decomposition of polyvinyl alcohol have been proposed[51,56–59], however, there are still some common intermediary and final functional modifications that need to be highlighted for proper analysis of results. The main characteristic is the formation of double bonds after the release of water during the dehydration and the formation of ketones through the migration of the double bond to an adjacent hydroxyl group followed by the enol ketone tautomerization[57,53]. The tautomerization will be at equilibrium, meaning that we should expect to see enols and ketones, nevertheless, thermodynamically, the ketones are favored making the presence of such species more abundant at a given time thanks

to the acid sites capabilities to catalyze the tautomerization process (Figure 9)[33]. Thus, the amount of water released and the presence of ketones and carbon double bonds would allow us to have a clear indication of the extent of reaction or dehydration that has occurred.

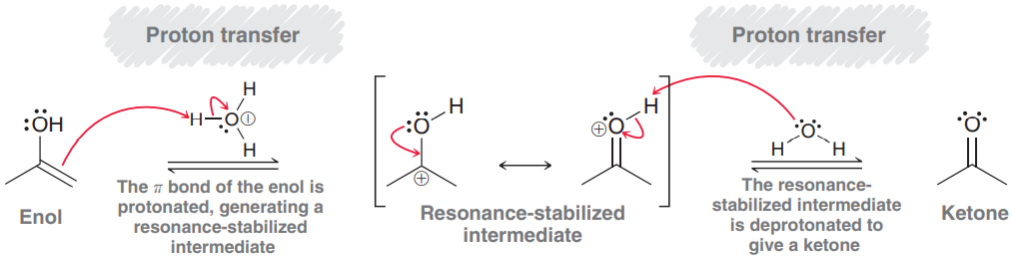

Figure 9: Acid Catalyzed Enol-Ketone Tautomerization[33]

The release of water in particular has been taken advantage of to study the dehydration using thermogravimetry (TGA). In this way, the mass loss from the sample at low dehydration temperature can be attributed to water loss from the dehydration process, thus providing an accurate way to track the reaction. Thus, it gives us a tool to have a proper exploration on the activity of different catalyst under molten conditions.

Therefore, in this study, the role of pore size, acid site density and external acid sites are investigated using different commercially available zeolites, modified zeolites and TGA.

2.3 Materials and methods

2.3.1 Catalysts

NH_4-ZSM-5 catalysts (framework type MFI), with Si/Al = 40 (CBV 8014) and Si/Al = 140 (CBV 28014), were obtained from Zeolyst International. To render them acidic, the zeolites were calcined under 40 ml/min of air (80% N2 / 20% O2) at 550°C for 5 hours, with a ramp rate of 1 °C/min.

In order to assess diffusion properties and role of external active sites, a core-shell zeolite (active ZSM-5 core, inert silicalite shell) was prepared based on the procedure described by Ghorbanpour et al.[61] In our work, however, we used Zeolyst MFI seeds to grow the silicalite layer, instead of synthesizing the zeolite entirely. Also, the annealing step was not performed, which considerably lowers the time necessary for this sample preparation. 750 mg of NH_4-ZSM-5 (Si/Al = 40) were added to a dilute growth solution – 1.3 ml tetraethyl orthosilicate (TEOS) 98%, and 2.8 ml tetrapropylammonium hydroxide 40% in 65 ml of water, in which TEOS was added dropwise and left reacting at 100°C for 24h in a rotisserie oven. The mixture was then centrifuged, and the zeolite was washed with deionized water 5 times. The solids were dried in a vacuum oven overnight at 80°C, and subsequently calcined under 40 ml/min air flow according to the following temperature program: 1 hour isothermal at 350°C (ramp rate = 1 °C/min) to clean the surface of any remaining water, followed by 5 hours at 600°C (ramp rate = 2 °C/min). The resulting catalyst is referred to as ZSM-5@Silicalite[62].

NH_4-Beta and H-Beta (framework type BEA), with Si/Al = 19 (CP814C) and Si/Al = 180 (No. 45875), were obtained from Zeolyst International and Alfa Aesar respectively. To render the NH_4-Beta acidic, the zeolites were calcined under 40 ml/min of air (80% N2 / 20% O2) at 550°C for 5 hours, with a ramp rate of 1 °C/min. The H-Beta was used as received.

H-Y and NH_4-Y catalysts (framework type FAU), with Si/Al = 40 (CBV 780) and Si/Al = 2.6 (CBV 300), were obtained from Zeolyst International. To render the NH_4-Y acidic, the zeolites were calcined under 40 ml/min of air (80% N2 / 20% O2) at 550°C for 5 hours, with a ramp rate of 1 °C/min.

H-ZSM22 catalyst (framework TON), with Si/Al = 65-80 (MSZ22H12), was obtained from ACS Material and used as received.

Amorphous silica-alumina (ASA) catalyst support grade 135, Si/Al = 6, was obtained from Aldrich and used as received.

2.3.2 Catalyst Characterization

To measure the acid sites of each zeolite, Isopropyl Amine Temperature Programmed Reaction (IPA-TPRx)[63,64] method was implemented in which a mixture of 50 mg of pelletized catalyst between 250 and 400 micrometers and 50 mg of glass beads was loaded into a 0.25-inch o.d. quartz reactor. The catalyst was pretreated in helium flow at 300 °C for 1 hour to eliminate any physisorbed water, then the reactor was cooled down to 100 °C and held there for 30 minutes. While keeping the temperature at 100 °C, injections of 2 μL of isopropyl amine (1 injection every 3 minute) were sequentially sent over the sample using a manual syringe until the area of the peaks were constant, signaling saturation of the zeolite which usually occurred at around 10 injections; then, the sample was flushed under He for 2 hours to remove any weakly adsorbed isopropyl amine. A linear temperature ramp of 10 °C/min from 100 to 600 °C was used to catalytically convert the chemisorbed IPA into propylene and ammonia which evolution was tracked using an MS. Afterwards, the MS was calibrated using a 500 μL gas injection coil with propylene to quantify the acid sites in the sample by assigning each propylene detected to an acid site.

Table 2: Catalyst Characterization, Pore Size obtained from literature, Acidity obtained from IPA-TPRx, SAR obtained from product description.

Catalyst	*Pore Size(A)*	*Acidity (mM/g)*	*SAR*
TON	4.5	0.384	65-80
MFI	5.3-5.6	0.106	140
MFI	5.3-5.6	0.391	40
BEA	6.7	0.119	180
BEA	6.7	0.547	19
Y	7.4	0.114	40
Y	7.4	0.366	2.6
ASA	20<	0.34	6

To verify the formation of the silicalite shell on ZSM-5, two probe reactions were performed in a flow reactor: acetic acid ketonization at 320°C, and triisopropylbenzene (TIPB) cracking at 400°C. The reactor consisted of a 0.25-in. OD quartz tube in a furnace, and the products were analyzed in a Hewlett Packard 6890 gas chromatograph (GC) equipped with an INNOWax column (30 m x 0.25 mm x 0.25 μm) and a flame ionization detector (FID). Both inlet and outlet lines were heated to avoid condensation of reactants and products. Reactions were performed under a 62.5 ml/min flow of helium and using 35 mg of fresh catalyst. W/F was 0.2 h for TIPB cracking, and 0.3 h for acetic acid, where F is the reactant feed rate. The zeolites were pretreated under the same flow of helium at the reaction temperature for 1 hour prior to the reaction start (Figure 10)[62].

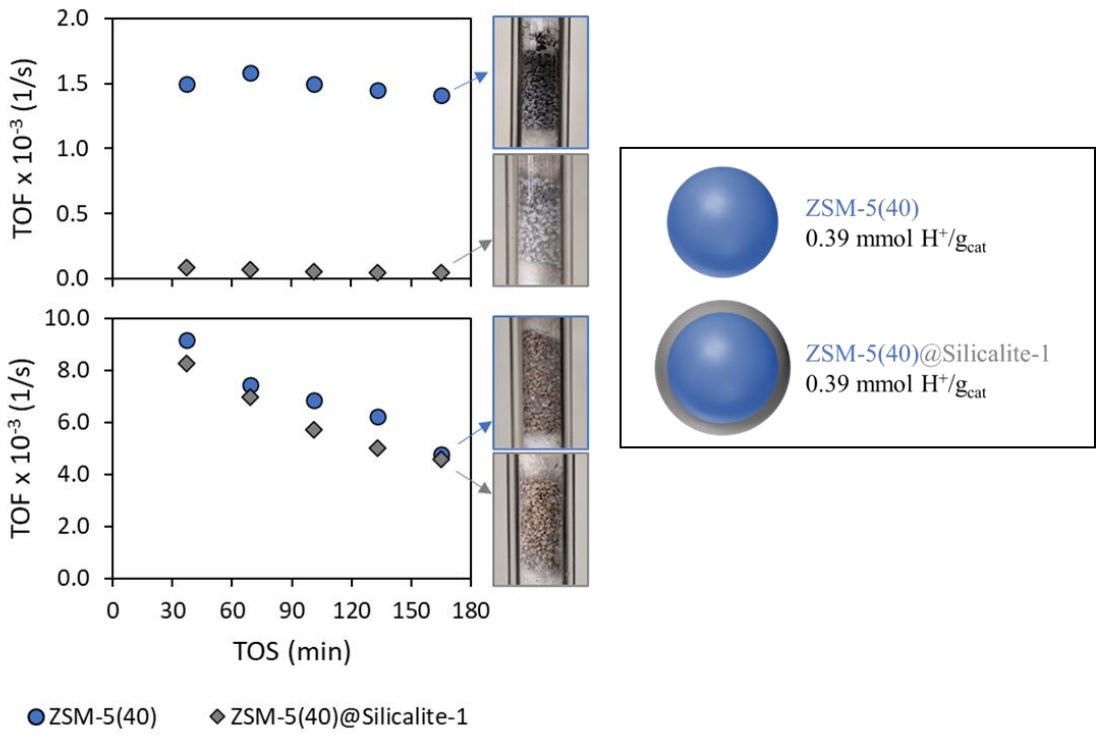

Figure 10: Turnover frequencies (TOF, 1/s) vs. time on stream (TOS, min) in a flow reactor for (A) TIPB cracking at 400 °C, and (B) acetic acid ketonization at 320 °C. (C) Visual representation of ZSM-5 and ZSM-5@Silicalite-1 (thickness of inert external shell is exaggerated for better visualization), and the BAS densities as measured by IPA-TPRx[62].

2.3.3 Catalyst Loading

In this study, the role of the zeolite framework, specifically the pore size, and the acid site density will be investigated. To compare fairly all the catalysts, the acid site to polymer ratio is kept constant throughout the different runs (Figure 11: Illustration for fair catalyst comparison by keeping the acid site to polymer ratio constant). In this way, we compare the different zeolites and structures in order to elucidate the roles and effects that each catalyst has on the catalytic dehydration of EVOH.

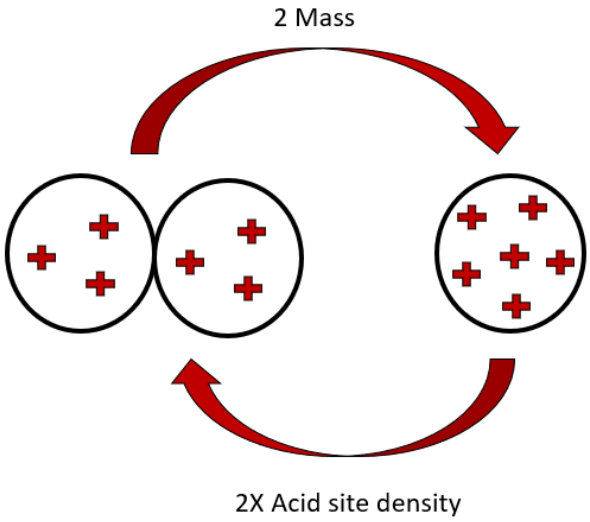

Figure 11: Illustration for fair catalyst comparison by keeping the acid site to polymer ratio constant.

2.3.4 Polymer

The polymer used in this reaction is Poly(vinyl alcohol-co-ethylene), with 32 ± 2 mol % of ethylene, fully hydrolyzed and obtained from Sigma Aldrich (No. 414093). The polymer was pulverized using a Retsch Mixer Mix CryoMill , with a 50 mL grinding jar, one 25 mm grinding ball with a profile of 10 minutes of pre-cooling at 5 Hz, followed by three cycles of 10 minutes of grinding at 25 Hz and an intermediary cooling of 5 minutes at 5 Hz. As polymer can degrade due to grinding[65], NMR experiments in a 400 MHz dual broadband probe system were conducted to corroborate that the polymer did not change after the treatment (Table 3)[66] . Prior to these experiments, an inverse recovery pulse sequence was performed to obtain the highest spin-lattice relaxation (T_1) for the solvent (DMSO) and the polymer (EVOH). This was with the intention of being able to set the relaxation time to five times the value of T_1 to assure quantitative measurements. For this sample, environment, and solvent the highest T_1 was 0.9 s, consequently the relaxation delay used for all measurements was set to 5s. The spectral width was set to

6410.3 Hz, acquisition time was 2.556 s, complex points was 16384, pulse angle set to 90 and 128 scans were made.

Table 3: NMR analysis of EVOH before and after cryomilling[66]

Pellets EVOH (EVOH before cryomilling)	**R-CH3**	**-CH2-**	**-CH-O**	**-CH(OH)-**	**Ethers and ketones**
Area	722.8	66529.8	17295.7	16845.2	Area of -CH-O minus Area of OH
Number of protons	3	2	1	1	4
Normalized area (Area/Number of protons)	220.9	33264.9	17295.7	16845.2	112.6
Total area	220.9 + 33264.9 +16845.2 + 112.6 = 50443.7				
% (Normalized area/Total area)	0.4%	65.9%	N/A	33.4%	0.1%
Estimated $M_W = M_{-CH2-} \times \%_{-CH2-}/(\%_{R-CH3}/2) + M_{CHOH} \times \%_{-CHOH-}/(\%_{R-CH3}/2) + 2 \times M_{CH3}$ ≈ 9653 (g/mol)					
Cryomilled EVOH (EVOH in this work)	**R-C*H3***	**-C*H2*-**	**-C*H*-O**	**-CH(O*H*)-**	**Ethers and ketones**
Area	609.0	72131.0	18687.0	18406.2	Area of -CH-O minus Area of OH
Number of protons	3	2	1	1	4
Normalized area (Area/Number of protons)	203.0	36065.5	18687.0	18406.2	70.2
Total area	203.0 + 36065.5 + 18406.2 + 70.2 = 54744.9				
% (Normalized area/Total area)	0.4%	65.9%	N/A	33.6%	0.1%
Estimated $M_W = M_{-CH2-} \times \%_{-CH2-}/(\%_{R-CH3}/2) + M_{CHOH} \times \%_{-CHOH-}/(\%_{R-CH3}/2) + 2 \times M_{CH3}$ ≈ 9683 (g/mol)					

The physical characteristics of the virgin EVOH were also investigated to corroborate the plastic was in the molten state during reaction conditions, as the degree of co-polymerization will ultimately affect the melting point. As such, DSC experiments on a TA Discovery series DSC 2500 with PerkinElmer standard aluminum pans (No. 02190041) were performed. The settings for the experiment were: initial temperature ramping at 10 K/min to 200 °C, followed by an isotherm for 5 minutes, then the sample was cooled to 40°C at 10 K/min followed by another ramping to 200 °C at 10 K/min. The data from the first step was discarded as its main purpose is to have a well

distributed plastic on the pan for the following steps. Results indicated that the melting temperature for poly (vinyl alcohol-co-ethylene) is 183.90 °C (Figure 12).

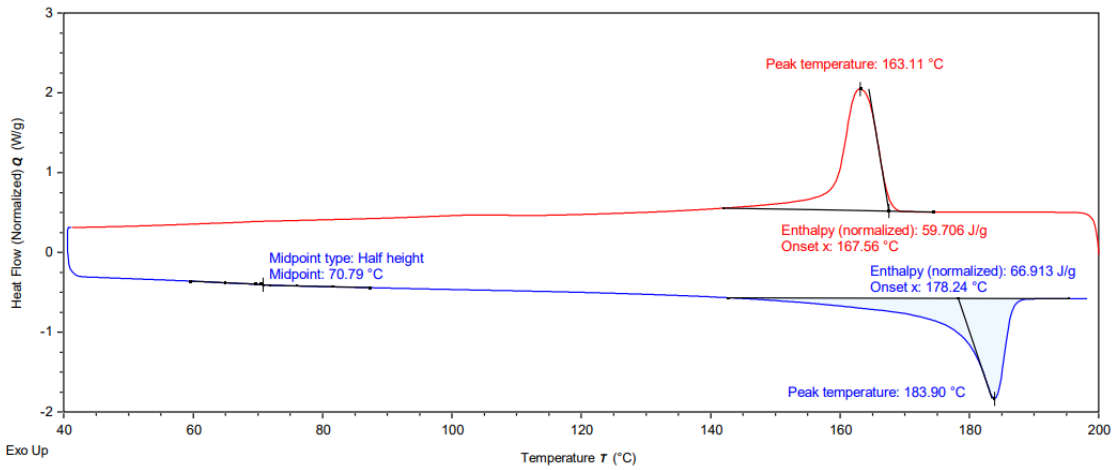

Figure 12: DSC of pure EVOH before reaction

2.3.3 Thermogravimetry

Reactions were carried out in a NETZSCH STA Jupiter 449 F1 thermogravimetric analysis (TGA) system, under 40 ml/min flow of argon. For each reaction, catalyst powder was mixed thoroughly with cryomilled EVOH before pouring the sample into the Al_2O_3 pan. The sample consisted of 70 mg of plastic coupled with the correct amount of catalyst to obtain the desired loading. The system was also coupled with an MS in which the water could be tracked to monitor the reaction progress (Figure 13).

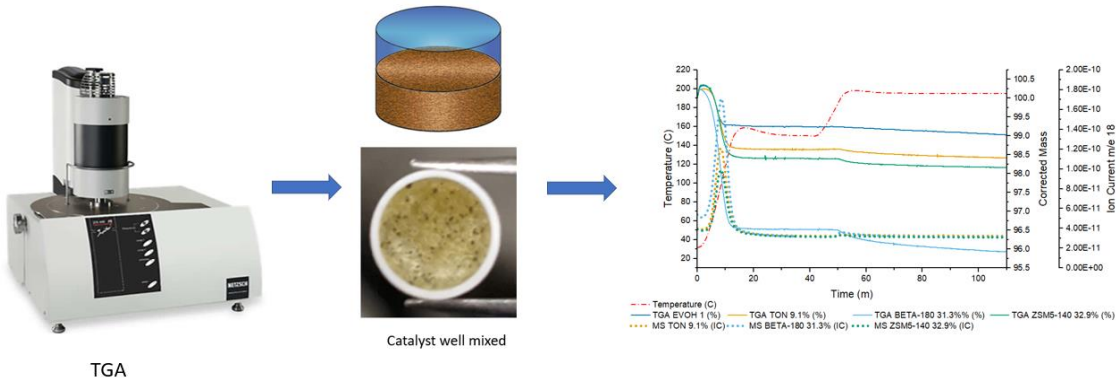

Figure 13: Reaction Procedure for TGA experiments.

The temperature profile used for this investigation consisted of an initial temperature ramping to 150°C at 10 Kelvin per minute, followed by an isotherm of 30 minutes. This step was with the intention of removing all the physisorbed water from the catalyst and the plastic to get a more accurate measurement of the true weight loss from water evolved during the dehydration reaction. Afterwards, a ramping of 5 Kelvin per minute to 195°C followed by a one-hour isotherm was performed to investigate the catalytic activity of the polymer (Figure 14). It is important to highlight that during the removal of physisorbed water, we do not expect any type of reaction as the plastic is still in a solid state at 150°C, Thus, this section of the data is not considered during analysis of the reaction (Figure 15). Once we reach 195°C, the plastic should be fully molten as the melting point for EVOH, found from DSC experiment (Figure 12), is 183.90°C and this would be the main data to be analyzed.

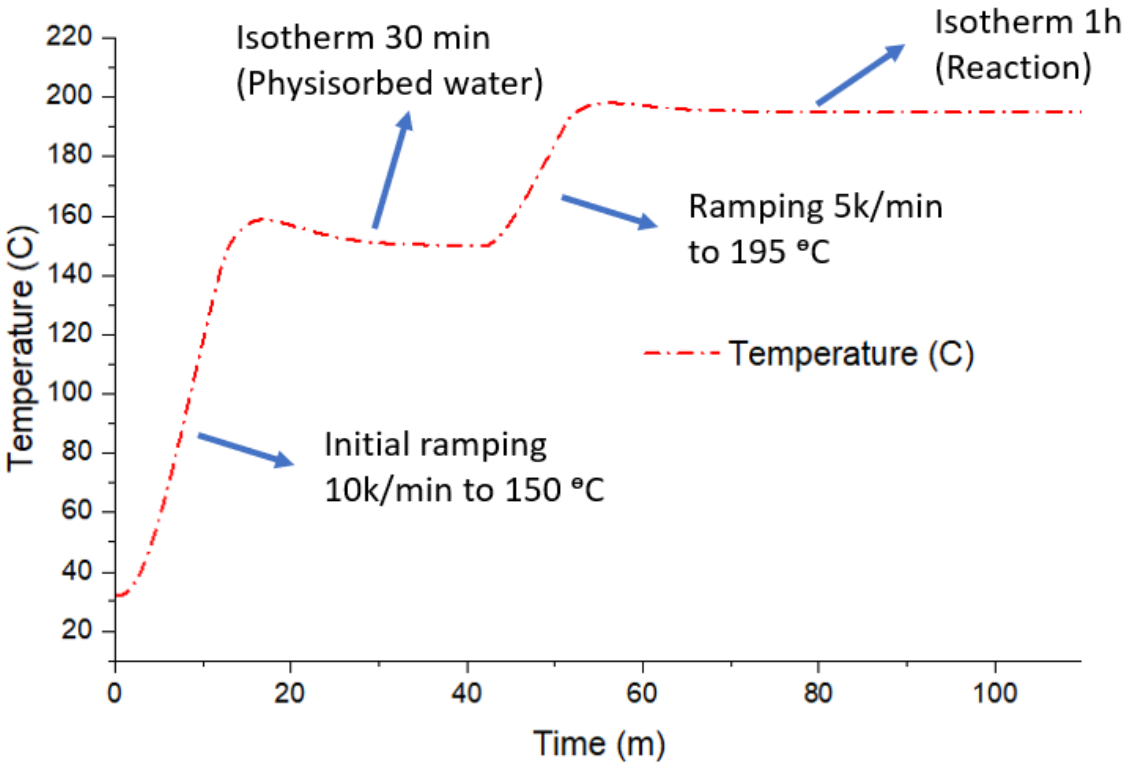

Figure 14: Temperature profile for TGA experiments

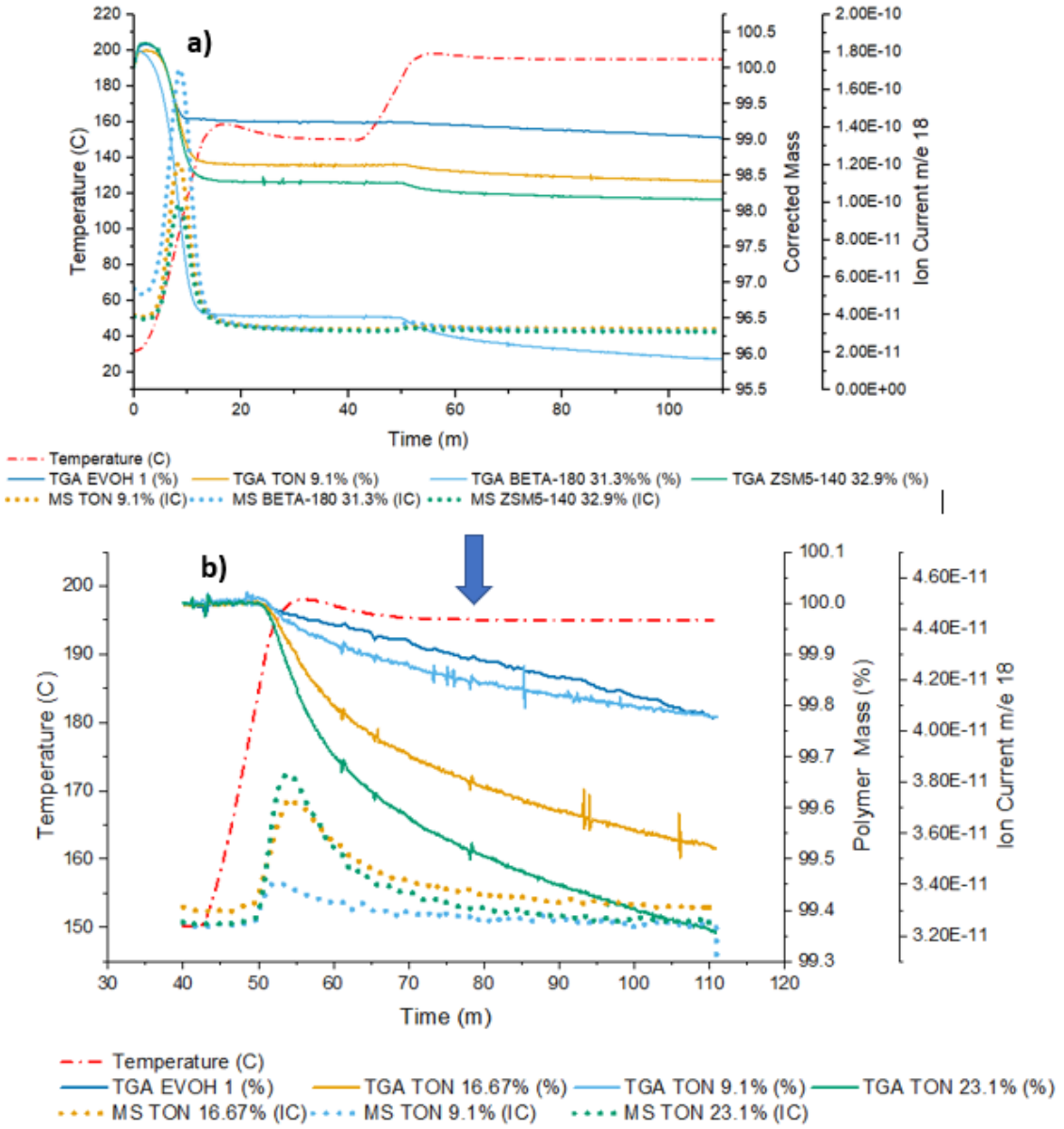

Figure 15: Figure depicting example TGA results before (a) and after (b) removal of the data in the physiosorbed water region.

2.3.4 Thiele Modulus Calculations

To be able to calculate the effectiveness factor for our reaction we are going to take advantage of the definition for this parameter[67]:

$$\eta = \frac{Actual\ overall\ rate\ of\ reaction}{Rate\ of\ reaction\ that\ would\ result\ if\ entire\ interior\ surface\ were\ exposed\ to\ the\ external\ pellet\ surface\ conditions}$$

Now, as can be seen on the equation, to be able to determine the effectiveness factor η we need to get the reaction rate in the surface. To accomplish this, the experiments using ZSM5 and ZSM5@Si will be leveraged by calculating the rates by getting the slopes of the mass loss found on the TGA experiments. Then the mass would be correlated to the amount of moles of water that would be release and normalize to the total amount of OH available in a single strand of EVOH, to get a rate in terms of polymer moles reacted. Also, as the TGA provides results in a %mass, for simplicity the mass of the sample was assumed to be equal to 100 g.

$$Rate = \frac{Slope * 100}{Mw_{H2O} * Mols\ of\ OH\ in\ a\ mol\ of\ EVOH}$$

The rates achieved by ZSM5 should be a combination of the internal active sites which are assumed to be completely limited by diffusion and the external active sites which provide the surface reaction rate. However, ZSM5@Si would only give the rate of the internal active sites as the surface-active sites were removed through the formation of the silicalite shell. As such, by subtracting the rate of ZSM5@Si from ZSM5 the rate of the external actives sites should be obtained.

$$R_{ZSM5} = R_{Surface} + R_{Internal}$$

$$R_{ZSM5@Si} = R_{Internal}$$

$$\rightarrow R_{Surface} = R_{ZSM5} - R_{ZSM5@Si}$$

However, to be able to use the rates calculated using this methodology, a normalization per acid site in the surface and in the pores would need to be made.

$$R_{Surface} = \frac{R_{Surface\ Observed}}{Number\ of\ External\ Active\ Sites}$$

$$R_{Internal} = \frac{R_{Internal\ Observed}}{Number\ of\ Internal\ Active\ Sites}$$

This in itself presents some difficulties as the number of actual external actives sites is unknown. Thus, for these calculations it is going to be assumed that the catalyst particles contain uniformly distributed active sites throughout its entire surface area (internal and external). The surface area in the pores (SAI) can be calculated using BET while the external surface area (SAE) can be estimated using SEM images to measure the particle size[62,68–74], assuming that the particles are spherical, and also as the surface area needs to be in a per gram bases, the theoretical crystal density would be used [75].

$$V_{Particle} = \frac{4}{3}\pi * r_{Particle}^3$$

$$V_{Pores} = V_{BET}$$

$$n_{pores} = \frac{2}{3} * \frac{r_{Particle}^2}{r_{Pore}^2}\frac{V_{Pore}}{V_{Particle}} * 2$$

$$SAE = \frac{4 * \pi * r_{Particle}^2 - \pi * r_{Pore}^2 * n_{Pore}}{V_{Particle} * \rho_{Crystal}}$$

$$SAI = SA_{BET}$$

$$SAT = SAE + SAI$$

$$\rho_{ZSM5} = \frac{n_{Al} * Mw_{Al} + n_{Si} * Mw_{Si} + n_O * Mw_O + n_H * Mw_H}{V_{Unit\ Cell} * N_{Avogadro}}$$

The Unit cell volume for ZSM5 can be estimated using as relationship derived by Mishin et al with respect to the number of alumina in the unit cell[76].

$$V_{Unit\ Cell} = 15.4 * n_{Al} + 5330$$

To calculate the number of atoms for each element the unit cell structure for HZSM5 can be used.

$$Si_{96-n}Al_nO_{192}H_n(n < 8)$$

Similarly, the unit cell volume for beta and Y zeolite can be estimated using literature measurements[77,78].

Thus, with these surface areas and densities we can calculate the number of internal and external actives sites from the IPA-TPD results.

$$Total\ Active\ Sites = Internal\ Active\ Sites + External\ Active\ Sites$$

$$= IPA\ TPD * Catalyst\ Loading$$

$$Internal\ Active\ Sites = Total\ Active\ Sites * \frac{SAI}{SAT}$$

$$External\ Active\ Sites = Total\ Active\ Sites * \frac{SAE}{SAT}$$

By calculating all these parameters for ZSM5 and ZSM5@Si the external rates and Internal rates can be calculated which, in tandem, will provide a Effectiveness Factor.

To be able to calculate Thiele modulus and diffusivities, further assumptions would need to be made. In this case it is going to be assumed that the process is first order and occur in an spherical particle[67].

$$\eta = \frac{3}{\phi^2} * (\phi coth(\phi) - 1)$$

To calculate other frameworks besides ZSM5 SAR 40, it is going to be assumed that the external turnover frequency would be the same across all the zeolites. Thus, permitting the calculation of the external turnover frequency by calculating the number of external acid sites based on the ratio between external and internal surface area. Then, the same procedure as before was done to get the effectiveness factor and Thiele modulus.

2.4 Results and Discussion

2.4.1 Acid Site Density

Initially, the role of the acid site density was explored on the different zeolite frameworks and acid site densities. To accomplish this, two sets of experiments were performed, one in which the same framework with equal total amount of acid sites but different total available pores were compared (Figure 16a), and the other in which the total available pores was set equal, but the amount of total acid sites varied (Figure 16b). These two types of experiments were performed on the zeolites with frameworks MFI, BEA and FAU as they possess different pore sizes. This

allowed to have a preview on how the acid site density impacts the performance of each type of framework and its respective pore size.

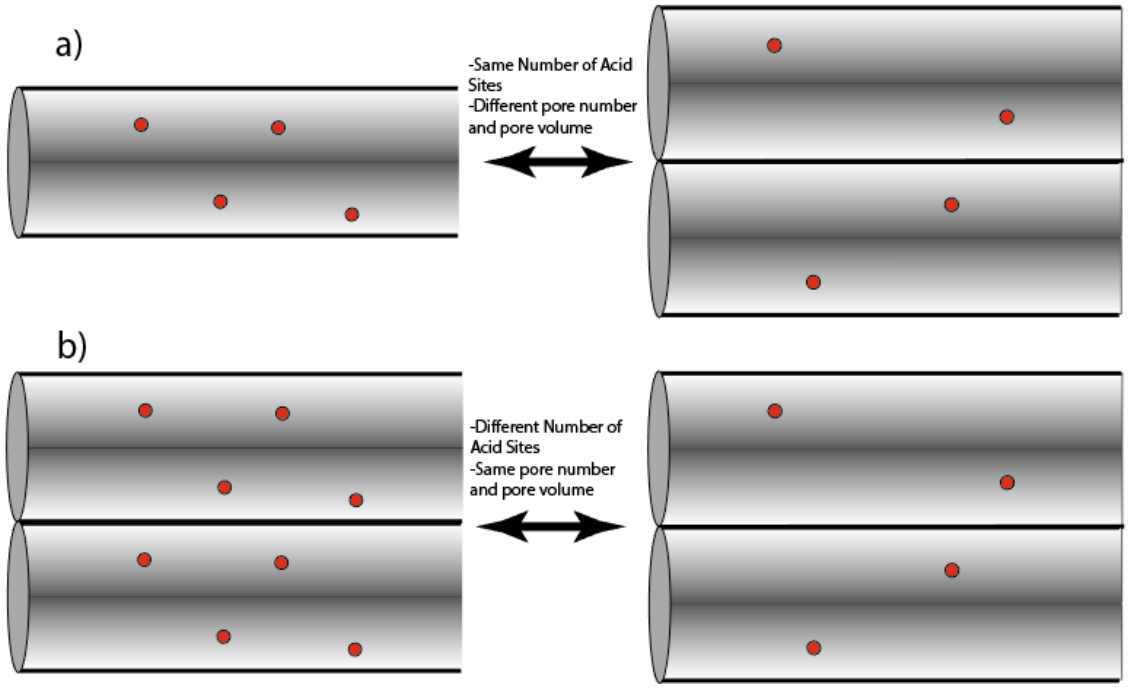

Figure 16: Experimental setup for acid site comparison. A) comparing the catalyst with the same total number of acid sites but with different total pore volume. b) Comparing the catalyst with the same total pore volume but with a different number of acid sites.

The first experiment was set with the intention of exploring how the number of available pores for a specific type of framework would affect the reaction rates. This is accomplished by setting the acid site to polymer ratio to a constant of $0.0349 \frac{mM\ Acid}{g\ Polymer}$, thus keeping the total number of acid sites on the experiment constant but changing the amount of available pores by altering the loadings of the catalyst to meet this constraint. Results for such experiment can be observed in Figure 17 where part a, b and c show the effects that the difference in acid site density, and thus catalyst loadings, for a particular zeolite at a given framework has on the dehydration rates for EVOH. The first trend that can be observed on Figure 17 and Table 4 shows

that regardless of the pore size, higher maximum rates were achieved over the catalyst with a lower acid site density (i.e., in the experiments with greater catalyst mass:polymer ratio). Also, the degree of difference between the maximum rates seems to be correlated with pore structure as well as it can be seen on Table 4, where a larger pore structure would lead to a higher absolute difference. However, the maximum rate percentage difference between FAU and MFI is about the same which could be related to the similar acid site densities of the pair of catalysts explored for these frameworks. Another pattern that can be observed from these results are that the final rate after deactivation is greater for zeolites that have a low acid site density and have big pores (Figure 17 and Table 5). Nevertheless, if these final rates are compared to the maximum rate achieved by the zeolite, it can be seen on Table 5 that there is shift on the maximum rate retention from high acid site density zeolites to low acid site density zeolites as the pore size increases.

Table 4: Maximum rates for the different zeolite frameworks with different acid site density but with a constant number of acid sites to polymer ratio. Thus, rates can be considered as rate per acid site because we need to divide all by the same number.

	Acidity (mM/g)	***Max Rate***	***Difference***	***% Difference***
MFI SAR 40	0.391	3.41E-03	6.66E-03	195.21%
MFI SAR 140	0.106	1.01E-02		
BEA SAR 19	0.547	2.89E-03	1.68E-02	583.68%
BEA SAR 180	0.119	1.97E-02		
FAU SAR 2.6	0.366	9.47E-03	1.84E-02	194.38%
FAU SAR 40	0.114	2.79E-02		

Table 5: Comparison of maximum rates to the final rate after deactivation

	Max Rate	***Final Rate***	***Difference***	***% Rate Retention***
MFI SAR 40	3.41E-03	1.00E-03	2.41E-03	29.39%
MFI SAR 140	1.01E-02	1.00E-03	9.07E-03	9.95%
BEA SAR 19	2.89E-03	7.15E-04	2.17E-03	24.77%
BEA SAR 180	1.97E-02	3.42E-03	1.63E-02	17.32%
FAU SAR 2.6	9.47E-03	2.84E-04	9.19E-03	2.99%
FAU SAR 40	2.79E-02	5.16E-03	2.27E-02	18.53%

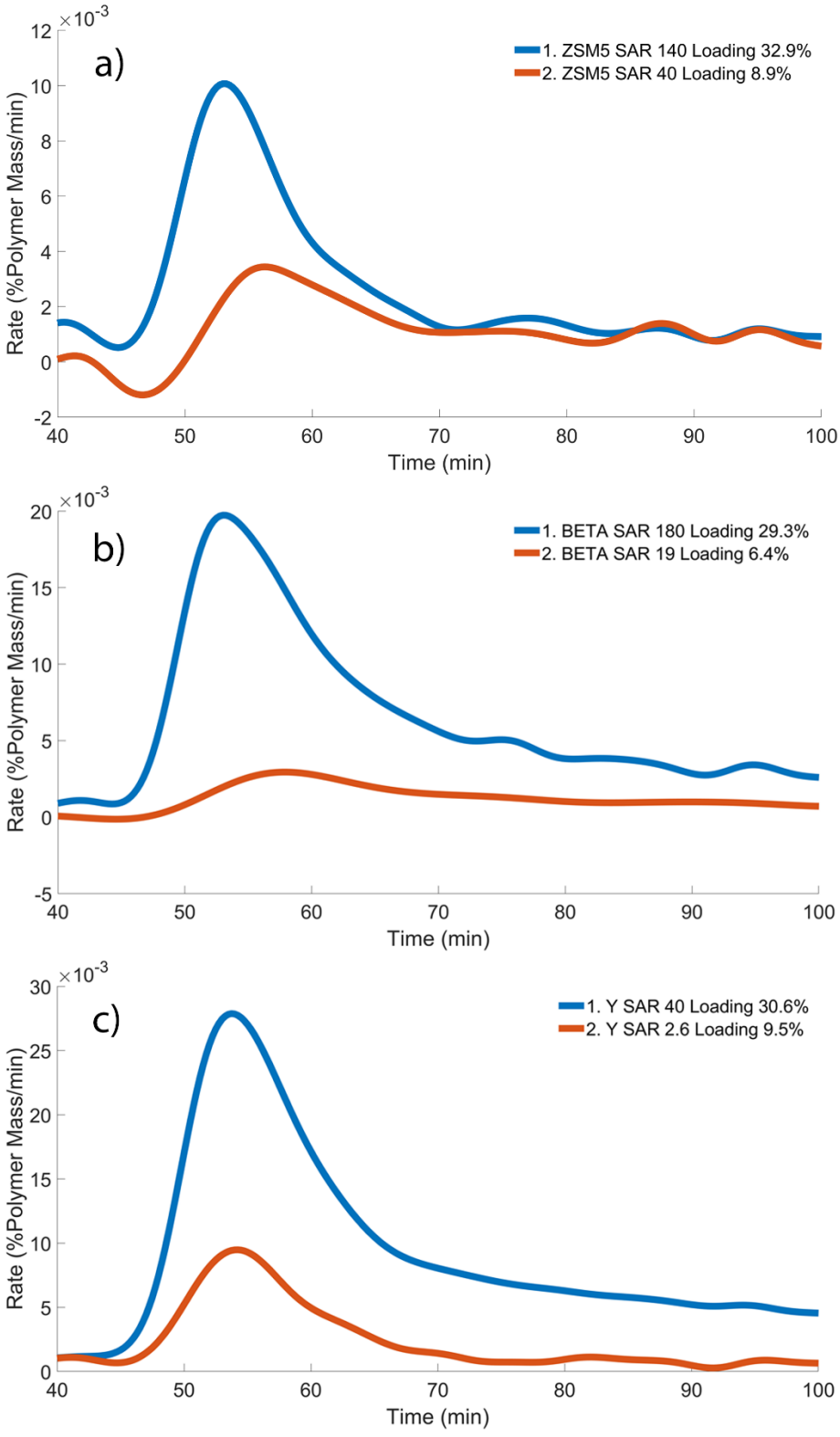

Figure 17: Catalytic Polymer dehydration rates using Zeolite ZSM5 (a), BEA (b) and FAU (c) at two different Silica to Alumina ratios but preserving a constant total acid site to polymer ratio.

In a second set of experiments, catalyst mass to polymer ratio was held constant with different acid site densities in order to explore dependence of rate on site availability in a constant volume of pores. Results for such experiments can be appreciated on Figure 18 where part a, b and c portray the effect of acid site densities at the same number of available pores in the dehydration reactions for different zeolite frameworks. At first glance the results from this experiment seem to produce an opposite trend compared to the previous experiment, the high acid site density zeolites show a consistent higher maximum rate for dehydration compared to their lower acid site counterparts regardless of the pore structure (Figure 18 and Table 6). Nevertheless, if the rates are normalized in a per acid site manner it can be seen that the pattern previously found holds. The maximum rate per acid site is higher for lower acid site density zeolites and when large pore zeolites are used (Table 6). Another pattern to be outlined is that at equal loading, the final rates observed for the zeolites seem to converge to single final rate of reaction for all frameworks as it can be seen of Figure 18 after 70 minutes for part a, b and c.

Table 6: Maximum rates for the different zeolite frameworks with different acid site density but with a constant number of available pores.

	Acidity (mM/g)	***Rate***	***Rate/Acid Site***
MFI 40	0.391	2.18E-02	1.70E-01
MFI 140	0.106	1.01E-02	2.89E-01
BEA 19	0.547	2.68E-02	1.67E-01
BEA 180	0.119	1.97E-02	5.66E-01
FAU 2.6	0.366	5.59E-02	4.99E-01
FAU 40	0.114	2.78E-02	7.98E-01

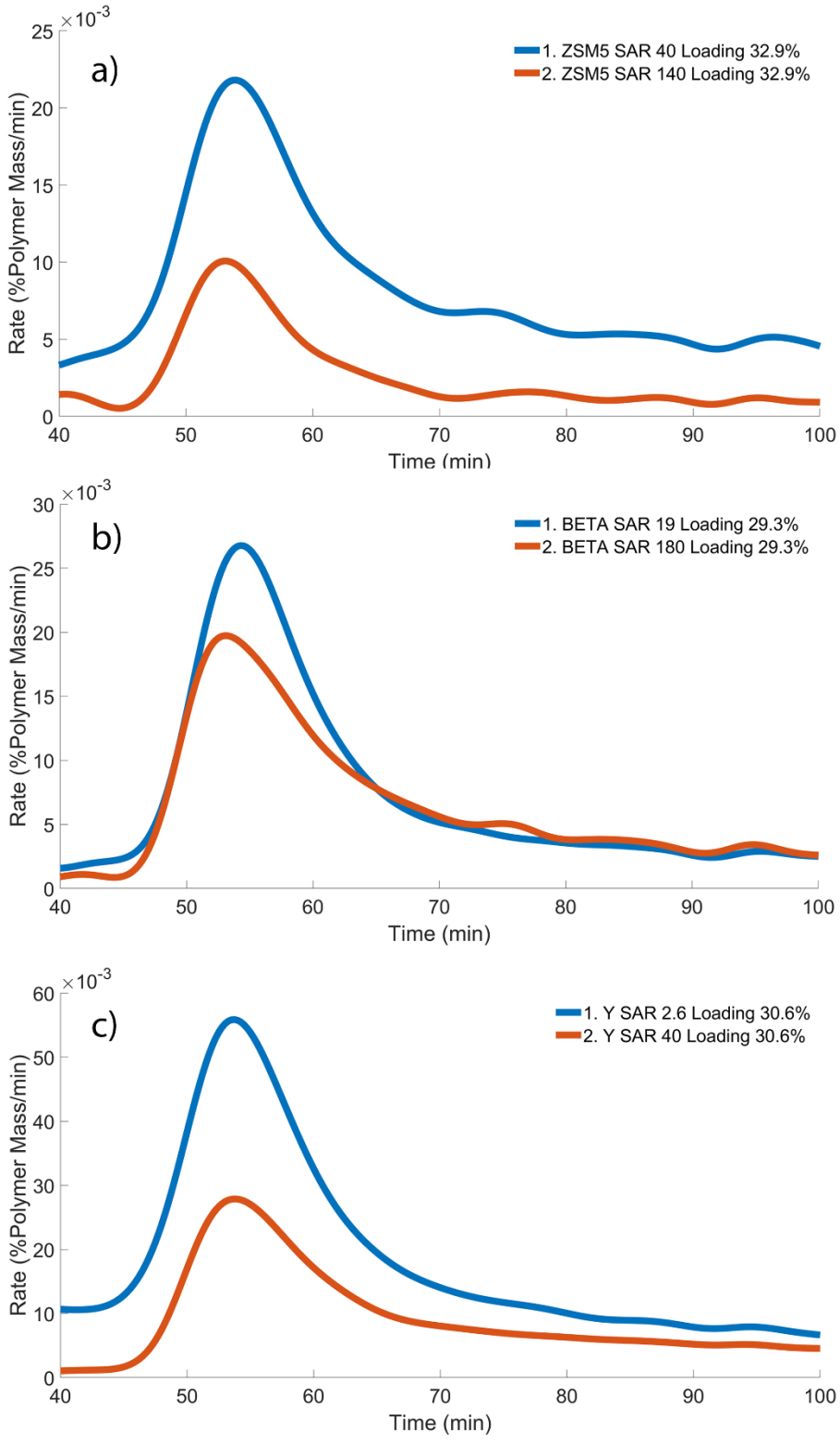

Figure 18: Catalytic Polymer dehydration rates using Zeolite ZSM5 (a), BEA (b) and FAU (c) at two different Silica to Alumina ratios but preserving a constant total available number of pores.

The behavior observed on the previous results could be explained in several ways, but the underlying principle of the ideas is the same: Mass transfer limitations. This overall constraint was confirmed by how the experiments fail the Koros-Nowark Criterion outlined by Madon and Boudart[79], where the conversion and thus the rate for experiments with the same acid site loadings but different catalyst mass loading show different results. One of the hypotheses for the difference in catalytic performance would be due to the number of available pores. It is well known that an increment on the number of available pores for a polymer to diffuse would increase the flux of the substrate which will in tandem show a higher catalytic rate when diffusion is the rate limiting step. This increase in the rate of mass transfer could further explain the results obtained in the number of available pores comparison experiment. The additional available pores for diffusion could contribute significantly to the apparent rate compared to the effects of shorter diffusion paths resulting from higher acid site density in zeolites. Thus, the zeolites with higher catalyst mass loading and lower acid site density would show better catalytic activity. This idea further explains the second observation, in which at the same number of total available pores, the lower acid site to polymer ratio samples outperforms the higher acid site to polymer ratio option when the turnover frequency was compared. Finally, the increase in the number of pores and the diffusion-limited behavior can explain why the catalyst with higher loadings and larger pore structures appears to have better activity retention. This is likely because the improved diffusion capabilities from these two aspects facilitate the mass transport of the polymer into and out of the zeolite porous structure, thus achieving a higher apparent steady state rate by improving the rate limiting step. This explanation is consistent with literature, as it has been show that polymers have a particularly hard time when diffusing out of porous structures[48].

2.4.2 Pore Size

Diffusion limitations have been shown to play a significant role in controlling reaction rates for these polymeric systems. Therefore, it is important to explore the significance of pore size as a tool to tune these limitations. To ensure fair comparison, this investigation focuses on zeolites with similar acid site densities, enabling comparable catalyst loading. The use of comparable catalyst loading is particularly relevant as previous findings indicate that the number of available pores, closely related to loading, greatly impacts apparent rates.

As can been seen in Figure 19, there is a trend where the maximum rate achieved is directly correlated to the pore size of the zeolite framework. This has been shown by how MFI, which has the smallest pore size, depicts the lowest rates while FAU which has the biggest pore size shows the highest rate. This behavior supports the previous results on the idea that this reaction is severely mass transfer limited, as the main two contributing factors that pore size can bring to this system are diffusion and coke prevention effects. Furthermore, it can be seen that the retention of activity after the fast deactivation is also correlated to the pore size, with FAU retaining the most activity while MFI retaining the least, about 5 times less compared to FAU. This result also suggests that the deactivation of our catalyst is probably not mainly driven by classic deactivation due to coke as the smaller pore size zeolites should have better capabilities on mitigating its production and thus retaining the activity which is not what its being seen. Thus, deactivation seems to be more likely due to diffusion limitations of the polymer strand which ultimately cause a fouling effect on the catalyst pores. As such, the mitigation of the mass transfer

issue brought by a bigger pore size zeolite would explain why FAU shows higher activity and activity retention compared to MFI.

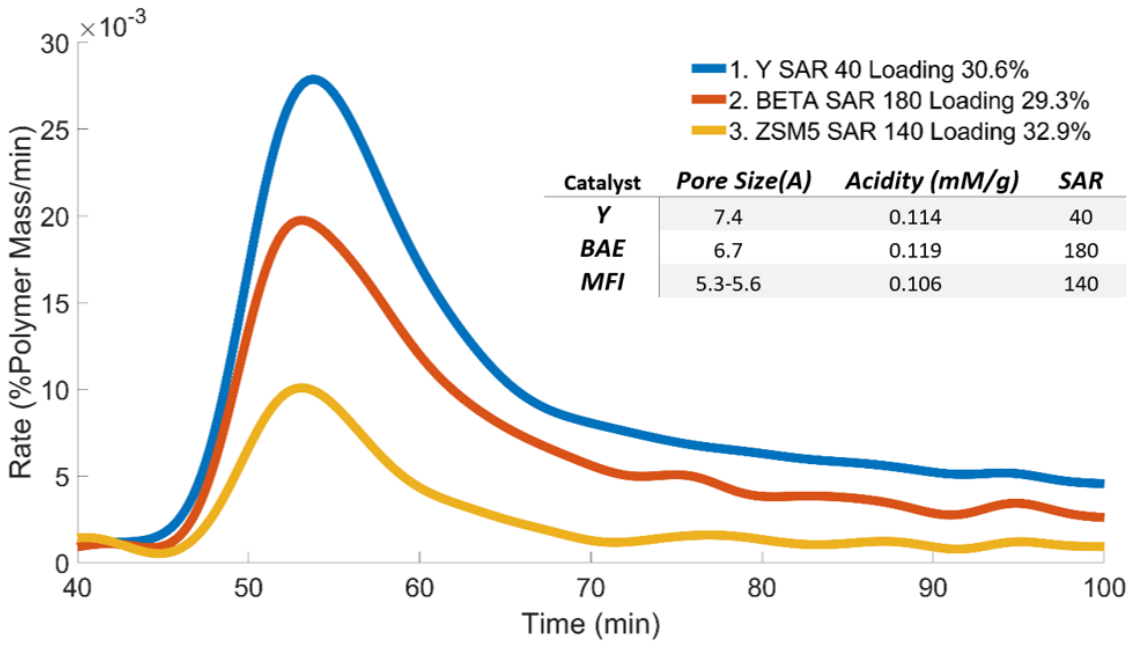

Catalyst	Pore Size(A)	Acidity (mM/g)	SAR
Y	7.4	0.114	40
BAE	6.7	0.119	180
MFI	5.3-5.6	0.106	140

Figure 19: Zeolite framework comparison (pore comparison) with relatively similar acid site density, while keeping the acid site to polymer ratio equal to $0.0349 \frac{mM\ Acid}{g\ Plastic}$

To explore in more depth the role of pore size on the reaction, it was decided to compare a wider range of zeolite frameworks and an amorphous silica alumina catalyst which has meso- and macro-porosity. As it can be seen on Figure 20, the general trend seen for the different zeolite frameworks in which a higher pore size leads to higher achievable rates still holds with FAU showing the highest activity and TON showing the least. However, the amorphous silica alumina catalyst which should have the least diffusion limitations compared to the zeolites shows lower performance compared to the zeolite Y but it retains better the activity after deactivation. In this sense, these results could point out that the cages from the zeolite frameworks have an initial improvement on either diffusion of the reactant to the acid sites or limiting the initial

deactivation of the catalyst. Nevertheless, once a certain extent of reaction has been achieved, the increase in diffusivity provided by the hierarchical pore structure from the amorphous material will improve activity retention of this catalyst. Another interesting takeaway that can be taken from this set of experiments is that the deactivation on the zeolites is not due to more than one polymer strand interacting and reacting with each other on the pore intersections as TON which has only straight channels show the same type of deactivation.

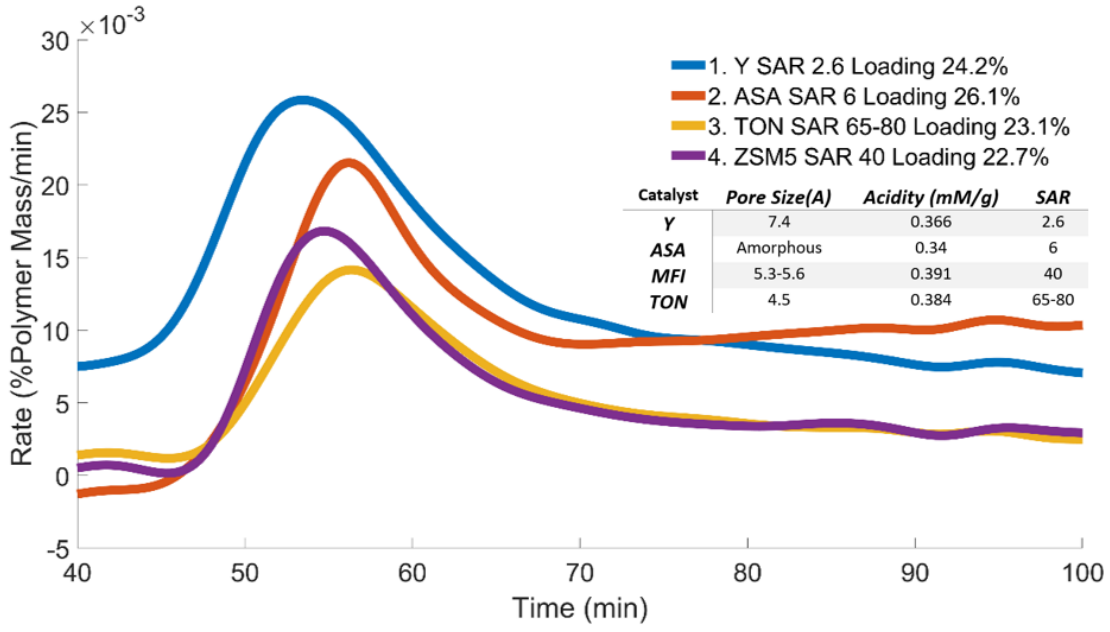

Catalyst	Pore Size(A)	Acidity (mM/g)	SAR
Y	7.4	0.366	2.6
ASA	Amorphous	0.34	6
MFI	5.3-5.6	0.391	40
TON	4.5	0.384	65-80

Figure 20: Zeolite framework comparison (pore comparison) with relatively similar acid site density, while keeping the acid site to polymer ratio equal to $0.08862 \frac{mM\ Acid}{g\ Plastic}$

2.4.3 External Active Sites

When the accessibility to the active sites within the pore of a catalyst is limited, such as the case of polymeric systems, the external active sites are expected to be a significant contributor to the rate. Thus, to explore in more detail to what degree the external active sites influence the activity of our reaction, a comparison between a normal MFI zeolite and an MFI

with a silica shell that removes all the external active sites was made. The results from this experiment can be seen in Figure 21 where it can be appreciated that once the external active sites are removed not only the maximum rate achieved is drastically decreased but also the catalyst seems to deactivate much faster, as the rate approaches zero in less time. It can be seen in Table 7 that the removal of the external active sites leads to a loss of more than 50% of the maximum achievable rate. Thus, this experiment reiterates that the external active sites are playing a crucial role on the activity of the polymer.

Table 7: Rate comparison for external active sites experiments.

	Max Rate
MFI	2.15E-02
MFI@Si	9.47E-03
Difference	1.20E-02
% Difference	55.94%

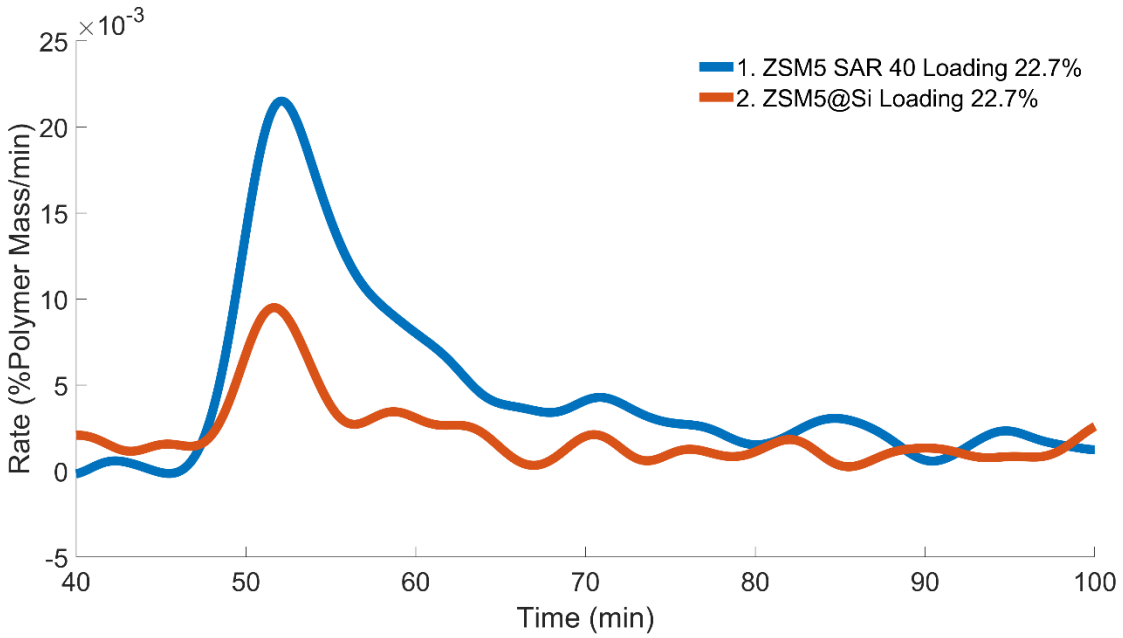

Figure 21: Evaluation of the role of external active sites during the catalytic dehydration of EVOH by comparing ZSM5 SAR 40 with a modify ZSM5 SAR 40 with a silica shell.

2.4.4 Thiele Modulus and Effectiveness Factors

The observed effectiveness factor and Thiele modulus was calculated using the methodology previously outlined and can be seeing on Table 8. It can be seen that the catalysts with smaller pore size seem to have higher Thiele modulus within the same range of acidity. Also, there seems to be a correlation between the acid site density and the magnitude of Thiele modulus, showing higher Thiele values for the catalyst with higher acid site densities.

Table 8: Thiele modulus and effectiveness factor for each catalyst

Catalyst	Acidity (mM/g)	Thiele Modulus	Effectiveness Factor
ZSM5 SAR: 40	0.391	452.0	0.0066
ZSM5 SAR: 140	0.106	400.6	0.0075
BETA SAR: 19	0.547	1702.5	0.0018
BETA SAR: 180	0.119	143.5	0.0208
Y SAR: 2.6	0.366	164.8	0.0181
Y SAR: 40	0.114	81.2	0.0365

One observable pattern is that the Thiele modulus values for all catalysts are significantly higher than one, clearly indicating that the reaction operates within the diffusion-limited regime and supporting the previous conclusions. Additionally, the Thiele modulus increases as the acid site density rises, which aligns with the earlier hypothesis. This increase implies even greater diffusion limitation, potentially due to stronger adsorption of the polymers functional groups in the catalyst, thereby impeding diffusion rates. Furthermore, the pattern of decreasing Thiele modulus with increasing pore size at the same acid site density range further reinforces the notion of diffusion limitation. Larger pores generally exhibit higher diffusion rates, so this observed decrease in Thiele modulus is expected. However, it is worth noting that the magnitude of the Thiele modulus obtained through this methodology is lower than anticipated. This discrepancy could stem from inaccuracies in the calculations resulting from underlying assumptions or the behavior of the reaction itself. Alternatively, another hypothesis proposes that the low Thiele modulus observed in this study may solely represent the reaction occurring at the polymer chain ends. This would explain the initial activity peak followed by rapid deactivation as the polymer chain ends diffuse into the catalyst, react, and becomes immobilized due to interactions with the catalyst walls and active sites.

2.5 Conclusion

In conclusion, the role of acid site density and pore size in zeolite catalysts has been investigated in the context of catalytic dehydration of Poly(vinyl alcohol-co-ethylene). Two sets of experiments were performed to explore the impact of these factors on reaction rates and activity retention.

The first set of experiments focused on comparing catalysts with the same total number of acid sites but different total available pores (catalyst loadings). The results showed that regardless of the pore size, higher maximum rates were achieved over catalysts with lower acid site densities. The difference in maximum rates was correlated with the pore structure, with larger pore structures exhibiting a higher maximum rate. Moreover, zeolites with lower acid site densities and larger pores demonstrated better activity retention after deactivation compared to high acid site density zeolites. These findings suggested that catalysts with higher loadings and lower acid site densities exhibited improved catalytic activity, likely due to enhanced mass transfer facilitated by additional available pores for diffusion.

In the second set of experiments, catalyst mass to polymer ratio was held constant while varying the acid site densities. Zeolites with higher acid site densities consistently exhibited higher maximum rates for dehydration, regardless of pore structure. However, when the rates were normalized per acid site (turn over frequency), the low acid site density zeolites outperformed their counterparts, reinforcing the idea that lower acid site density zeolites with larger pores had higher maximum rates per acid site.

Lastly, the significance of external active sites was investigated by comparing MFI zeolites with and without external active sites. The removal of external active sites resulted in a drastic decrease in the maximum achievable rate and faster deactivation of the catalyst, indicating the crucial role of external active sites in the polymer dehydration reaction. Thus, reinforcing how crucial mass transfer is for this type of reactions.

Overall, these findings highlight the importance of considering acid site density and pore size when selecting zeolite catalysts for catalytic polymer dehydration. Lower acid site densities and larger pores can enhance mass transfer and improve catalytic activity, while external active sites contribute significantly to the overall reaction rate. Understanding these factors can aid in the development and selection of more efficient catalysts for polymer conversion processes.

Chapter 3: Catalytic Dehydration of Polyvinyl alcohol in solvent system

3.1 Abstract

The study focuses on the selection of solvents and exploration of catalytic activity for the dehydration of EVOH (ethylene vinyl alcohol). Two solvents were explored, DMSO (dimethyl sulfoxide) and a combination of water and propanol. DMSO was found to have excellent solvation effects on EVOH but its use resulted in limited reactivity of the catalysts that were studied. The inhibition of the reaction by DMSO could be attributed to its competition for acid sites or a possible interference with certain transition steps in the dehydration process. On the other hand, the water-propanol mixture also showed promise by allowing the dissolution of EVOH and offering the potential for additional chemistry, such as alcohol addition through the formation of an ether. Various catalysts were tested, and Beta 19 demonstrated the highest activity. The study also investigated the optimal proportions of propanol and water and found that water adversely affected the reaction rate, with a significant burst of activity observed when water proportions were below 25% of the solvent mixture.

The analysis of the reactions involved the use of NMR (nuclear magnetic resonance) and DSC (differential scanning calorimetry) techniques and FTIR (Fourier Transform Infrared Spectroscopy). However, sampling inconsistencies posed challenges in quantifying the overall reaction conversion. Cryomilling was employed to improve the acquisition of a uniform random sampling, but even with this method, results showed some inconsistencies. Additionally, NMR experiments, which were critical for conversion analysis, not only suffered from the sampling

heterogeneity but also from incomplete dissolution which hindered accurate quantification using NMR. The difficulties encountered highlight the complexity and challenges of characterizing the overall conversion of plastic.

3.2 Introduction

Mass transfer limitation in polymer melts is one of the key challenges that need to be overcome to achieve good conversion for catalytic transformation of polymers. Nevertheless, understanding of catalytic mechanisms and rates even without that limitation in polymer mixtures is still important to build fundamental knowledge for the more complex system. As such, studying the reaction in solvent systems could bring insight into the reaction mechanism and how the molten polymer system should be approached.

To accomplish this task, several zeolites with different frameworks were studied. It is important to highlight that in solvent systems, the presence of water can play a major role during the dehydration mechanism and also in the stability of the zeolite[37,43,44]. Thus, the use of zeolites with low defects and controlling the water concentration can help elucidate ideal conditions for this reaction.

3.3 Materials and methods

3.3.1 Catalysts

NH_4-Beta and H-Beta (framework type BEA), with Si/Al = 19 (CP814C) and Si/Al = 180 (No. 45875), were obtained from Zeolyst International and Alfa Aesar respectively. To render the NH_4-Beta acidic, the zeolites were calcined under 40 ml/min of air (80% N2 / 20% O2) at 550°C for 5 hours, with a ramp rate of 1 °C/min. The H-Beta was used as received.

H-Y and NH_4-Y catalysts (framework type FAU), with Si/Al = 40 (CBV 780) and Si/Al = 2.6 (CBV 300), were obtained from Zeolyst International. To render the NH_4-Y acidic, the zeolites were calcined under 40 ml/min of air (80% N2 / 20% O2) at 550°C for 5 hours, with a ramp rate of 1 °C/min.

Amorphous silica-alumina (ASA) catalyst support grade 135, Si/Al = 6, was obtained from Aldrich and used as received.

3.3.2 Catalyst Characterization

To measure the acid sites of each zeolite, Isopropyl Amine Temperature Programmed Reaction (IPA-TPRx)[63,64] method was implemented in which a mixture of 50 mg of pelletized catalyst between 250 and 400 micrometers and 50 mg of glass beads was loaded into a 0.25-inch o.d. [63,64] method was implemented in which a mixture of 50 mg of pelletized catalyst between 250 and 400 micrometers diameter and 50 mg of glass beads was loaded into a 0.25-inch o.d. quartz reactor. The catalyst was pretreated in helium flow at 300 °C for 1 hour to eliminate any physisorbed water, then the reactor was cooled down to 100 °C and held there for 30 minutes. While keeping the temperature at 100 °C, injections of 2 μL of isopropyl amine (1 injection every 3 minute) were sequentially sent over the sample using a manual syringe until the area of the peaks were constant, signaling saturation of the zeolite which usually occurred at around 10 injections; then, the sample was flushed under He for 2 hours to remove any weakly adsorbed isopropyl amine. A linear temperature ramp of 10 °C/min from 100 to 600 °C was used to catalytically convert the chemisorbed IPA into propylene and ammonia which evolution was tracked using an MS. Afterwards, the MS was calibrated using a 500 μL gas injection coil with

propylene to quantify the acid sites in the sample by assigning each propylene detected to an acid site.

Table 9: Catalyst Characterization, Pore Size obtained from literature, Acidity obtained from IPA-TPRx, SAR obtained from product description.

Catalyst	Pore Size(A)	Acidity (mM/g)	SAR
BEA-180	6.7	0.119	133
BEA-19	6.7	0.547	19
Y-40	7.4	0.114	40
Y-2.6	7.4	0.366	2.6
ASA	20<	0.34	6

3.3.3 Polymer

The polymer used in this reaction is poly(vinyl alcohol-co-ethylene), with 32 ± 2 mol % of ethylene, fully hydrolyzed and obtained from Sigma Aldrich (No. 414093). The plastic was dissolved in either 20mL of distilled water and alcohol in a 1:1 ratio for a 1 g of plastic to 20 mL solvent concentration or in pure DMSO for a 2g of plastic in 20 mL of solvent concentration. The process was carried out at a temperature of 50 °C while stirring at 350 rpm overnight. Once the reaction experiment was finished, the alcohol-water mixture was exposed to liquid nitrogen while in DMSO samples, water was used as antisolvent to crash the polymer out of solution. The plastic was collected through centrifugation, washed with distilled water, and dried in a vacuum oven overnight at 90 °C. After drying, the samples were cryomilled in a Retsch Mixer Mix CryoMill with a 10 mL chamber and two 12 mm balls. The samples were precooled for 5 minutes at 5 Hz, followed by three cycles of milling for 2 min at 25 Hz and intermediary cooling for 2 minutes at 5 Hz.

For analysis of the polymer, NMR experiments in a 400 MHz dual broadband probe system were performed. The samples were dissolved in deuterated DMSO overnight at 80°C. Prior to these experiments, an inverse recovery pulse sequence was performed to obtain the highest spin-lattice relaxation (T_1) for the solvent (DMSO-d6) and the polymer (EVOH and reacted EVOH). This was with the intention of being able to set the relaxation time to five times the value of T_1 to assure quantitative measurements. For this sample, environment, and solvent the highest T_1 was 0.9 s, consequently the relaxation delay used for all measurements was set to 5s. The spectral width was set to 6410.3 Hz, acquisition time was 2.556 s, complex points was 16384, pulse angle set to 90 and 128 scans were made. Carbon NMR was also performed on the samples, with the experimental setup being relaxation 2s coupled with 528 scans. It is important to note that the carbon NMR measurements are not quantitative as the relaxation time is not sufficiently large, but they give a qualitative representation of the functional groups present in the polymer.

Another way in which the polymer modification was quantified was through the melting point calculation. It is known that the polymer melting point decreases with the extent of dehydration[53,54]. Furthermore, changes to these physical properties do not occur at temperature below 200 °C which is below the reaction temperatures of this study[53]. Thus, this change in melting point is a qualitative tool to measure the degree of conversion. To accomplish this, DSC experiments on a TA Discovery series DSC 2500 with PerkinElmer standard aluminum pans (No. 02190041) were performed. The settings for the experiment were: initial temperature ramping at 10 K/min to 200 °C, followed by an isotherm for 5 minutes, then the sample was cooled to 40°C at 10 K/min followed by another ramping to 200 °C at 10 K/min. The data from the first step

was discarded as its main purpose is to have a well-distributed plastic on the pan for the following steps.

3.3.4 Conversion Calculations

To calculate the fractional conversion (dehydration) of the polymer, the quantitative results from NMR were used. To accomplish this, firstly the NMR peaks were identified for each functional group. Using literature[80–84], and carbon NMR the following peak identifications were assigned (Figure 22).

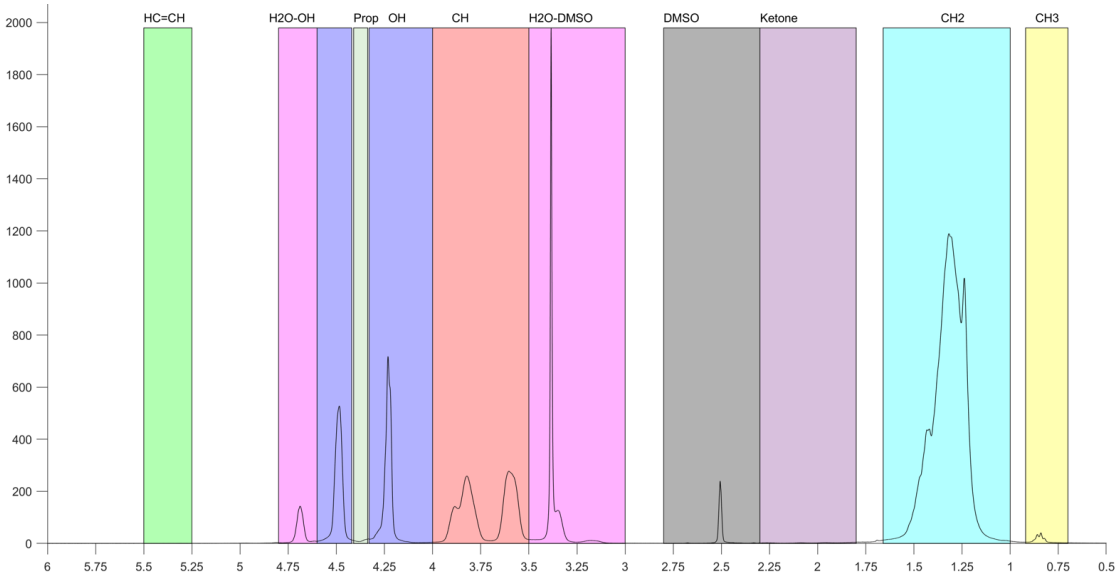

Figure 22: H-NMR of EVOH peak identification

Once the peaks were identified, a normal trapezoidal integration was performed to get the area for each peak. Then the area was divided by the respective number of protons in each functional group. It is important to highlight that the ketone functional group is a special case, as this functionality is going to be detected through the signal of its adjacent CH_2 hydrogen, not the ketone itself. So, extra corrections for this consideration need to be made.

To properly correct the areas and thus find the conversion results, firstly it has to be highlighted the three possible reactions, their products and how each will affect the polymer.

The first reaction is normal dehydration of the polymer chain (Figure 23). In this reaction, for every alcohol that is dehydrated, the polymer chain loses one CH_2 and the four CH_2 protons adjacent to the C=C would be shifted on the NMR spectrum. Thus, in terms of NMR, for every C=C, the CH_2 main peak loses 3 times the area loss of the OH peak (6 times if the areas have not been corrected by the number of hydrogens in the functional group). Additionally, the remaining RCHR and the additional RCHR formed would be shifted, thus reducing the normal RCHR area by an equal amount as the OH area and creating a new vinylic RCHR equal to double the amount of OH loss.

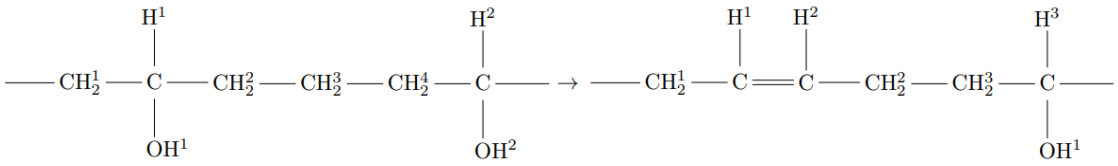

Figure 23: Dehydration of the polymer chain and formation of C=C with counting of functional groups present

The second reaction that could occur is that the double bond created on the dehydration can migrate until an enol is formed. The enol is not favored thermodynamically which will lead to it being converted to a ketone (Figure 24). Thus, the creation of a ketone will entail the loss of two OH groups, the shift of two CH_2 in the NMR spectrum, the creation of a new normal CH_2 and the loss of two RCHR groups. Consequently, for every increase in the ketone area for HNMR, the OH, the RCHR and the CH_2 would decrease by two times the area gained by ketones and the main CH_2 area would increase by the same amount as the ketones due to the creation of a new CH_2, giving a net decrease of the main CH_2 area equal to the amount gained in the ketone area.

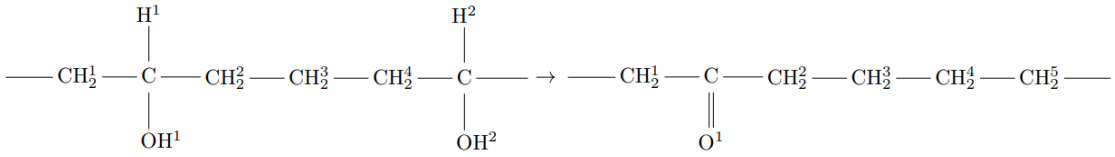

Figure 24: Migration of the C=C bond in the polymer chain and formation of C=O with counting of functional groups present

The last way in which the polymer can react, when alcohol is used as solvent, is through the attachment of the alcohol through ether formation (Figure 25). In this case where 1-proanol was used as the co-solvent, the polymer chain would gain two additional CH_2, one CH_3 but it will lose an OH group. It is important to highlight that from HNMR perspective, one of the gained CH_2 would be shifted, thus it won't contribute to the main CH_2 area. Therefore, for every unit of area loss on the OH by this reaction, the main CH_2 and CH_3 peak will gain one unit while another peak for CH_2 would be formed.

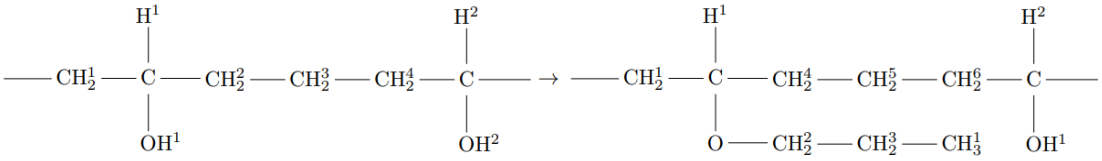

Figure 25: Attachment of alcohol during reaction to form an ether.

Now, based on the products for these reactions, the following corrections can be applied: the initial RCHR concentration for the reacted polymer can be calculated by adding two times the area of the ketone signal and half the area of the vinylic CH to the RCHR.

Once the area for each peak has been found and corrected, comparison between each experiment and the virgin EVOH was performed by taking advantage of functional groups' ratios. As the RCHR group from the virgin polymer and the corrected RCHR group from the reacted

polymer must be equal, the areas of the other functional groups can be translated to represent the intensity of each test and as such it can be used to quantify fractional conversion.

$$\%Conversion = \frac{OH_{Reacted} * \frac{RCHR_{Unreacted}}{RCHR_{Reacted}} - OH_{Unreacted}}{OH_{Unreacted}} * 100$$

Where

$$RCHR_{Unreacted} = Area_{RCHR} + Area_{Ketones} * 2 + \frac{Area_{C=C}}{2}$$

$$Area_{Ketones} = \frac{Area_{Ketones-CH_2}}{4}$$

3.3.5 Parr Reactor

All the reactions in the solvent system were performed in a Parr reactor outlined in Figure 26. The procedure for the experiments began by loading all the reactants into their respective sections: the 20 mL of solvated polymer was loaded into the injection chamber and the catalyst powder was loaded into the main chamber followed by 20 mL of solvent. The solvent added into the reaction chamber changed depending on experimental setup. Once the system was set up, it was flushed by loading 600 psi of N2 and removing it. Then, the system was pressurized to 200 PSI and all the valves were closed. Next, the main chamber was heated to the reaction temperature while stirring at 400 rpm and the injection vessel was also heated to reaction temperature through the use of heating tapes, a thermocouple and a temperature controller. The system was left heating and equilibrating for 1h before three injections with 600 PSI of N2 were performed. The time at which the injections were finalized was considered as the t=0. Once

the reaction time reached the intended value, the reactor was quenched with an ice bath which signaled the end of the reaction.

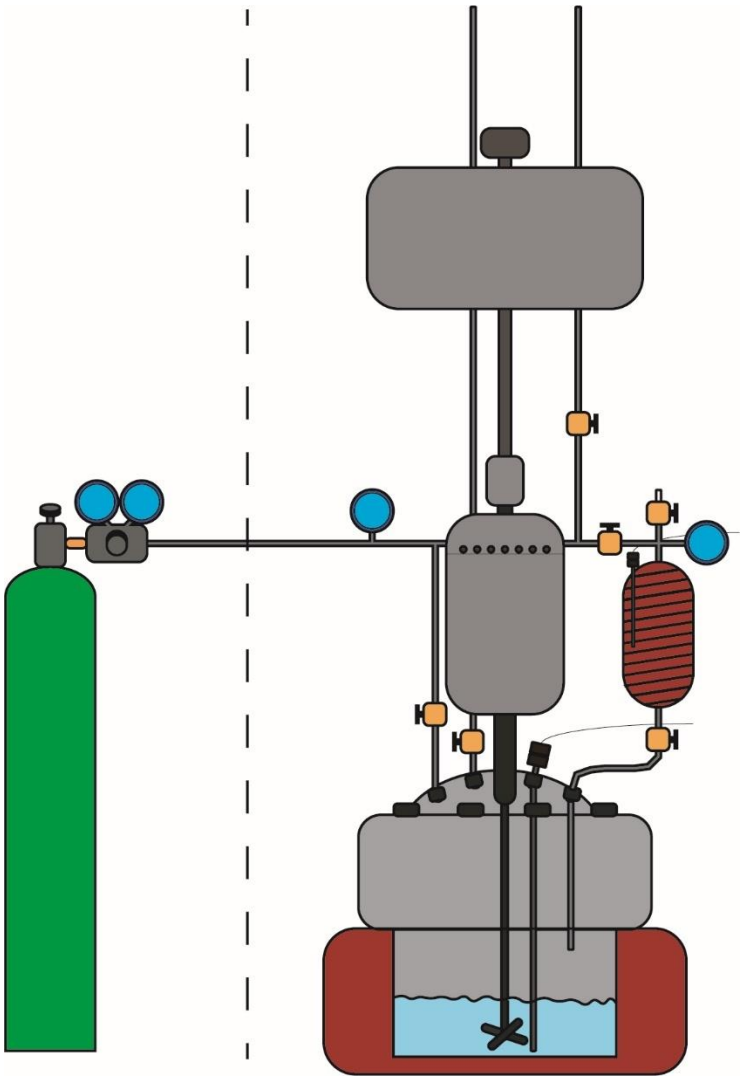

Figure 26: Parr reactor system setup

3.3.6 Solvent and Gas analysis

The gas phase after reaction was analyzed using GCMS loaded with an Agilent 19091P-Q04PT 30m x 320 µm x 20 µm column. The flow was set to 0.79135 mL/min, column inlet pressure

was 0.554 psi, average velocity 32.208 cm/sec and holdup time was 1.5524 min. The oven temperature program began with a 4-minute hold at 37 °C followed by a ramp of 15°C/ min to 200°C where it was held for 60 minutes. The split inlet was set to 250°C with a split ratio of 20:1. The MS was set to analyze from 3 to 110 m/e.

The liquid phase, specifically the final amount of water, was analyzed using a Karl Fisher titrator loaded with Hydranal medium K (Cat. 34698-1L-US) and Hydranal Nextgen Composite 5 SC (Cat. 34805-1L-SC). An injection with 10 µL was made for each run. Three runs were made for averaging and statistical significance.

3.4 Results and Discussion

3.4.1 DMSO

DMSO was chosen as one of the promising candidate solvents due to its excellent solvation effects on EVOH[3,25,85]. Experiments with different catalysts such as ZSM5 SAR 140, ZSM5-22 (TON), Beta SAR 180, and Beta SAR 19 were done to study the reaction viability. Only zeolite beta SAR 19 showed some reactivity when the reaction was carried out at 190°C with loading of 13% catalyst with respect to the polymer mass, though with a small rate. It was calculated that the rate for this reaction was about 0.16% conversion per hour (Figure 27 and Figure 28). This low rate could be due to DMSO competing for acid sites by forming hydrogen bonds with the acidic protons on the catalyst surface or DMSO could affect certain transition steps which could inhibit the reaction, both behaviors have already been reported in the literature for other reactions[86]. Thus, use of DMSO as solvent for the catalytic dehydration of EVOH does not seem viable for this set of zeolite catalysts.

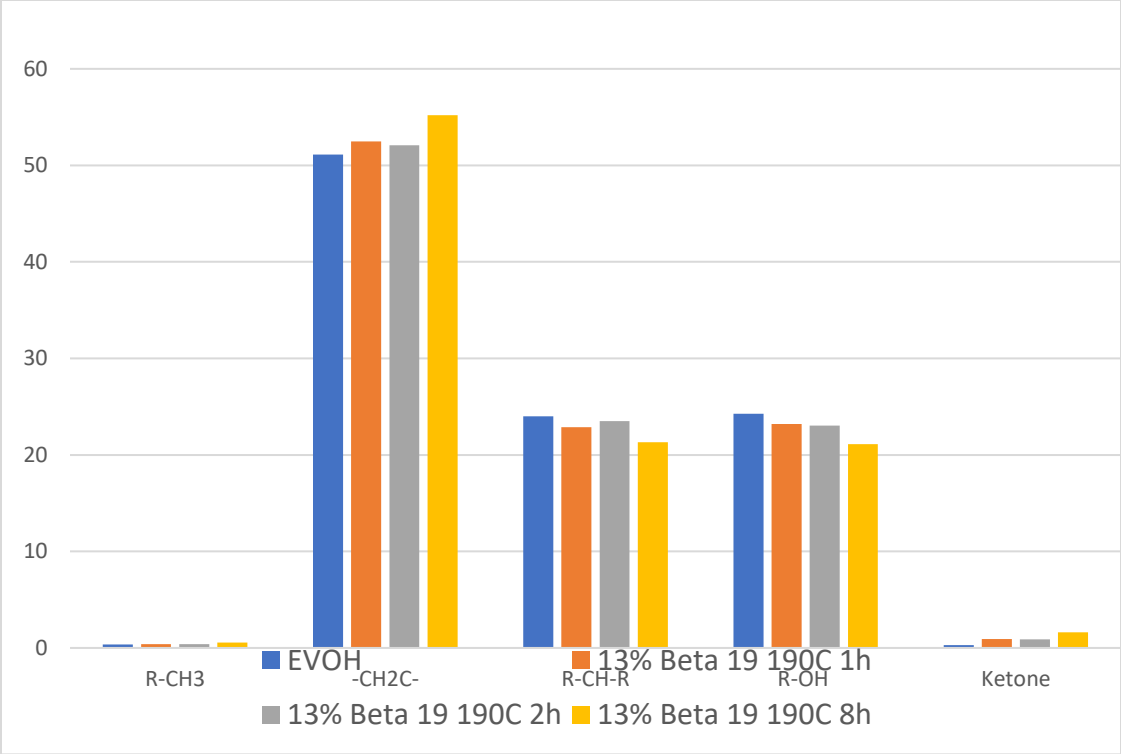

Figure 27: NMR results for dehydrated EVOH in DMSO using Beta SAR 19

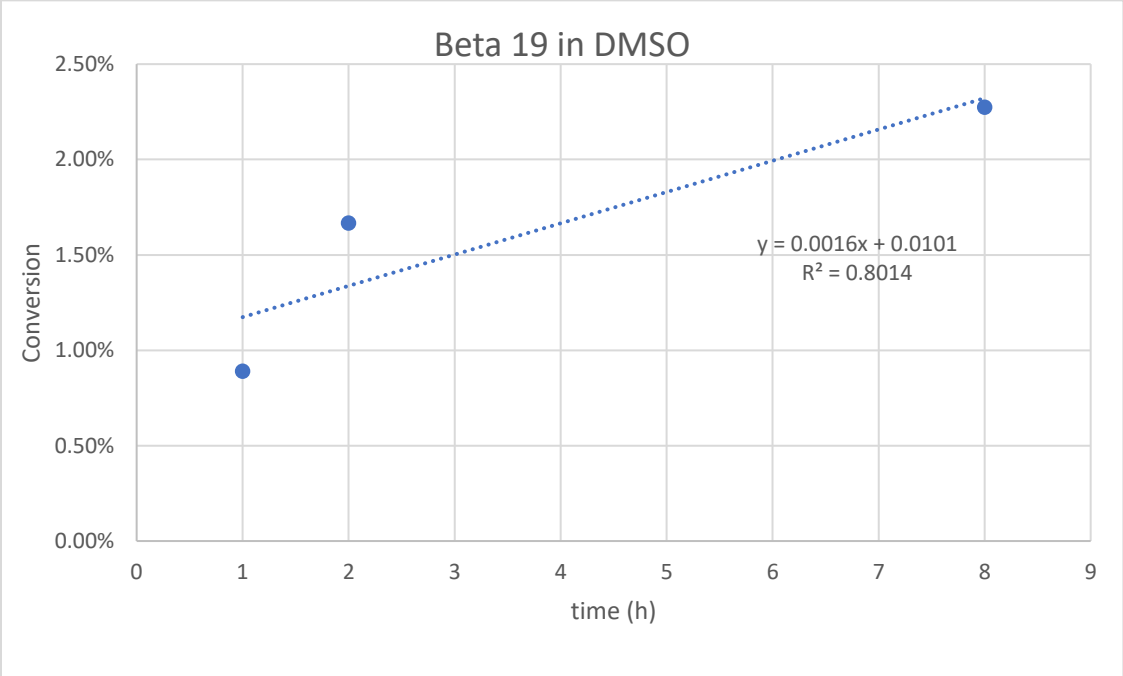

Figure 28: Conversion vs time achieve by Beta SAR 19 in DMSO

3.4.2 Propanol and water

Another promising solvent that could be used is a mixture of water and alcohol. It has been shown that the combination of water and alcohol could allow the dissolution of EVOH when stirred and heated[87]. This system would hopefully reduce the inhibition behavior observed with DMSO while also allowing other types of chemistry to occur, specifically the addition of alcohol through the formation of an ether. This could, in theory, open a new path to modify the functional groups of the polymer, thus allowing compatibilization by choosing the alcohol structure.

For this study, a water/1-propanol mixture was prepared as the solvent of choice. Once the solvent of choice has been selected, the next question would be what are the ideal proportions between 1-propanol and water for the catalytic dehydration of EVOH. To address this question several experiments with zeolites ZSM5 140, Beta 180, ASA, Y 40, Y2.6 and Beta 19 were made. While all these catalysts showed some conversion on FTIR and DSC results, only Beta 19 showed measurable catalytic activity on NMR results. Therefore, Beta 19 was used as the main catalyst for this exploration. In Figure 29, it can be seen that water seems to detrimentally affect the rates, showing significant activity once the water proportions go below 25% of the total amount of the solvent (Figure 29 and Figure 30).

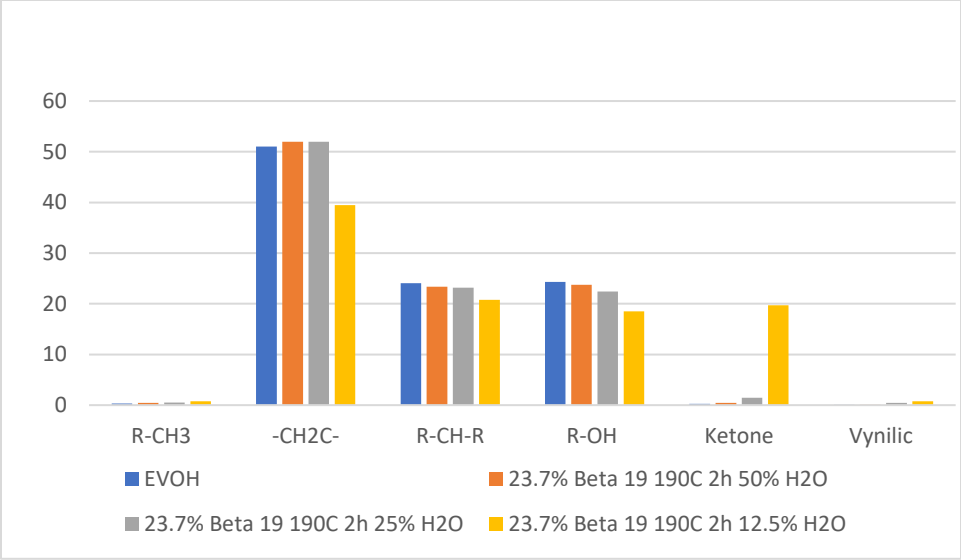

Figure 29: NMR results for catalytic dehydration of EVOH using Beta 19 with 2 hour reaction at 190C using various solvent combinations

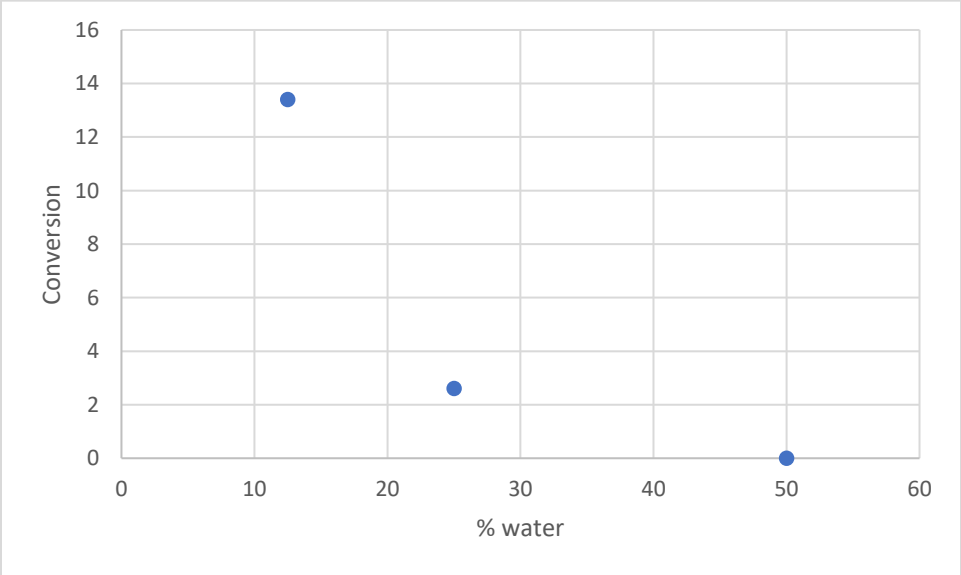

Figure 30: Conversion vs water loading for zeolite Beta 19 with 23.7% loading at 190 C for 2 h

DSC results supported this trend by showing decreasing melting point temperature as the proportion of water was decreased until 12.5% water loading was achieved. Once the water proportion went below the 12.5% threshold, the final melting point started to increase again (Figure 31). This suggest the highest rate is achieved when the water is between 10% and 25%.

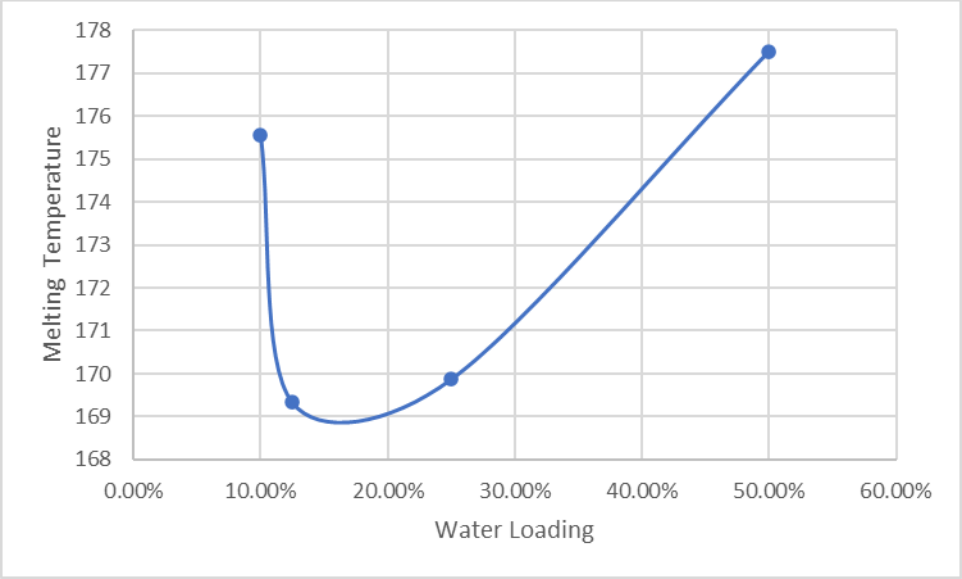

Figure 31: DSC results measuring the melting temperature for reacted plastic at different water to 1-propanol ratios. The melting point for virgin EVOH is 183.9 °C.

Following these results, experiments were conducted with 12.5% water. Several experiments with beta 19 were performed in which the catalyst loading, the reaction time and the temperature were varied. NMR results obtained when the catalyst loading was below 23.7 mass% and the temperature below 190C indicated that no reaction happened. Nevertheless, these measurements were not consistent with results obtained in DSC and FTIR where evidence of some reaction is observed. This inconsistency can be clearly seen on Figure 32 where catalyst loadings of 6.6% do show some decrease in the OH functionality, though not as much as 23.7%, but NMR measurements for such samples did not show any modification of the polymer.

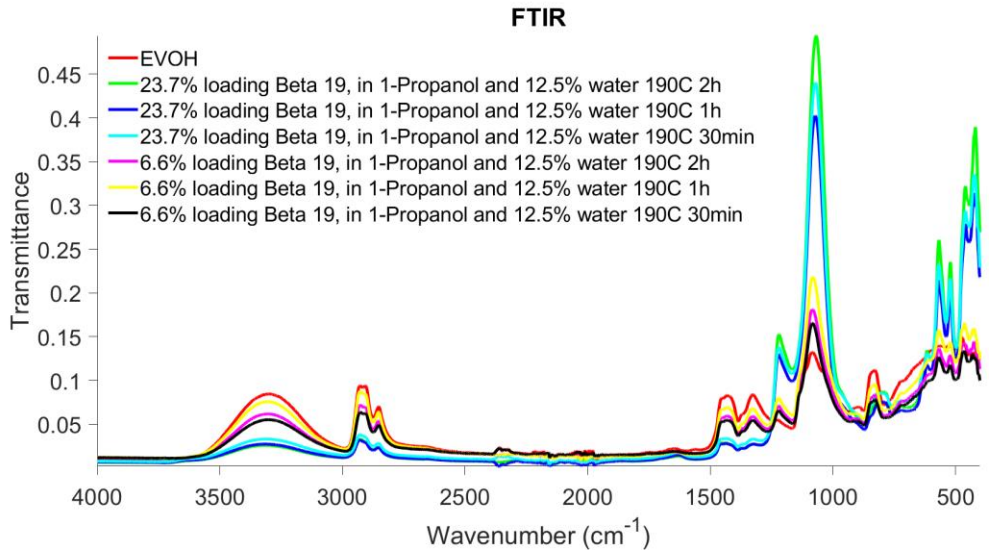

Figure 32: FTIR measurements for catalyst with different loadings and time for beta 19 in a water propanol mixture

Now, if the focus is drawn to the results obtained from a single set of experiments on FTIR, it can be seen that even though there is a clear reduction of the OH groups once a catalyst is introduced into the system, the change of such decrease is not as evident with time which implies a fast initial rate of reaction followed by deactivation (Figure 33). Thus, lower times or characterization with higher sensitivity would be required for proper analysis of the rates.

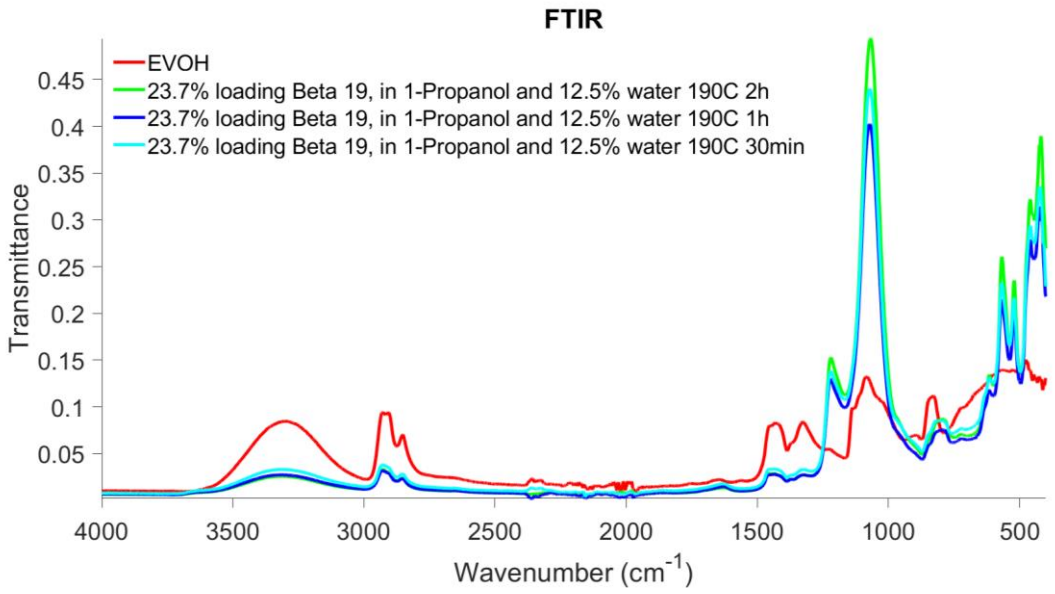

Figure 33: FTIR measurements comparing EVOH and the samples from the reaction of 23.7% loading of Beta 19 in a water propanol mixture for 2 hours, 1 hour and 30 minutes at 190C

While these inconsistencies were present, analysis of the NMR results that showed reactivity were still performed, and conversion was calculated. These results did show some conversion dependence in time as can be seen on Figure 34, Figure 35 and Figure 36, but the validity of such results are still in question due to the inconsistencies previously outlined.

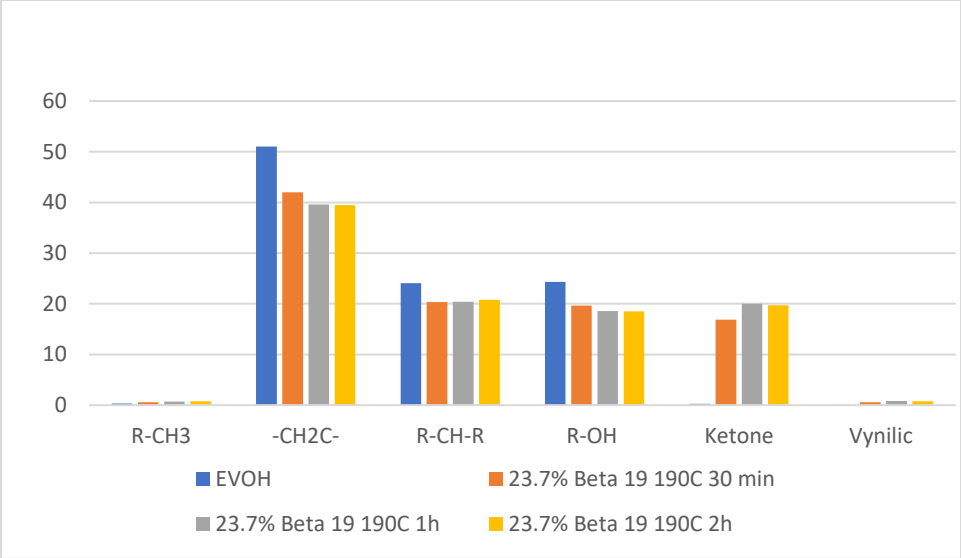

Figure 34: HNMR results for the reaction of 23.7% loading of Beta 19 in a water propanol mixture at different times and at 190C

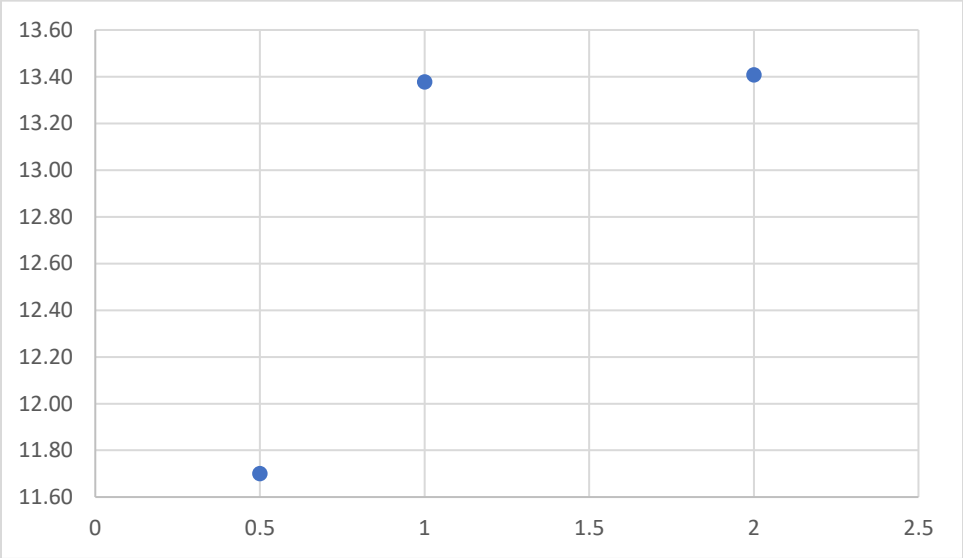

Figure 35: Conversions calculated from HNMR results for the reaction of 23.7% loading of Beta 19 in a water propanol mixture at different times and at 190C

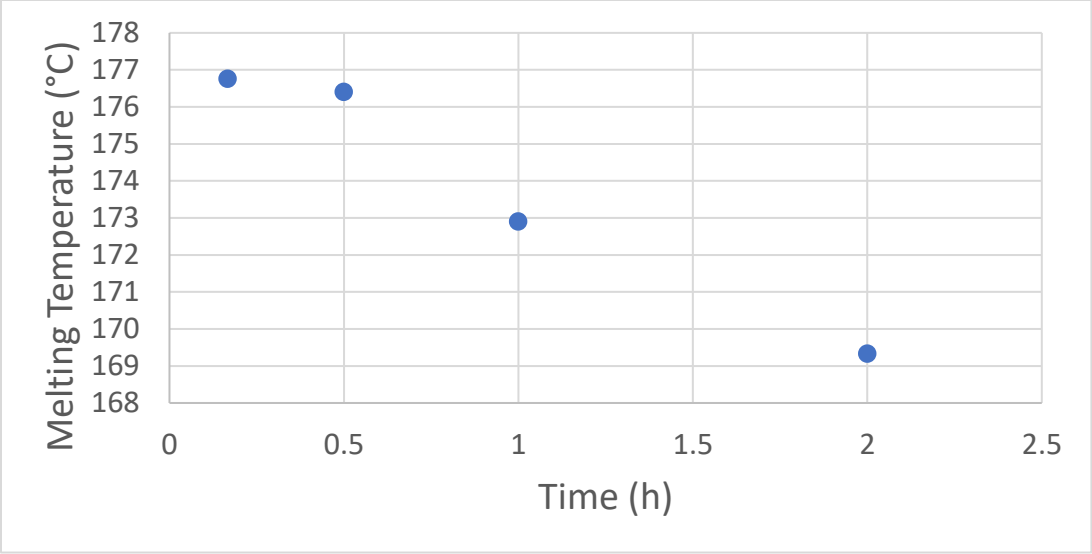

Figure 36: Melting temperatures for the reaction of 23.7% loading of Beta 19 in a water propanol mixture at different times and at 190C

Unfortunately, these inconsistencies are not limited to the previously shown results. For example, when a catalyst loading of 13% of Beta 19 was used, FTIR and DSC showed reduction of the OH peaks and the melting point which are clear indication of conversion (Figure 37 and Figure 38). Nevertheless, liquid HNMR indicated no conversion. This raises the question of why FTIR and DSC can detect the change in characteristic of the polymer while liquid NMR cannot.

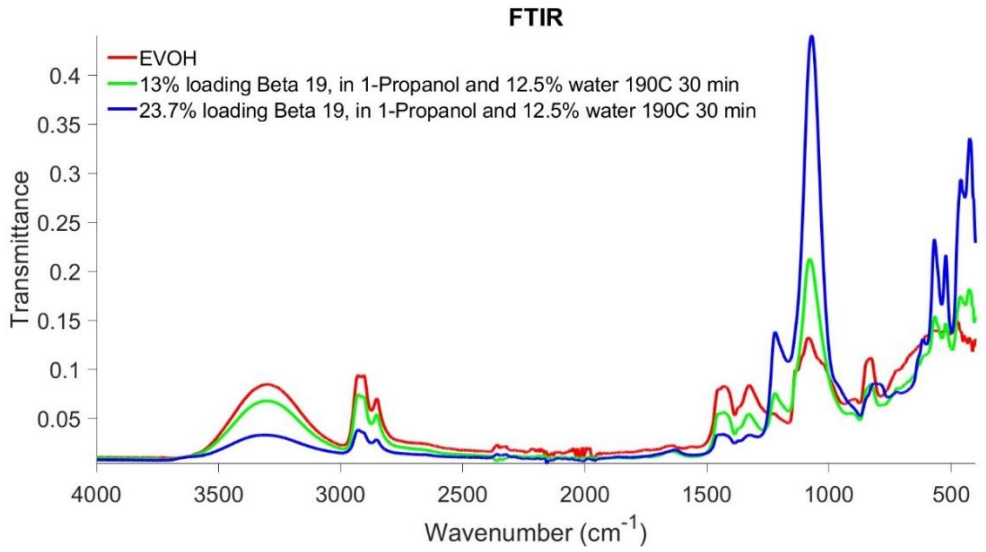

Figure 37: FTIR results showing a comparison of the plastic after catalytic conversion with 13% and 23.7% loadings, same reaction times, solvent proportions and temperature .

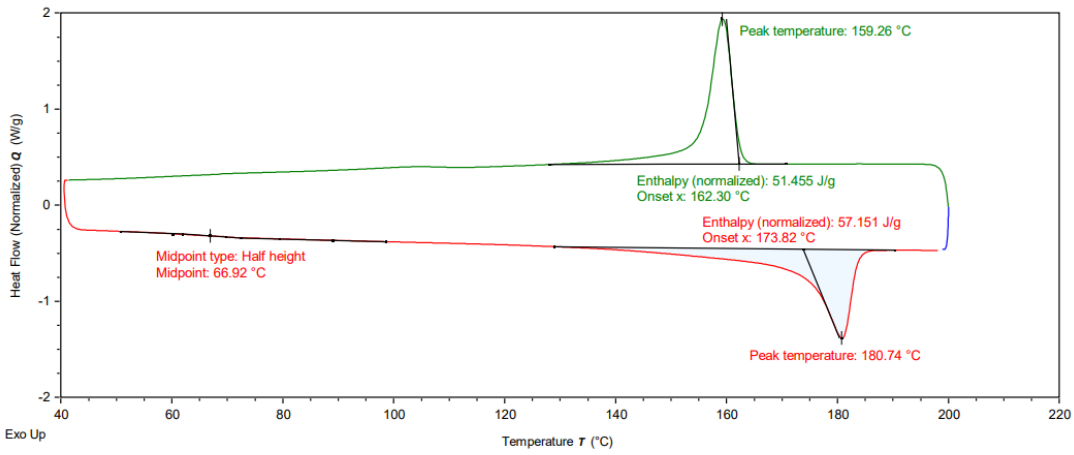

Figure 38: DSC results for catalytic conversion of EVOH with 13% loading of Beta 19 at 30 min reaction time and 190C, showing a decrease in melting temperature of 3 degrees.

It is hypothesized that the inconsistency in results may be due to sampling inconsistencies caused by polymer product heterogeneity. In the DSC plot (Figure 39) for the 2-hour reaction at 190C with 23.7% loading of Beta 19, it can be seen that not only the melting point for the plastic reduces from 183 C to 169 C, but also that there is a second peak which corresponds to the melting point of unreacted polymer. This implies that the conversion of the polymer does not

happen uniformly, but instead certain chains, or portions of chains, may be converted while others are not, creating heterogeneities and thus making the sampling difficult when only small quantities of the material can be used such as in NMR measurements. To mitigate this issue, cryomilling of the final sample was done prior to analysis to improve the random sampling and thus increase the likeliness of getting a representative sample. Nevertheless, even with this method, results are not consistent, such as the case previously outlined where DSC (Figure 39) and FTIR (Figure 33) results showed clear conversions, but two different random samples taken from the same cryomilled reacted polymer in NMR show in one case a conversion of 13% but no conversion in the other case. These results highlight the difficulty of accurately quantifying the fractional conversion. Another issue that was found during the analysis, specifically for NMR, was that the polymer did not dissolve entirely in the deuterated solvent, even at low sample loadings, which could directly affect the quantification and proper representation that this tool could provide for these results. To try to circumvent this issue, other deuterated solvents were tried, but with no success.

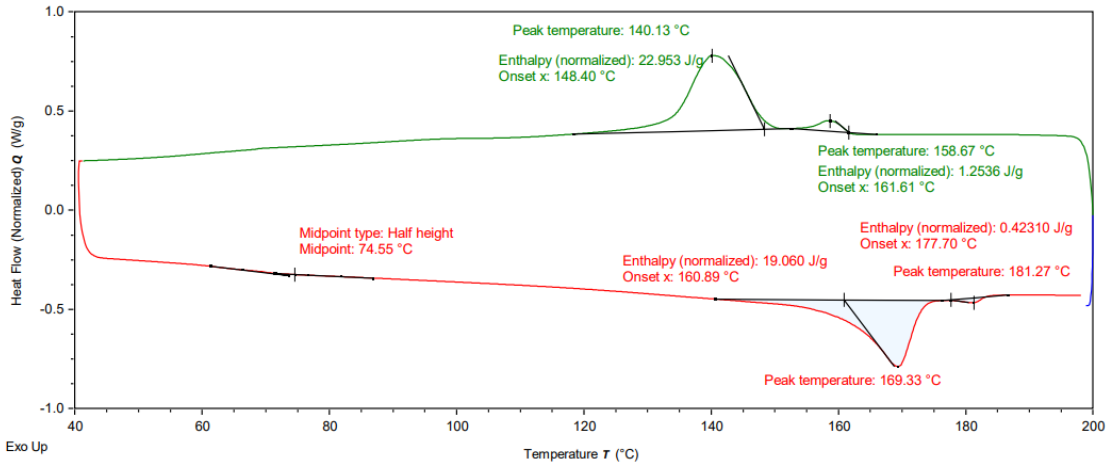

Figure 39: DSC measurements for the reaction of 23.7% loading of Beta 19 in a water propanol mixture for 2 hours at 190C

3.5 Conclusion

In conclusion, the study investigated the catalytic dehydration of EVOH using different solvents and catalysts. Initially, DMSO was chosen as a solvent, but it showed limited reactivity with the different zeolites tested. This could be attributed to DMSO competing for acid sites on the catalyst surface or affecting certain transition steps, inhibiting the reaction.

To explore alternative solvents, a combination of water and propanol was investigated. It was found that this solvent system allowed for the dissolution of EVOH and showed potential for additional chemistry, such as the addition of alcohol through the formation of an ether. Zeolite beta 19 exhibited the most significant activity among the catalysts tested in this solvent system.

However, the presence of water had a detrimental effect on the reaction rates, except at low proportions. Further experiments show that maximum rates were obtained when the water loading was set to 12.5% for the tested proportions. Thus, consequent experiments were performed using a 12.5% loading of water, which resulted in successful conversion of some of the hydroxyl groups to mainly ketones.

The analysis of the results was challenging due to sampling inconsistencies and difficulties in quantifying the conversion of the polymer as a whole. Cryomilling was employed to improve random sampling, but inconsistent results were still obtained, indicating the presence of heterogeneities withing the final polymer sample. DSC results and FTIR further confirmed the presence of heterogeneities and emphasized the need to develop a methodology to get representative samples for the measurements.

Overall, the study suggests that the use of DMSO as a solvent for the catalytic dehydration of EVOH with the tested zeolite catalysts is not viable. However, a water-propanol mixture shows promise, although further development of sampling techniques are require to get an accurate characterization of the polymer and thus elucidate the mechanism and limitations for such reaction.

Chapter 4: Conclusions and future work

4.1 Overall Conclusions

In conclusion, the study provides valuable insights into the role of acid site density, pore size, and solvent selection in the catalytic dehydration of Poly (vinyl alcohol-co-ethylene) (EVOH) using zeolite catalysts.

Regarding acid site density and pore size, the first set of experiments showed that catalysts with lower acid site densities and larger pores exhibited higher maximum rates and better activity retention after deactivation. This suggests that catalysts with higher loadings and lower acid site densities perform better due to enhanced mass transfer facilitated by additional available pores for diffusion. In the second set of experiments, zeolites with higher acid site densities consistently showed higher maximum rates, but when normalized per acid site, low acid site density zeolites outperformed their counterparts, emphasizing the importance of larger pores in achieving higher maximum rates per acid site. Additionally, the study highlighted the significance of external active sites, as the removal of these sites led to a significant decrease in the maximum achievable rate and faster catalyst deactivation, underscoring the crucial role of external active sites in the polymer dehydration reaction.

The investigation of solvents revealed that DMSO exhibited limited reactivity with the tested zeolite catalysts, possibly due to competition for acid sites or inhibition of certain transition steps. However, a water-propanol mixture was found to not only be capable of dissolving EVOH effectively but also offered better activity and potential for additional chemistry, such as the formation of ethers through the addition of alcohol. Nevertheless, the proportions

between water and 1-propanol showed to be of significant importance on the performance of the catalyst. The presence of water negatively affected the reaction rates, except in low proportions. Further experiments determined that a 12.5% water loading resulted in maximum rates, leading to successful conversions of hydroxyl groups to ketones.

The study encountered challenges in analyzing the results, including sampling inconsistencies and difficulties in quantifying polymer conversion. Cryomilling was employed to improve random sampling, but heterogeneities within the final polymer sample persisted. DSC and FTIR analyses further confirmed the presence of heterogeneities and emphasized the need for a methodology to obtain representative samples for accurate measurements.

In summary, the study suggests that considering acid site density and pore size is crucial when selecting zeolite catalysts for catalytic polymer dehydration. Lower acid site densities and larger pores enhance mass transfer and improve catalytic activity, while external active sites significantly contribute to the overall reaction rate. The use of DMSO as a solvent may not be economically viable, but a water-propanol mixture shows promise. However, further development of sampling techniques is necessary to accurately characterize the polymer and understand the mechanism and limitations of the reaction.

4.2 Recommendations for future work

To gain a more detailed understanding of bigger pore size zeolites and catalysts, it is important to conduct further exploration. This can be achieved by exploring additional zeolite frameworks and amorphous catalysts with different ranges of mesopores. Additionally, investigating the role of external acids in the performance of bigger pore catalysts, such as through the use of silicalite layered zeolites like FAU@Si, would be beneficial.

Another crucial area for development is the characterization of the polymer itself after the reaction. Liquid NMR analysis has demonstrated limitations for polymer characterization due to changes in solubility brought about by the reactions. Therefore, it is recommended to utilize solid NMR for polymer characterization. Furthermore, the presence of inherited heterogeneities in the reacted polymer necessitates the use of higher sample percentages during characterization to minimize the analysis of biased samples.

Finally, the implementation of a twin-screw extruder could help alleviate potential limitations in external mass transfer and diffusion of catalyst particles between phases after the reaction has occurred. Thus, allowing for the exploration of the reactions process in a more realistic setup that can be easily transferred to industrial applications.

Appendix

Raw TGA Data

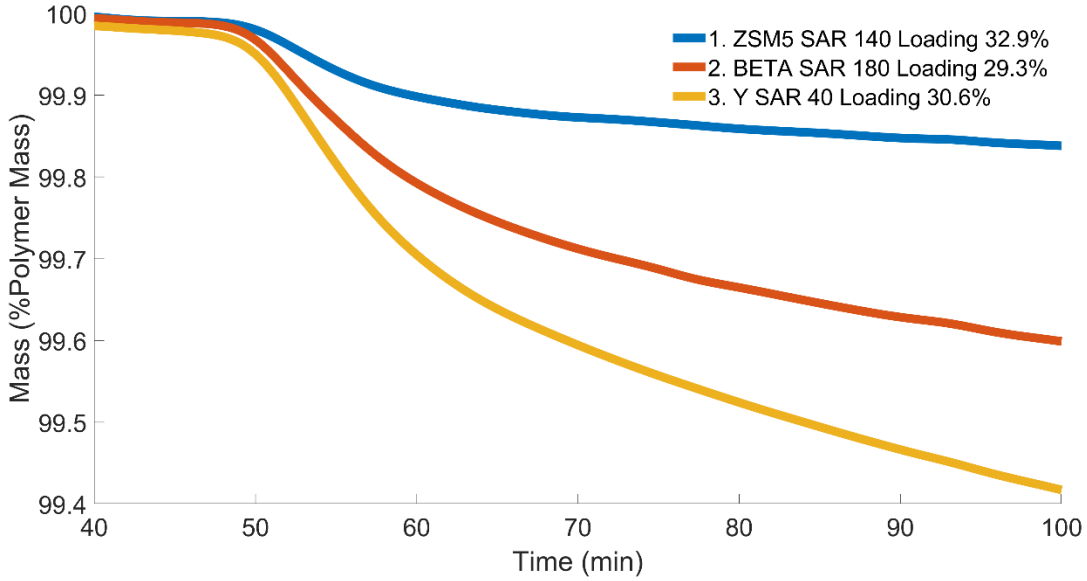

Figure 40: Zeolite framework comparison (pore comparison) with relatively similar acid site density, while keeping the acid site to polymer ratio equal to $0.0349 \frac{mM\ Acid}{g\ Plastic}$

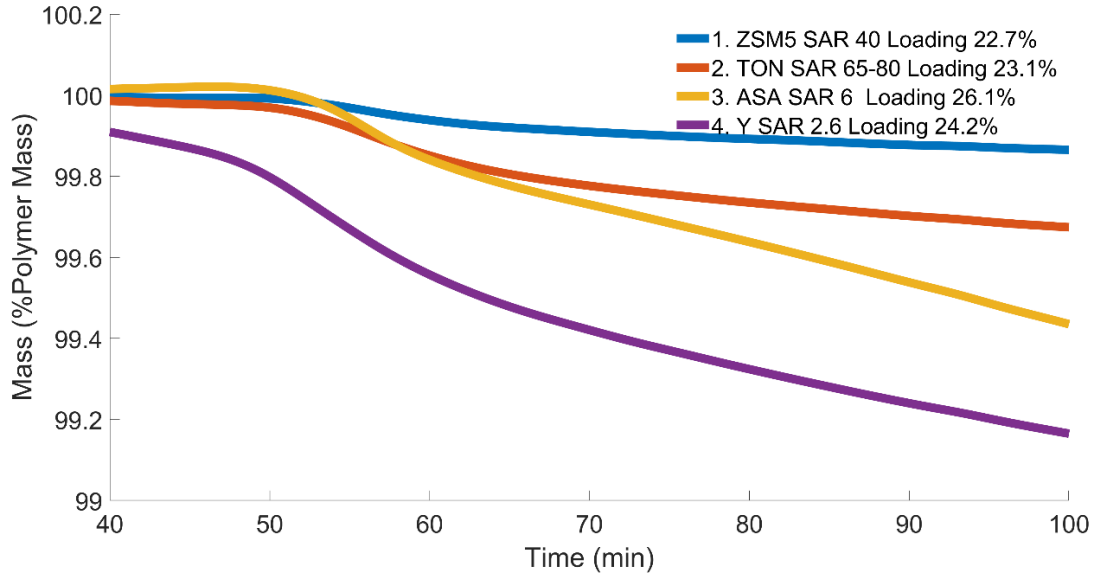

Figure 41: Zeolite framework comparison (pore comparison) with relatively similar acid site density, while keeping the acid site to polymer ratio equal to $0.08862 \frac{mM\ Acid}{g\ Plastic}$

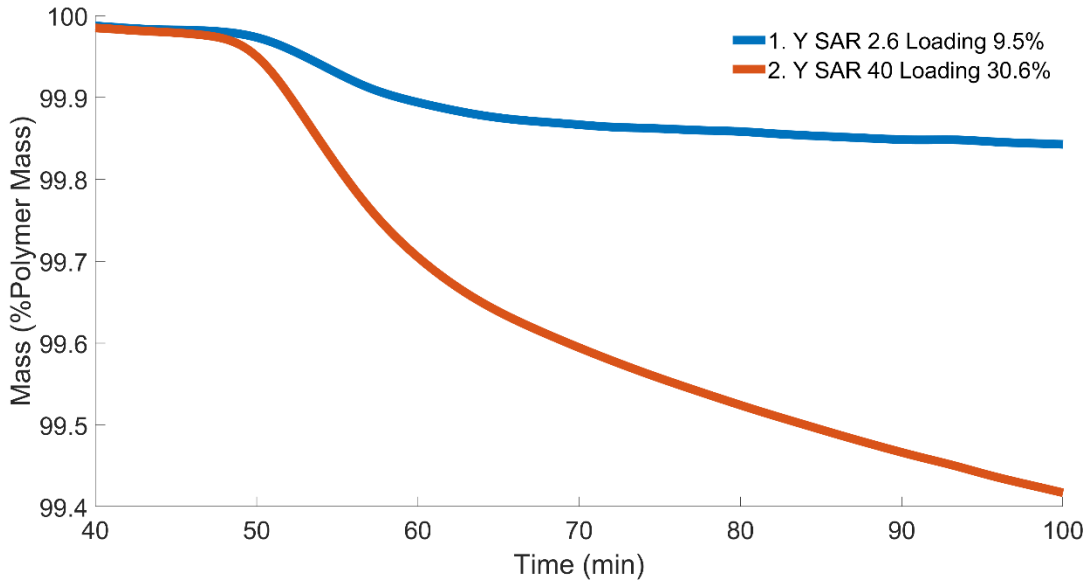

Figure 42: Y comparison holding the same acid site concentration

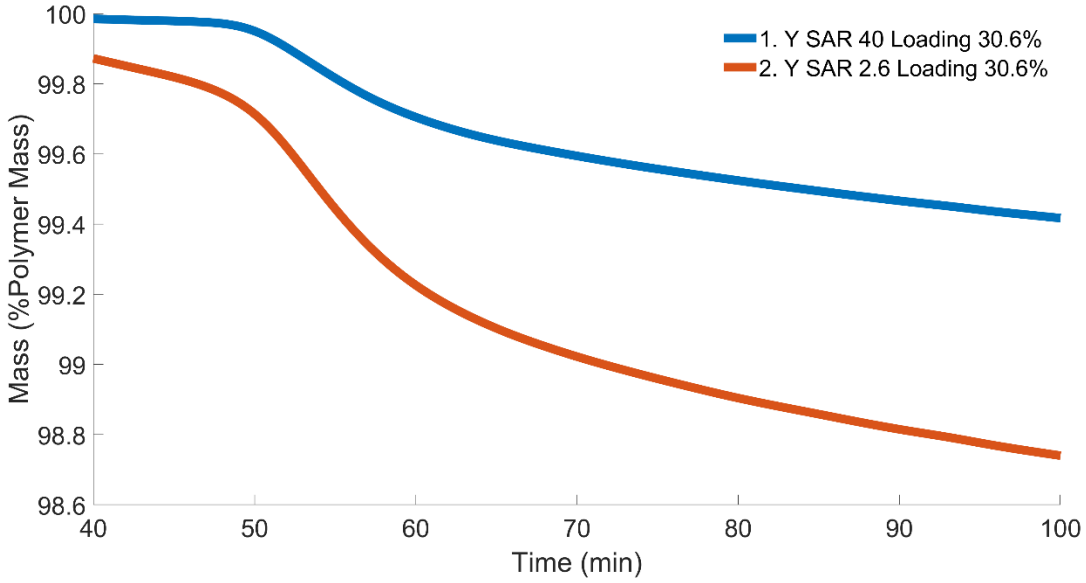

Figure 43: Y comparison holding the amount of catalyst loading constant

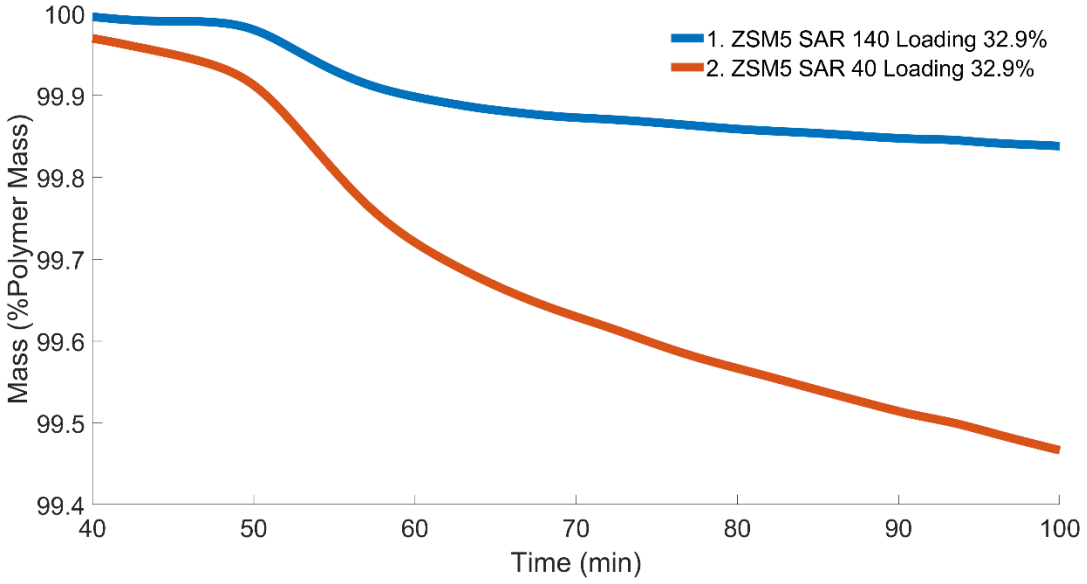

Figure 44: ZSM5 comparison holding the amount of catalyst loading constant

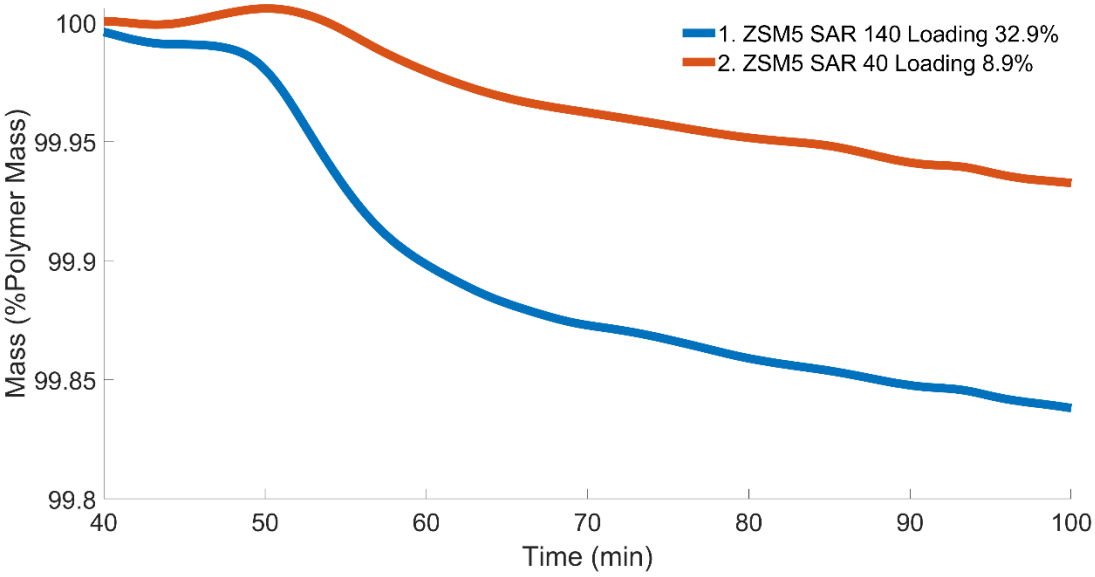

Figure 45: ZSM5 comparison holding the same acid site concentration

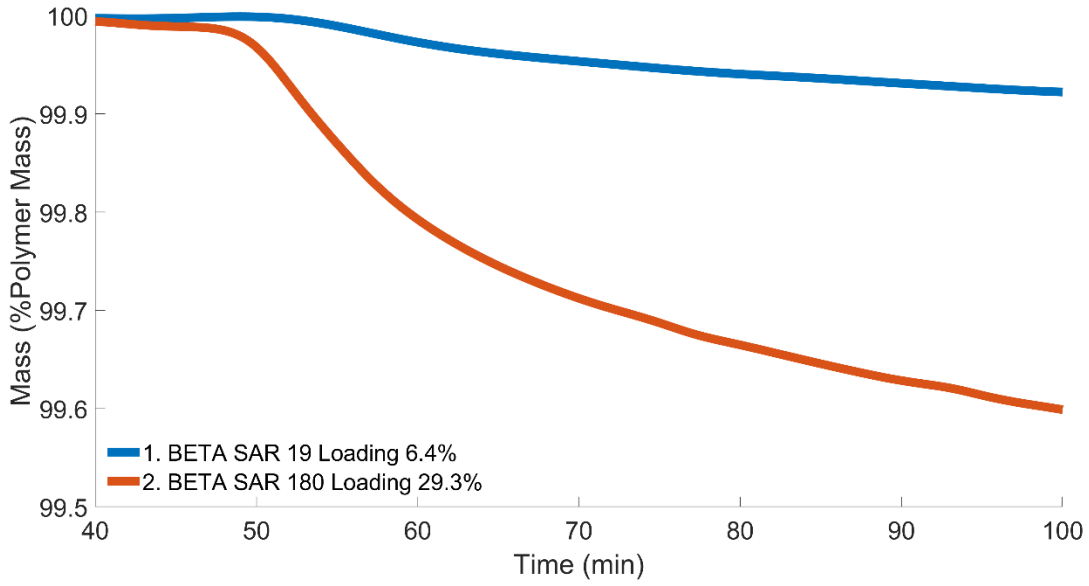

Figure 46: Beta comparison holding the same acid site concentration

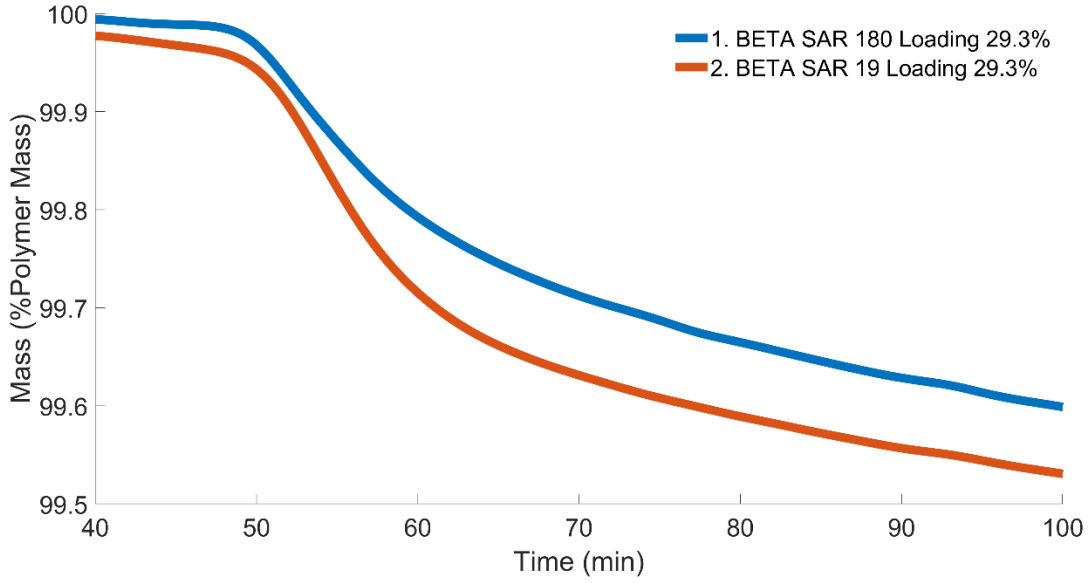

Figure 47: Beta comparison holding the amount of catalyst loading constant

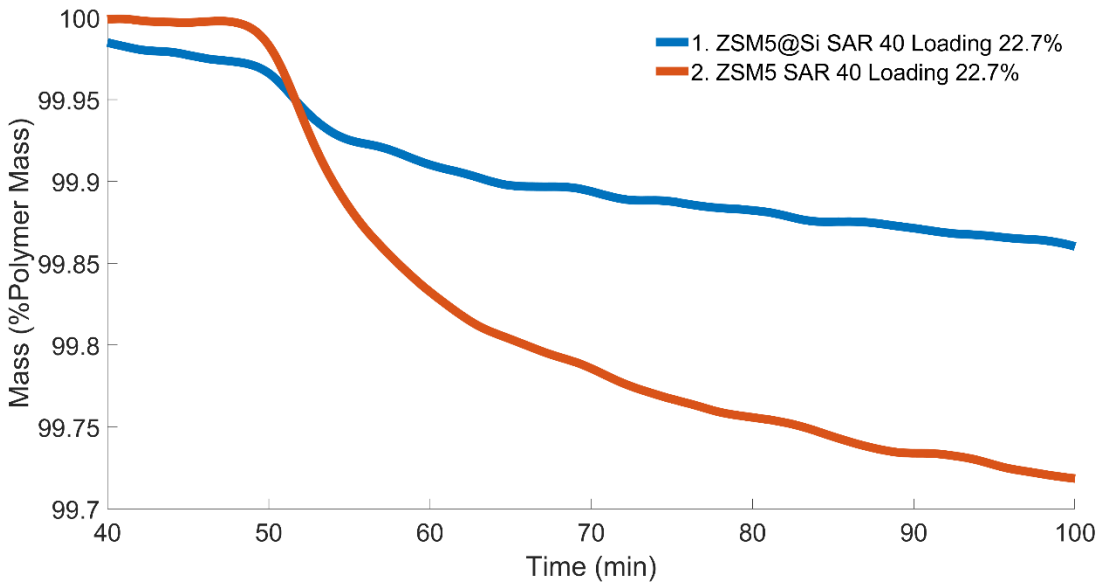

Figure 48: Role of external active sites in ZSM5 zeolite

Raw Data DSC

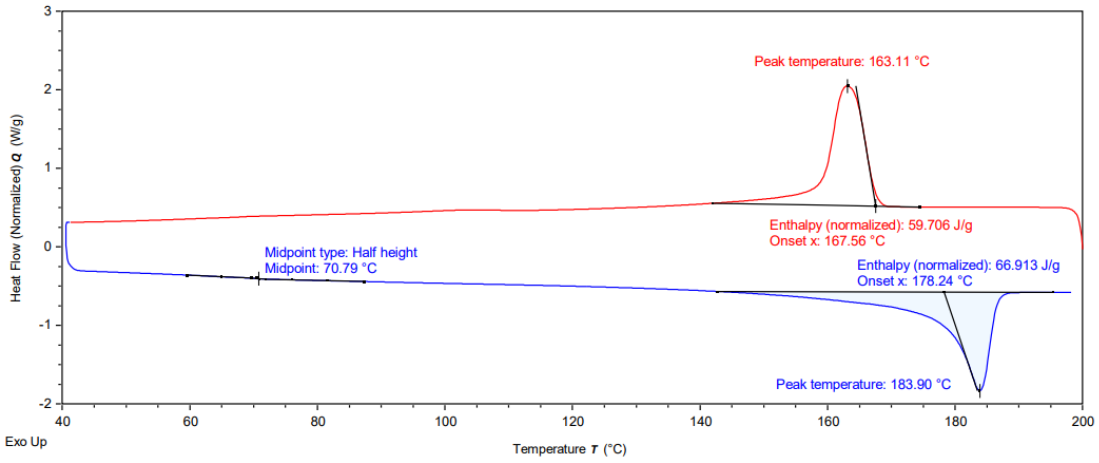

Figure 49: DSC for EVOH

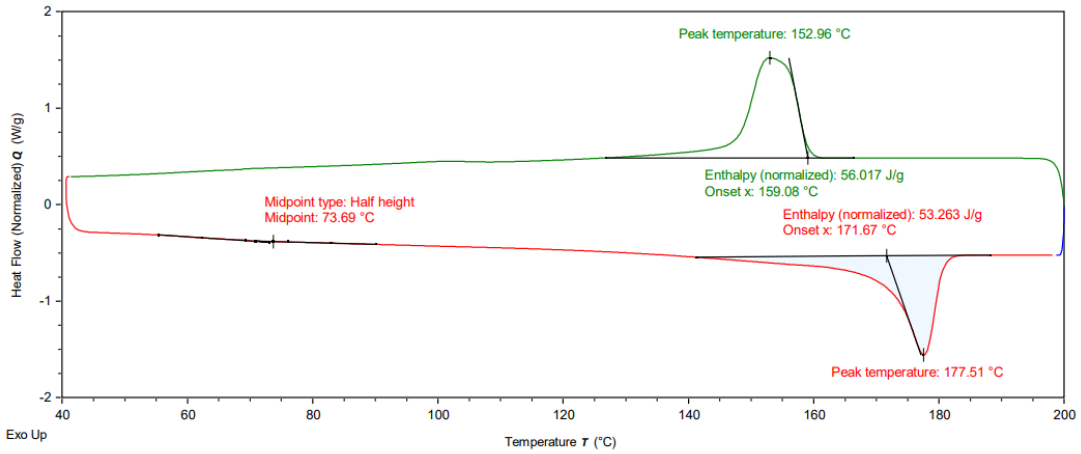

Figure 50: DSC for 50% Water Loading

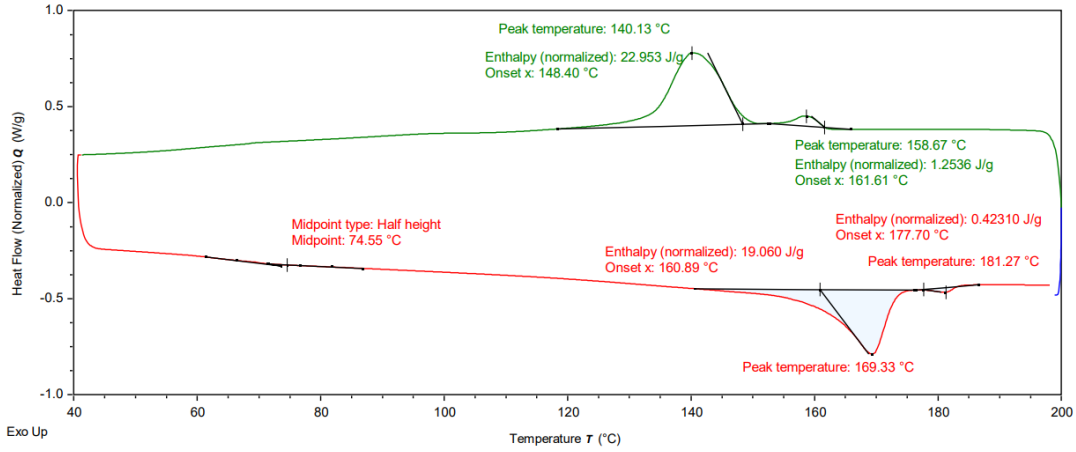

Figure 51: DSC for 12.5% Water Loading

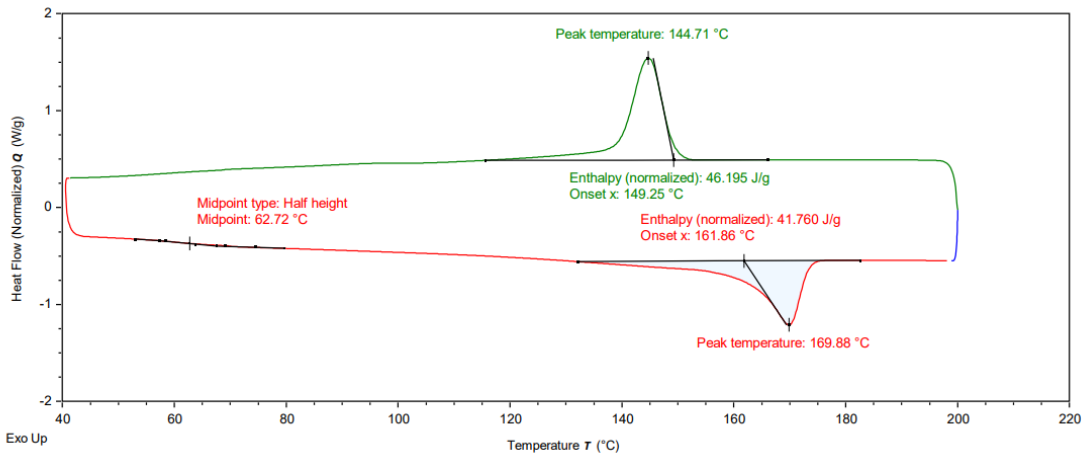

Figure 52: DSC for 25% Water Loading

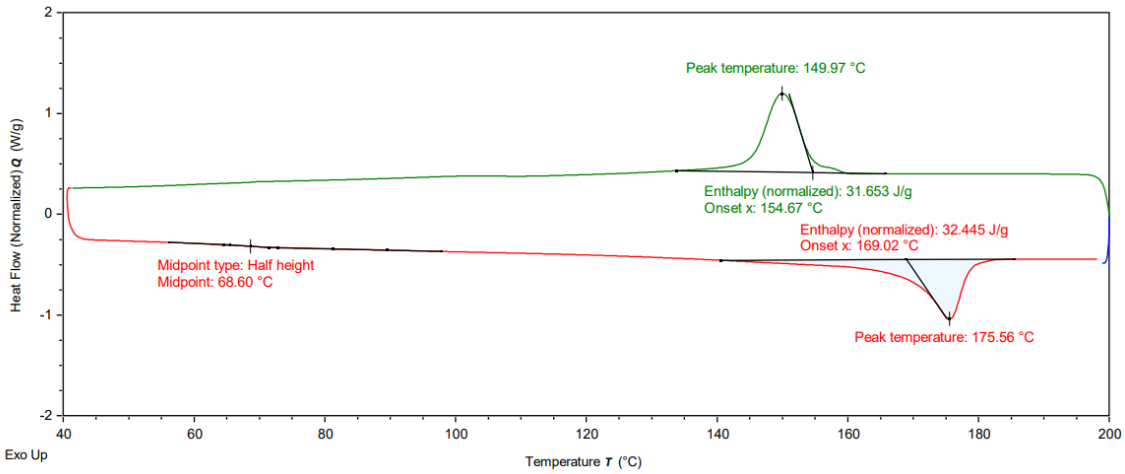

Figure 53: DSC for 10% Water Loading

Raw Data NMR

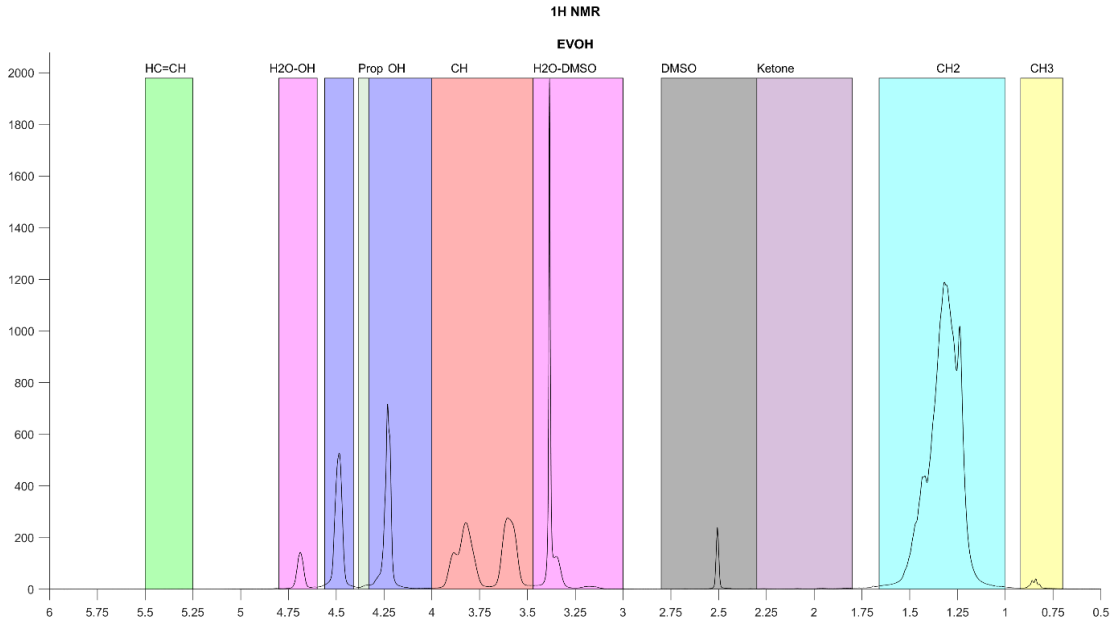

Figure 54: Hydrogen NMR for EVOH

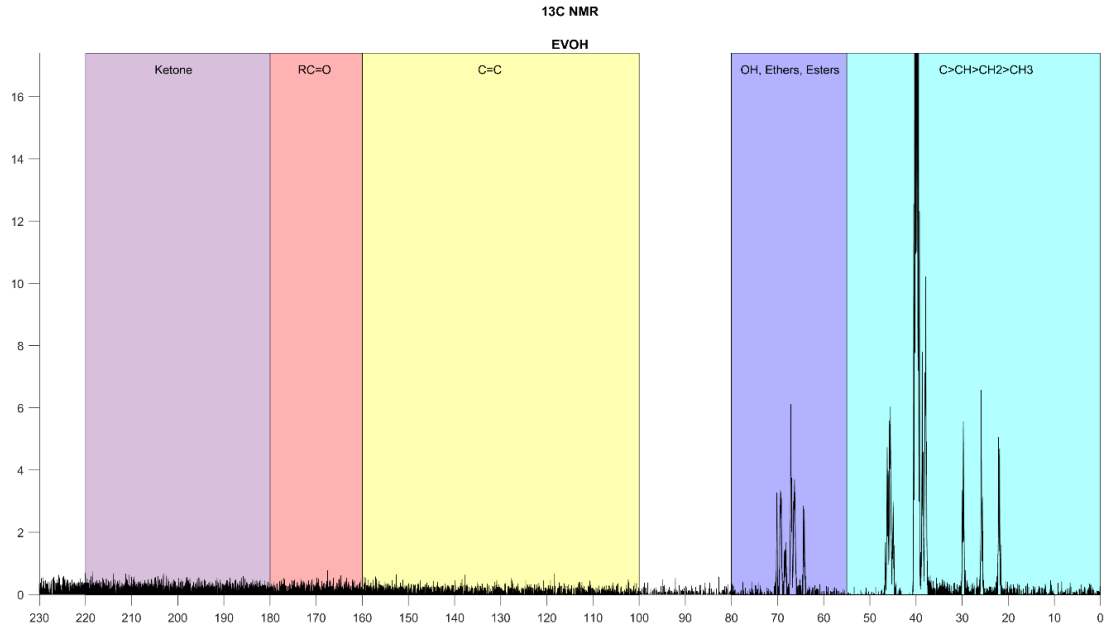

Figure 55: Carbon NMR for EVOH

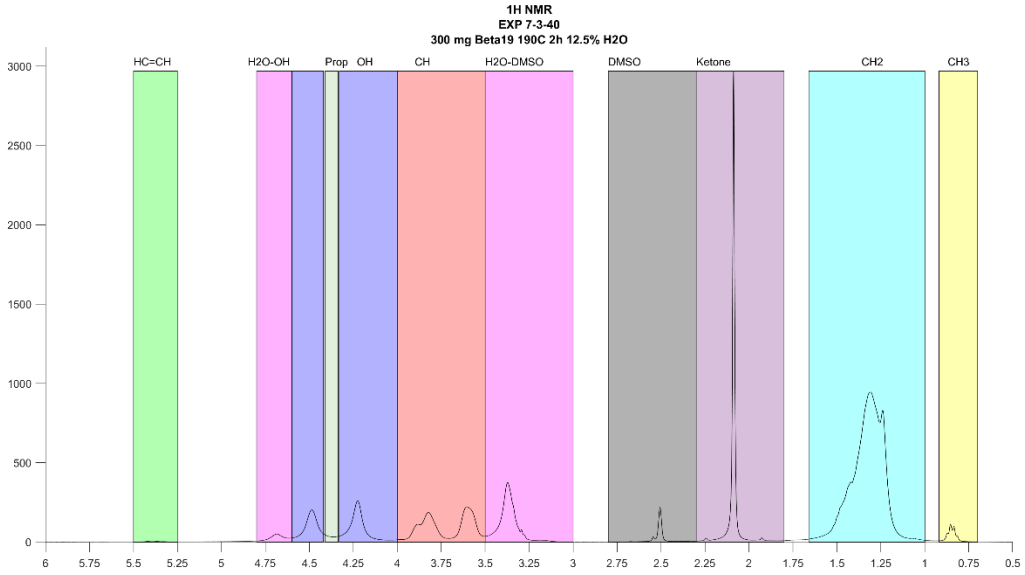

Figure 56: Hydrogen NMR for Reacted EVOH while taking a 30mg sample of the total plastic for characterization. Reaction was done with a 23.7% loading of beta 19 for 2 hours at 190C at 12.5% H2O.

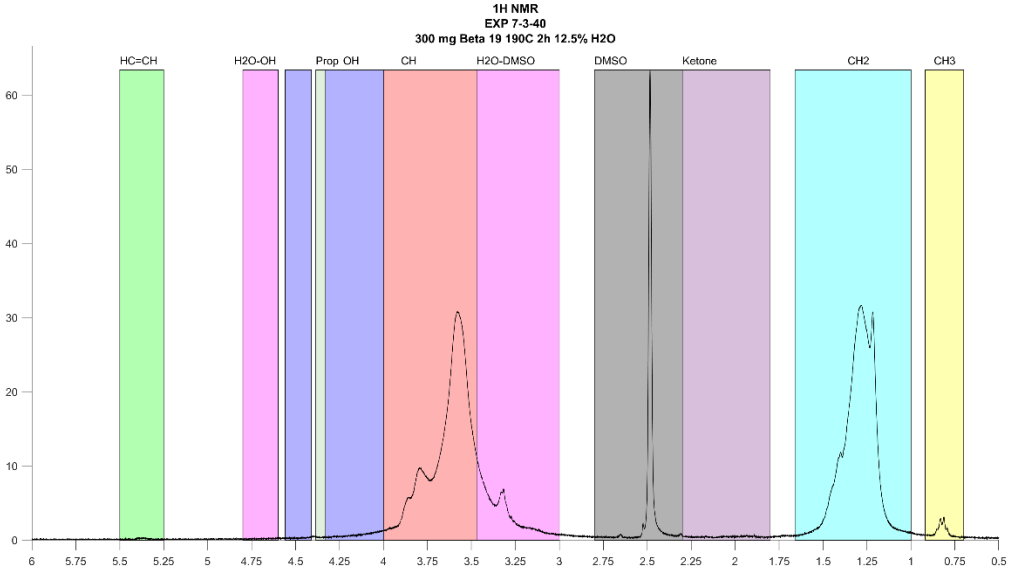

Figure 57: Hydrogen NMR for Reacted EVOH while taking a 5mg sample of the total plastic for characterization. Reaction was done with a 23.7% loading of beta 19 for 2 hours at 190C at 12.5% H2O.

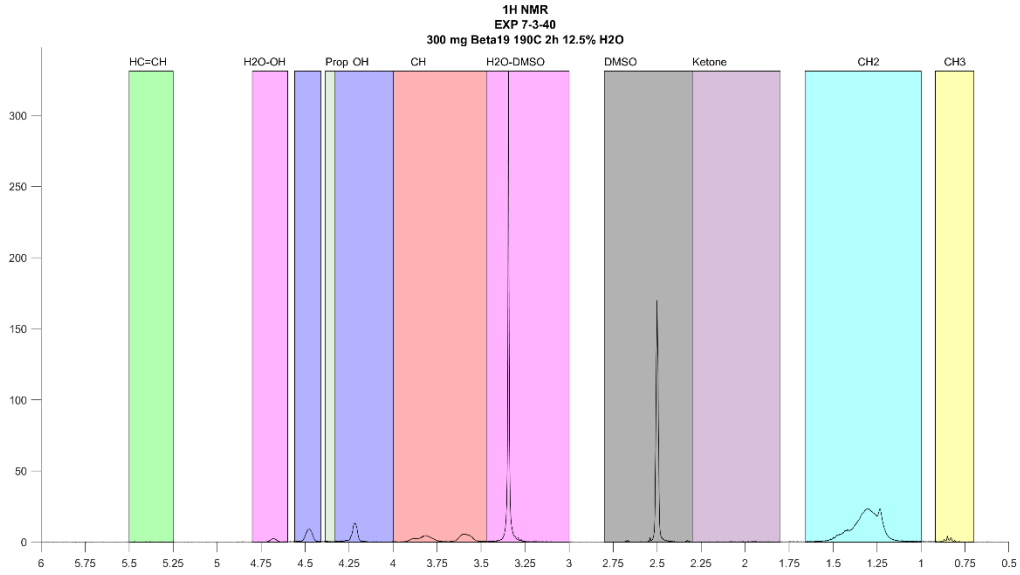

Figure 58: Hydrogen NMR for Reacted EVOH while taking a 2mg sample of the total plastic for characterization. Reaction was done with a 23.7% loading of beta 19 for 2 hours at 190C at 12.5% H2O.

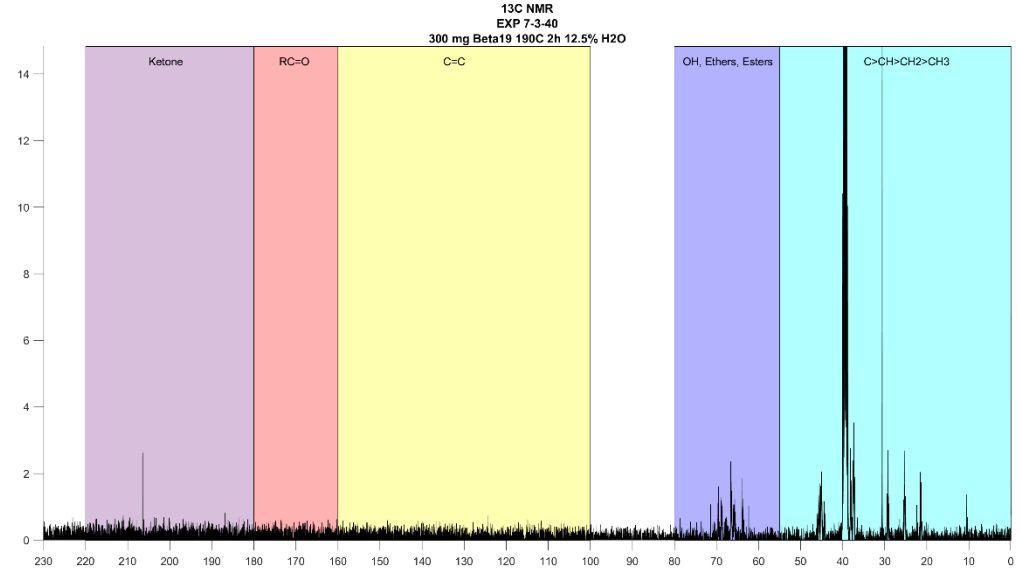

Figure 59: Carbon NMR for Reacted EVOH while taking a 30mg sample of the total plastic for characterization. Reaction was done with a 23.7% loading of beta 19 for 2 hours at 190C at 12.5% H2O.

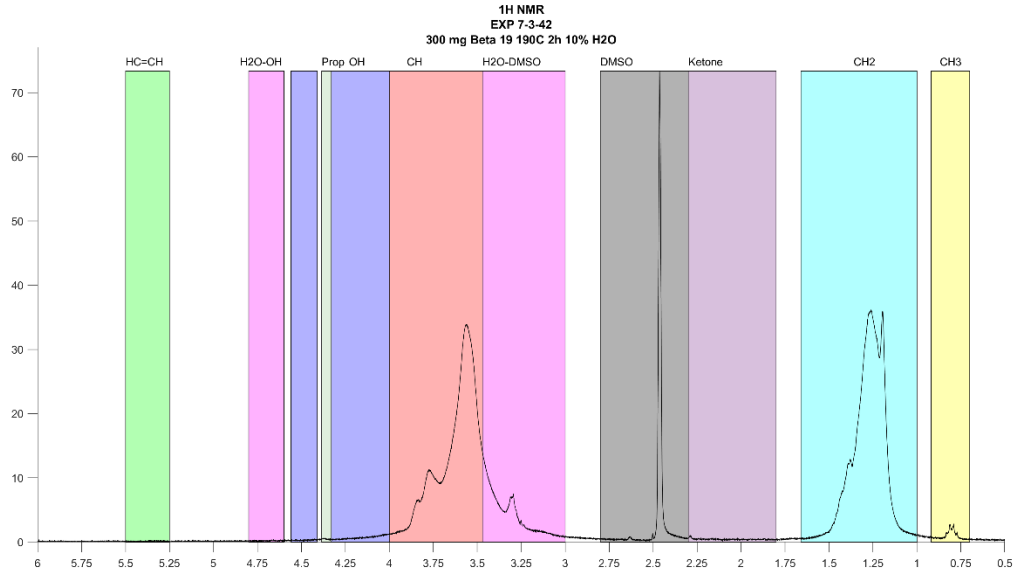

Figure 60: Hydrogen NMR for Reacted EVOH while taking a 5mg sample of the total plastic for characterization. Reaction was done with a 23.7% loading of beta 19 for 2 hours at 190C at 10% H2O.

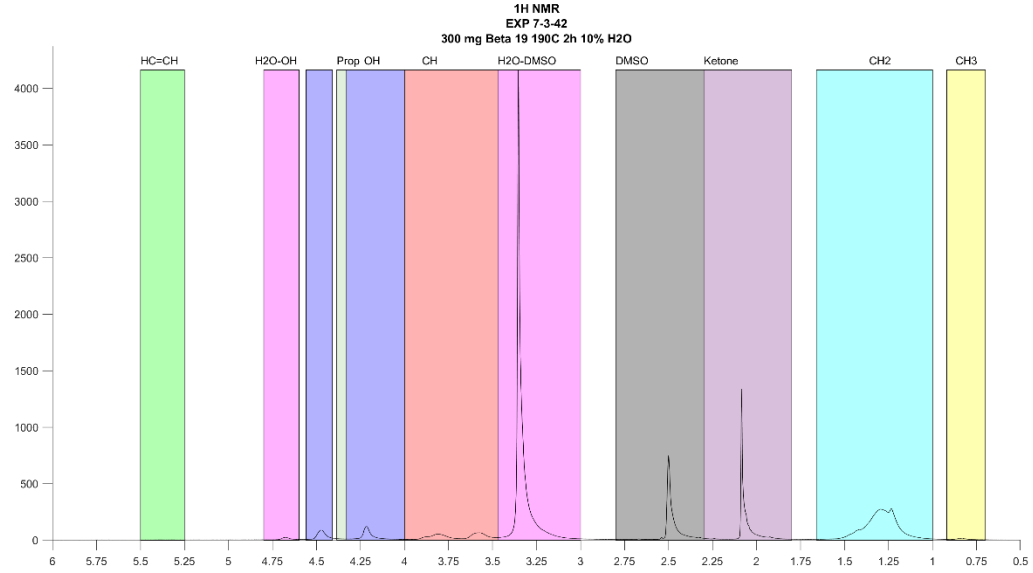

Figure 61: Hydrogen NMR for Reacted EVOH while taking a 2mg sample of the total plastic for characterization. Reaction was done with a 23.7% loading of beta 19 for 2 hours at 190C at 10% H2O.

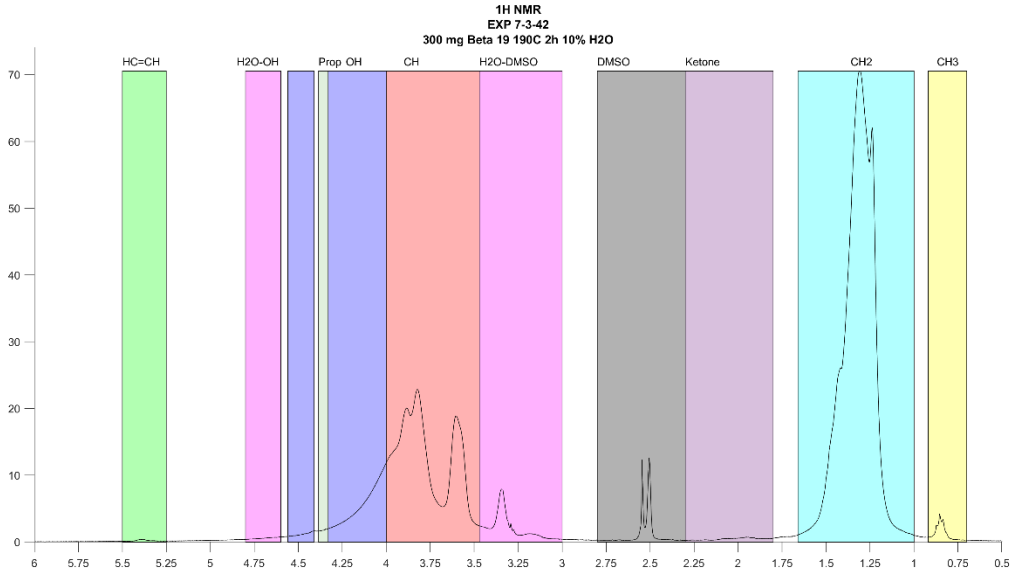

Figure 62: Hydrogen NMR for Reacted EVOH while taking a 30mg sample of the total plastic for characterization. Reaction was done with a 23.7% loading of beta 19 for 2 hours at 190C at 10% H2O.

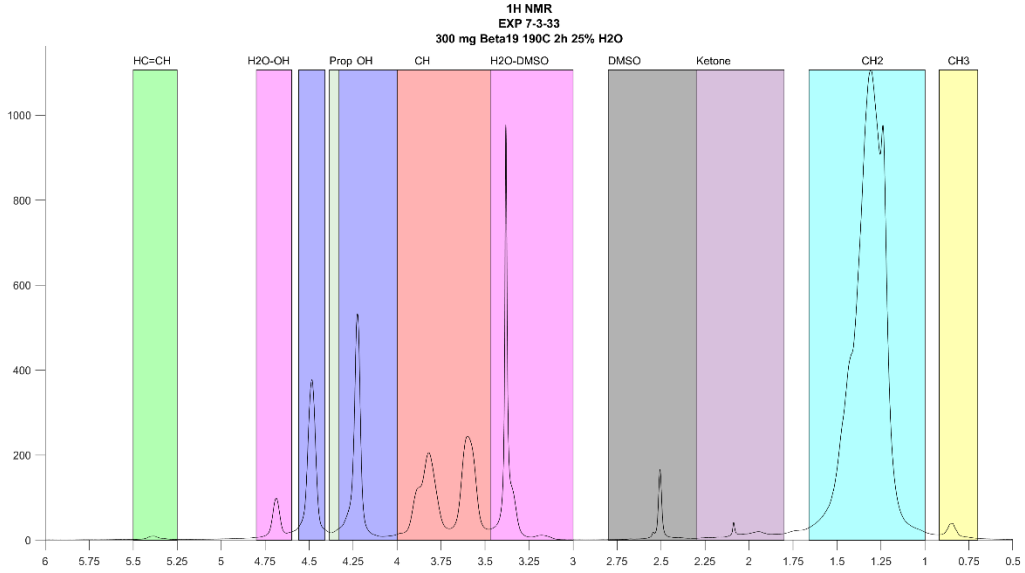

Figure 63: Hydrogen NMR for Reacted EVOH while taking a 30mg sample of the total plastic for characterization. Reaction was done with a 23.7% loading of beta 19 for 2 hours at 190C at 25% H2O.

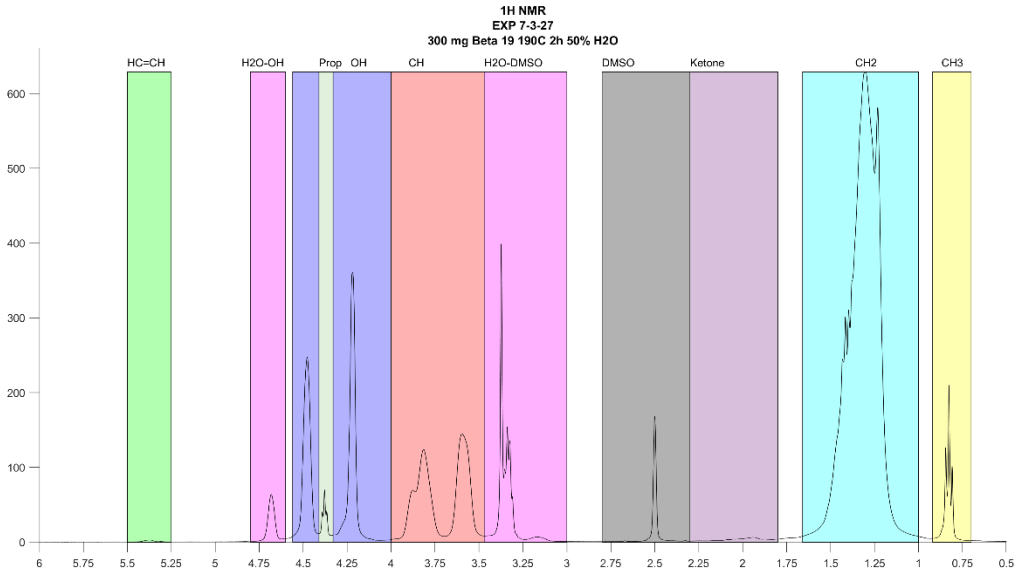

Figure 64: Hydrogen NMR for Reacted EVOH while taking a 30mg sample of the total plastic for characterization. Reaction was done with a 23.7% loading of beta 19 for 2 hours at 190C at 50% H2O.

Effectiveness Factor MATLAB Code

```
clear all
clc
%
Thiele = zeros(6,1);
Effectiveness_Factor = zeros(6,1);
Frameworkname = strings(6,1);
Acidity = zeros(6,1);
DiffusionCoefficient = zeros(6,1);
colnames = { 'Catalyst' 'Acidity' 'Thiele Modulus' 'Effectiveness Factor' 'De
(cm^2/s)'};
MwPlastic = 9683; %molecular weight plastic (g/mol)
MwH2O = 18; % molecular weight water (g/mol)
MolOHperMolEVOH = 68; % there are 68 mols of OH per 1 mol of EVOH

% ZSM5 40 calc
Acid_Site_Densit = 0.391; % (Mm/g-catalyst)
Catalyst_Loading = 29.3; % mg of catalyst per 100 mg of plastic
Total_Acid_Sites = Acid_Site_Densit* Catalyst_Loading;
Total_Max_Rate = 0.0215066*100/MwH2O/MolOHperMolEVOH;
Internal_Max_Rate = 0.0094749*100/MwH2O/MolOHperMolEVOH;
Internal_Surface_Area_BET = 398.6; % m^2/g
Pore_Volume_BET = 0.231; % cm^3/g
Partice_Radius = 0.864988889 * 10^(-6)/2; % m
Pore_Radius = 5.3*10^-10/2;% m
Framework  = "ZSM5";
```

```
SAR = 40; % Si/Al
Frameworkname(1) = strjoin ([Framework ' SAR: ' SAR]);
Acidity(1) = Acid_Site_Densit;
[Thiele(1),Effectiveness_Factor(1),External_Max_TurnOver_Frequency,DiffusionCoefficie
nt(1)]= Theta_and_Effectiveness_CoreShell(Total_Acid_Sites,Total_Max_Rate,
Internal_Max_Rate,Internal_Surface_Area_BET,Partice_Radius,Pore_Radius,Framework,SAR,
Pore_Volume_BET);

% ZSM5 140 Calculation
Acid_Site_Densit = 0.106; % (Mm/g-catalyst)
Catalyst_Loading = 49.09; % mg of catalyst per 100 mg of plastic
Total_Acid_Sites = Acid_Site_Densit* Catalyst_Loading;
Total_Max_Rate = 0.0100726*100/MwH2O/MolOHperMolEVOH;
Internal_Surface_Area_BET = 372.7; % m^2/g
Pore_Volume_BET = 0.224; % cm^3/g
Partice_Radius =  0.968873846 * 10^(-6)/2; % m
Pore_Radius = 5.3*10^-10/2;% m
Framework  = "ZSM5";
SAR = 140; % Si/Al
Frameworkname(2) = strjoin ([Framework ' SAR:' SAR]);
Acidity(2) = Acid_Site_Densit;
[Thiele(2),Effectiveness_Factor(2),DiffusionCoefficient(2)] =
Theta_and_Effectiveness_Extrapolation(External_Max_TurnOver_Frequency,Total_Max_Rate,
Partice_Radius,Pore_Radius,Framework,SAR,Total_Acid_Sites,Internal_Surface_Area_BET,P
ore_Volume_BET);

% Beta 19 Calculation
Acid_Site_Densit = 0.547; % (Mm/g-catalyst)
Catalyst_Loading = 41.5; % mg of catalyst per 100 mg of plastic
Total_Acid_Sites = Acid_Site_Densit* Catalyst_Loading;
Total_Max_Rate = 0.0267746*100/MwH2O/MolOHperMolEVOH;
Internal_Surface_Area_BET = 707; % m^2/g
Pore_Volume_BET = 0.14; % cm^3/g
Partice_Radius = 0.657057143 * 10^(-6)/2; % m
Pore_Radius = 6.7*10^-10/2;% m
Framework  = "Beta";
SAR = 19; % Si/Al
Frameworkname(3) = strjoin ([Framework ' SAR:' SAR]);
Acidity(3) = Acid_Site_Densit;
[Thiele(3),Effectiveness_Factor(3),DiffusionCoefficient(3)] =
Theta_and_Effectiveness_Extrapolation(External_Max_TurnOver_Frequency,Total_Max_Rate,
Partice_Radius,Pore_Radius,Framework,SAR,Total_Acid_Sites,Internal_Surface_Area_BET,P
ore_Volume_BET);

% Beta 180 Calculation
Acid_Site_Densit = 0.119; % (Mm/g-catalyst)
Catalyst_Loading = 41.5; % mg of catalyst per 100 mg of plastic
Total_Acid_Sites = Acid_Site_Densit* Catalyst_Loading;
Total_Max_Rate = 0.0197329*100/MwH2O/MolOHperMolEVOH;
Internal_Surface_Area_BET = 485; % m^2/g
Pore_Volume_BET = 0.301; % cm^3/g
Partice_Radius = 0.5905625 * 10^(-6)/2; % m
Pore_Radius = 6.7*10^-10/2;% m
Framework  = "Beta";
SAR = 180; % Si/Al
```

```
Frameworkname(4) = strjoin ([Framework ' SAR:' SAR]);
Acidity(4) = Acid_Site_Densit;
[Thiele(4),Effectiveness_Factor(4),DiffusionCoefficient(4)] =
Theta_and_Effectiveness_Extrapolation(External_Max_TurnOver_Frequency,Total_Max_Rate,
Partice_Radius,Pore_Radius,Framework,SAR,Total_Acid_Sites,Internal_Surface_Area_BET,P
ore_Volume_BET);

% Y 2.6 Calculation
Acid_Site_Densit = 0.366; % (Mm/g-catalyst)
Catalyst_Loading = 44.13; % mg of catalyst per 100 mg of plastic
Total_Acid_Sites = Acid_Site_Densit* Catalyst_Loading;
Total_Max_Rate = 0.0558739*100/MwH2O/MolOHperMolEVOH;
Internal_Surface_Area_BET = 549; % m^2/g
Pore_Volume_BET = 0.26; % cm^3/g
Partice_Radius = 0.796377419 * 10^(-6)/2; % m
Pore_Radius = 7.4*10^-10/2;% m
Framework  = "Y";
SAR = 2.6; % Si/Al
Frameworkname(5) = strjoin ([Framework ' SAR:' SAR]);
Acidity(5) = Acid_Site_Densit;
[Thiele(5),Effectiveness_Factor(5),DiffusionCoefficient(5)] =
Theta_and_Effectiveness_Extrapolation(External_Max_TurnOver_Frequency,Total_Max_Rate,
Partice_Radius,Pore_Radius,Framework,SAR,Total_Acid_Sites,Internal_Surface_Area_BET,P
ore_Volume_BET);

% Y 40 Calculation
Acid_Site_Densit = 0.114; % (Mm/g-catalyst)
Catalyst_Loading = 44.13; % mg of catalyst per 100 mg of plastic
Total_Acid_Sites = Acid_Site_Densit* Catalyst_Loading;
Total_Max_Rate = 0.0278789*100/MwH2O/MolOHperMolEVOH;
Internal_Surface_Area_BET = 678; % m^2/g
Pore_Volume_BET = 0.25+0.27; % cm^3/g
Partice_Radius =  0.694706667 * 10^(-6)/2; % m
Pore_Radius = 7.4*10^-10/2;% m
Framework  = "Y";
SAR = 40; % Si/Al
Frameworkname(6) = strjoin ([Framework ' SAR:' SAR]);
Acidity(6) = Acid_Site_Densit;
[Thiele(6),Effectiveness_Factor(6),DiffusionCoefficient(6)] =
Theta_and_Effectiveness_Extrapolation(External_Max_TurnOver_Frequency,Total_Max_Rate,
Partice_Radius,Pore_Radius,Framework,SAR,Total_Acid_Sites,Internal_Surface_Area_BET,P
ore_Volume_BET);

%----------------------Make Export Table--------------------
Export_Table = table(Frameworkname,Acidity,
Thiele,Effectiveness_Factor,DiffusionCoefficient,'VariableNames',colnames);
% clearvars -except Export_Table
%================================================================================
===============
%---------------Functions-------------------------------------------------------
---------------
%================================================================================
===============
```

```
function
[Thiele,Effectiveness_Factor,External_Max_TurnOver_Frequency,DiffusionCoefficient] =
Theta_and_Effectiveness_CoreShell(Acid_Site_Density_Total,Max_Rate_Normal,
Max_Rate_CoreShell,Internal_Surface_Area_BET,Particle_Radius,Pore_Radius,Framework,SA
R,Pore_Volume_BET)
Particle_Volume = (4/3)*pi()*Particle_Radius^3; %m^3
Crystal_Density= Density(Framework,SAR); % g/m^3
Pore_Volume_BET = Pore_Volume_BET/(10^2)^3*Particle_Volume*Crystal_Density;%m^3
Number_of_Pores =
(2/3)*(Particle_Radius^2/Pore_Radius^2)*(Pore_Volume_BET/Particle_Volume)*2; % number
of pore entraces (last *2 is because each channel has two entraces)
% External_Surface_Area =
(4*pi()*Particle_Radius^2)/(Particle_Volume*Crystal_Density); % Surface Area from
spherical particle minus pore entrance size
External_Surface_Area = (4*pi()*Particle_Radius^2-
pi()*Pore_Radius^2*Number_of_Pores)/(Particle_Volume*Crystal_Density); % Surface Area
from spherical particle minus pore entrance size
External_Acid_Sites= Acid_Site_Density_Total *
External_Surface_Area/(External_Surface_Area+Internal_Surface_Area_BET); %External
Acid Sites Stimation based on surface area
Internal_Acid_Sites = Acid_Site_Density_Total *
Internal_Surface_Area_BET/(External_Surface_Area+Internal_Surface_Area_BET); %
internal Acid Site Estimation Based on Surface Area
External_Max_TurnOver_Frequency = (Max_Rate_Normal-
Max_Rate_CoreShell)/External_Acid_Sites; % Turn Over Frequency for External Rate
Internal_Max_TurnOver_Frequency = Max_Rate_CoreShell/Internal_Acid_Sites; % Turn Over
Frequency for Internal Rate
Effectiveness_Factor =
Internal_Max_TurnOver_Frequency/External_Max_TurnOver_Frequency;
eqn = @(T) abs((3./T^2).*(T.*coth(T)-1)-Effectiveness_Factor);
Thiele = fminsearch(eqn,450);
Cplasticsurface = 1.19*10^3/9683; % mol/L
DiffusionCoefficient =
Internal_Max_TurnOver_Frequency*Particle_Radius*10/Cplasticsurface*100/60*Internal_Ac
id_Sites; %Diffusion coefficient in cm^2/s
end
function [Thiele,Effectiveness_Factor,DiffusionCoefficient] =
Theta_and_Effectiveness_Extrapolation(External_Max_TurnOver_Frequency,Max_Rate,Partic
le_Radius,Pore_Radius,Framework,SAR,Acid_Site_Density_Total,Internal_Surface_Area_BET
,Pore_Volume_BET)
Particle_Volume = (4/3)*pi()*Particle_Radius^3; %m^3
Crystal_Density= Density(Framework,SAR); % g/m^3
Pore_Volume_BET = Pore_Volume_BET/(10^2)^3*Particle_Volume*Crystal_Density;%m^3
Number_of_Pores =
(2/3)*(Particle_Radius^2/Pore_Radius^2)*(Pore_Volume_BET/Particle_Volume)*2; % number
of pore entraces (last *2 is because each channel has two entraces)
External_Surface_Area = (4*pi()*Particle_Radius^2-
pi()*Pore_Radius^2*Number_of_Pores)/(Particle_Volume*Crystal_Density); % Surface Area
from spherical particle minus pore entrance size
External_Acid_Sites= Acid_Site_Density_Total *
External_Surface_Area/(External_Surface_Area+Internal_Surface_Area_BET); %External
Acid Sites Stimation based on surface area
Internal_Acid_Sites = Acid_Site_Density_Total *
Internal_Surface_Area_BET/(External_Surface_Area+Internal_Surface_Area_BET); %
internal Acid Site Estimation Based on Surface Area
```

```
Internal_Max_TurnOver_Frequency= (Max_Rate-
External_Max_TurnOver_Frequency*External_Acid_Sites)/Internal_Acid_Sites; % Turn Over
Frequency for Internal Rate
Effectiveness_Factor =
Internal_Max_TurnOver_Frequency/External_Max_TurnOver_Frequency; % from definition
eqn = @(T) abs((3./T^2).*(T.*coth(T)-1)-Effectiveness_Factor);
Thiele = fminsearch(eqn,450);
Cplasticsurface = 1.19*10^3/9683; % mol/L
DiffusionCoefficient =
Internal_Max_TurnOver_Frequency*Particle_Radius*10/Cplasticsurface*100/60*Internal_Ac
id_Sites; %Diffusion coefficient in cm^2/s
% Graphical Solution
% x = 100:1:1000;
% y = (3./x.^2).*(x.*coth(x)-1);
% y1 = zeros(1,size(y,2))+Effectiveness_Factor;
% plot(x,y);
% hold on
% plot(x,y1)
end

function D = Density(framework,SAR)
if framework == "ZSM5"
Number_of_Alumina = 96*1/(SAR+1);
Molecular_Weight_Alumina = 26.982;
Number_of_Silica = 96*SAR/(SAR+1);
Molecular_Weight_Silica = 28.085;
Number_of_Oxygen = 192;
Molecular_Weight_Oxygen = 15.999;
Number_of_Hydrogen = Number_of_Alumina;
Molecular_Weight_Hydrogen = 1.008;
Avogadro_Number = 6.022*10^23;
Unit_Cell_Volume = 15.4*Number_of_Alumina+5330; % A^3
D =
(Number_of_Alumina*Molecular_Weight_Alumina+Number_of_Silica*Molecular_Weight_Silica+
Number_of_Oxygen*Molecular_Weight_Oxygen+Number_of_Hydrogen*Molecular_Weight_Hydrogen
)/(Unit_Cell_Volume*Avogadro_Number)*(1/(10^-10))^3;% g/m^3
elseif framework == "Beta"
D = 1.56*100^3;% g/m^3
else
Number_of_Alumina = 192*1/(SAR+1);
Molecular_Weight_Alumina = 26.982;
Number_of_Silica = 192*SAR/(SAR+1);
Molecular_Weight_Silica = 28.085;
Number_of_Oxygen = 384;
Molecular_Weight_Oxygen = 15.999;
Number_of_Hydrogen = Number_of_Alumina;
Molecular_Weight_Hydrogen = 1.008;
Avogadro_Number = 6.022*10^23;
Unit_Cell_Volume = (Number_of_Alumina+Number_of_Silica)/12.7*1000; % A^3
D =
(Number_of_Alumina*Molecular_Weight_Alumina+Number_of_Silica*Molecular_Weight_Silica+
Number_of_Oxygen*Molecular_Weight_Oxygen+Number_of_Hydrogen*Molecular_Weight_Hydrogen
)/(Unit_Cell_Volume*Avogadro_Number)*(1/(10^-10))^3;% g/m^3
end
end
```

TGA Data Processing Code

```
clear all;
clc;
close all;
%% Information
% ------------------------------------------------------------------------------------
------------
% Made by: Luis Mario Trevisi
% Updated by: Luis Mario Trevisi
% Date: 2022/11/09
%------------------------------------------------------------------------------------
------------
%% Experimental Setup & initial data (Variables/Inputs)

%general information
Pcatalyst = 0.3195; % % of catalyst by weight of plastic Pcatalyst = Mcat/Mplastic
Solvent =0; % 0: Non Solvent, 1: Solvent system. Variable to choose the type of
system
Solution = 9/55; % ratio of grams of plastic to grams of solvent from experimental
setup
MSInterest = 18; % the m/e of interest for internal plotting and MS integration
analysis

%determining the limits of integration for MS
Npeaks = 2; % number of peaks interested on the plot
time11 = 11.49; % initial time of peak 1 for integration
time12 = 38.4; % final time of peak 1 for integration
time21 = 50; % initial time of peak 2 for integration
time22 = 80; % final time of peak 2 for integration

%specifying the text file location to import the data
TGAfilename  ="C:\Users\lmtre\OneDrive - University of
Oklahoma\CATALY~1\EXPERI~1\EXP6CA~1\CATALY~2\EXFF30~1\EXPDAT~1.TXT"; % address of TGA
text file
MSfilename = ""; % address of MS text file, left as "" for no MS data recorded
savefolder = "C:\Users\lmtre\OneDrive - University of Oklahoma\Catalyst Polymer
Separation\Experimental Results\EXP6 Catalysis comparison at 220C 3h\Catalyst
comparison at 195C 1h\Processed Data\"; % address of folder to save output
Catalyst = "Y-2.6_";
EXP = "EXP_6-3-35_";
filename =
strcat(EXP,Catalyst,num2str(round(Pcatalyst/(1+Pcatalyst)*100,1)),'%.xlsx'); % name
of the file for t
% data to be saved


%Cutting the data and re-scale it.
TargetTime = 10; %  if bigger than zero it will cut everthing before the given time
and re scale it.

% level of smoothing
smoothing = 0.05;
```

```
%Note: The output of this program is in a variable called exportformat.
%% loading data (DO NOT MODIFY FROM HERE ON)

% Extracting the matrix numbers
TGA = readmatrix(TGAfilename);
if ~strcmp(MSfilename, "")
MS = readmatrix(MSfilename);
end

% extracting intial mass
 % open the file
 fid=fopen(TGAfilename);
 % find linenum for the initial mass.
linenum = 0;
n = 0;
 while (linenum == 0)
    n = n+1;
    MassIntial = textscan(fid,'%s',1,'delimiter','\n', 'headerlines',linenum);
    MassIntial = split(MassIntial{1,1}{1,1});
    s = size(MassIntial);
    if s(1)>1
        if (string(MassIntial(1)) == "#SAMPLE" && string(MassIntial(2)) == "MASS")
            linenum = n;
        end
    end
 end
% linenum = 15; % this line is where the initial mass information is located
 % use '%s' if you want to read in the entire line or use '%f' if you want to read
only the first numeric value
%  MassIntial = textscan(fid,'%s',1,'delimiter','\n', 'headerlines',linenum-1); %
read the line with the initial mass specifics
%  MassIntial =split(MassIntial{1,1}{1,1}); % split the initial mass specifics
%  c = size(MassIntial);
 MassIntial([1 2],:) = [ ];
 MassIntial = split(MassIntial,":");
 MassIntial(1,:) = [ ];
 MassIntial = str2double(MassIntial); % get the initial mass as a double.
% extracting the MS information
if ~strcmp(MSfilename, "")
 % open the file
 fid=fopen(MSfilename);
 % find linenum to for the targeted masses
linenum = 0;
n = 0;
 while (linenum == 0)
    n = n+1;
    C = textscan(fid,'%s',1,'delimiter','\n', 'headerlines',linenum);
    C = split(C{1,1}{1,1});
    c = size(C);
    if s(1)>1
        if (string(C(1)) == "#SAMPLE:" && string(C(2)) == "Mass")
            linenum = n;
        end
    end
```

```
 end

%  linenum = 14; % this line is where the MS information is located
%  % use '%s' if you want to read in the entire line or use '%f' if you want to read
only the first numeric value
%  C = textscan(fid,'%s',1,'delimiter','\n', 'headerlines',linenum-1); % read the
line with the MS specifics
%  C =split(C{1,1}{1,1}); % split the MS specifics
%  c = size(C);
 C(1,:) = [ ];
 for n = 1:1:c(1)/2 % remove the strings
     C(n,:)= [];
 end
 C = str2double(C); % get an array with the specific m/e
 c = size(C);
 k = 0;
 % Removing repeating MS from different sections in the MS array.
 for n=2:1:c(1)
     if C(n,1) == C(1,1)
         k = n;
         break
     end
 end
 if k>0
 t = c(1)-k+1;
 for n = 1:1:t
     C(k-1,:)= [];
 end
 end
 c = size(C);
 Nmass = c(1); % count the number of masses
end
% extracting TGA information
 % open the file
 fid=fopen(TGAfilename);
 % find the line where the TG headers are located
linenum = 0;
n = 0;
 while (linenum == 0)
    n = n+1;
    TGAColumname = textscan(fid,'%s',1,'delimiter','\n', 'headerlines',linenum);
    TGAColumname = split(TGAColumname{1,1}{1,1},';');
    a = size(TGAColumname);
    if s(1)>1
        if (string(TGAColumname(1)) == "##Temp./°C" && string(TGAColumname(2)) ==
"Time/min" )
            linenum = n;
        end
    end
 end

%% Indexing
%TGA index
    % intial guess
TGATemp = 1;
```

```
TGAtime = 2;
TGADSC = 3;
TGAMass = 4;
TGAPurge = 5;
TGAProtec = 6;
TGASensit = 7;
% assigning actual index for tga values base on file column name
for n = 1:1:a(1)
    if strcmp('##Temp./øC',TGAColumname(n))
        TGATemp = n;
    end
    if strcmp('Time/min',TGAColumname(n))
        TGAtime = n;
    end
     if strcmp('DSC/(uV/mg)',TGAColumname(n))
        TGADSC = n;
     end
    if strcmp('Mass/%',TGAColumname(n))
        TGAMass = n;
    end
    if strcmp('Gas Flow(purge2)/(ml/min)',TGAColumname(n))
        TGAPurge = n;
    end
    if strcmp('Gas Flow(protective)/(ml/min)',TGAColumname(n))
        TGAProtec = n;
    end
    if strcmp('Segment',TGAColumname(n))
        TGASensit = n;
    end
end

%MS Index
if ~strcmp(MSfilename, "")
    MStime = 1;
    targetmassarray = 1;
    for n= 1:c(1) % finding the array position in the MS data of interest
    if C(targetmassarray,1) ~= MSInterest
        targetmassarray = targetmassarray+1;
    end
    end
end
%% pre-processing TGA data

%Correction for non solvent system
if Solvent == 0
TGA(:,TGAMass) = ((TGA(:,TGAMass)./100).*(1+Pcatalyst)-Pcatalyst).*100;
end
%Correction for solvent system
if Solvent == 1
TGA(:,TGAMass) = ((TGA(:,TGAMass)./100)*(1+Solution+Pcatalyst)-
Pcatalyst)./(1+Solution).*100;
end
%% Processing MS data
if ~strcmp(MSfilename, "")
    %Joining sections for multi-step temperature program.
```

```
    x = size(MS);
    t = 0;
    p = 0;
    for n = 1:1:x(1)
       for m = 2:1:Nmass+1
       if isnan(MS(n,m+t))
           t = t+Nmass;
           p=p+1;
       end
       if t>0
           MS(n,m) = MS(n,m+t);
           MS(n,m+t) = NaN;
       end
       end
    end
    % for n = 1:1:x(1)
    %      for m = Nmass+1:1:Nmass*p+1
    %          MS(n,m) = NaN;
    %      end
    % end
end
%% exporting format
% making the arrays the same size to be able to export in a single array by
% getting the MS values at the same t step as TGA data
h = size(TGA);
fixequaltime = TGA(:,TGAtime);
MStimecorrected(:,1) = fixequaltime;
if ~strcmp(MSfilename, "")
    for n = 1:1:c(1)
        MStimecorrected(:,n+1) = interp1(MS(:,MStime),MS(:,n+1),fixequaltime);
    end
MS = MStimecorrected;
MS(isnan(MS)) = 0;
end
% making the exporting array
exportformat(:,1) = TGA(:,TGAtime);
exportformat(:,2) = smoothdata(TGA(:,TGAMass),'gaussian',smoothing*h(1));
if ~strcmp(MSfilename, "")
    exportformat(:,3) = MS(:,MStime);
    exportformat(:,4) = MS(:,targetmassarray+1); % ion current of target mass.
end

% finding the derivative
DevColNum = size(exportformat,2)+1;
 for n= 2:1:h(1)-1
     % Performing the average of foward and backward interpolation
     exportformat(n,DevColNum) = ((exportformat(n,2)- exportformat(n-
1,2))/(exportformat(n,1)- exportformat(n-1,1))+(exportformat(n+1,2)-
exportformat(n,2))/(exportformat(n+1,1)- exportformat(n,1)))/2;
     % Removing negative negative slopes by equaling to the last one.
%      if exportformat(n,5)<0
%          exportformat(n,5) = exportformat(n-1,5);
%      end
 end
```

```
 exportformat(:,DevColNum) =
smoothdata(exportformat(:,DevColNum),'gaussian',smoothing*h(1));
 exportformat(:,DevColNum) = (-1).*exportformat(:,DevColNum);

%% finding area under the curve for MS
% smoothing the MS signal
if Npeaks>=2 && ~strcmp(MSfilename, "")
MS(:,targetmassarray+1) = smoothdata(MS(:,targetmassarray+1),'sgolay'); % smoothing
the data

%finding the cells position for the integration (correlating time to cell
%index)
for n=1:1:h(1)
if MS(n,MStime) < time11
    if MS(n+2,MStime)>time11
        peak11 = n+1;
    end
end
if MS(n,MStime) < time12
    if MS(n+2,MStime)>time12
        peak12 = n+1;
    end
end
end
% integrating the first peak
coeff1 = polyfit(MS([peak11 peak12], MStime),MS([peak11
peak12],targetmassarray+1),1);
integration1 = 0;
for n=peak11:1:peak12
integration1 = integration1 + ((MS(n,targetmassarray+1)-
(coeff1(1)*MS(n,MStime)+coeff1(2)))+(MS(n+1,targetmassarray+1)-
(coeff1(1)*MS(n+1,MStime)+coeff1(2))))*(MS(n+1,MStime)-MS(n,MStime))/2;
end
% the total mass change for this section
deltaM1p = TGA(peak11,TGAMass)-TGA(peak12,TGAMass);
%finding the cells position for the integration (correlating time to cell
%index)
if Npeaks >= 2
for n=1:1:h(1)
if MS(n,MStime) < time21
    if MS(n+2,MStime)>time21
        peak21 = n+1;

    end
end
if MS(n,MStime) < time22
    if MS(n+2,MStime)>time22
        peak22 = n+1;
        break
    end
end
end
% integrating the second peak
coeff2 = polyfit(MS([peak21 peak22], MStime),MS([peak21
peak22],targetmassarray+1),1);
```

```
integration2 = 0;
for n=peak21:1:peak22
integration2 = integration2 + ((MS(n,targetmassarray+1)-
(coeff2(1)*MS(n,MStime)+coeff2(2)))+(MS(n+1,targetmassarray+1)-
(coeff2(1)*MS(n+1,MStime)+coeff2(2))))*(MS(n+1,MStime)-MS(n,MStime))/2;
end
% final mass of second peak
deltaM2p = TGA(peak21,TGAMass)-TGA(peak22,TGAMass);
end
% trying to find the onset automatically
%Nonset = 4; % determine the number of onsets ( 2 onsets per signal peak)
% try to find onset automatically
%[ipt, residual] =
ischange(MS(:,targetmassarray+1),'variance','MaxNumChanges',Nonset);
%  [ipt, residual] =
findchangepts(MS(:,targetmassarray+1),'Statistic','std','MinThreshold',5000);
% [ipt, residual] =
findchangepts(MS(:,targetmassarray+1),'MaxNumChanges',Nonset,'Statistic','std');
%% Mass analysis

deltaM2H2Op = deltaM1p/integration1*integration2; % Mass lost predicted from MS
calibration.
deltaM2H2Omg = deltaM1p/100/integration1*integration2*MassIntial; % Mass lost
predicted from MS calibration.
deltaM1mg = deltaM1p/100*MassIntial;
deltaM2mg = deltaM2p/100*MassIntial;
%% Display importat results/values
disp(['Initial Mass: ' num2str(MassIntial)]);
disp(['Area peak 1: ' num2str(integration1)]);
disp(['Area peak 2: ' num2str(integration2)]);
disp(['Experimental Mass Loss peak 2: ' num2str(deltaM2p) ' %']);
disp(['Predicted (MS) Mass Loss peak 2: ' num2str(deltaM2H2Op) ' %']);
disp(['Experimental Mass Loss peak 2: ' num2str(deltaM2mg) ' mg']);
disp(['Predicted (MS) Mass Loss peak 2: ' num2str(deltaM2H2Omg) ' mg']);

end
%% ploting results for integration of MS
% figure
% plot(MS(:,MStime),MS(:,targetmassarray+1));
% hold on
% plot(MS([peak11 peak12],MStime),MS([peak11 peak12],targetmassarray+1),'o');
% plot(MS(peak11:peak12,MStime),coeff1(1).*MS(peak11:peak12,MStime)+coeff1(2));
% ylabel("Ion Current"); xlabel("time");
% if Npeaks>=2
% plot(MS([peak21 peak22],MStime),MS([peak21 peak22],targetmassarray+1),'o');
% plot(MS(peak21:peak22,MStime),coeff2(1).*MS(peak21:peak22,MStime)+coeff2(2));
% end
% yyaxis right
% plot(TGA(:,TGAtime),TGA(:,TGAMass));
% ylabel("Corrected mass lost");
% hold off

% figure
```

```
%
plotyyy(TGA(:,TGAtime),TGA(:,TGATemp),TGA(:,TGAtime),TGA(:,TGAMass),MS(:,MStime),MS(:
,targetmassarray+1),["temperature" "Mass" ["MS18" num2str(C(targetmassarray,1))]])
% figure
% plot(MS(:,MStime),MS(:,targetmassarray+1));

%% cut data
if TargetTime > 0
    n=1;
    while TGA(n,TGAtime)~=TargetTime
    n=n+1;
    end
    exportformat(1:n-1,:) = [];
    exportformat(:,2) = exportformat(:,2)+(100-exportformat(1,2));
end

%% Creating exportable table
if ~strcmp(MSfilename, "")
    colnames = {'TGA time' 'TGA Corrected Mass' 'MS time' ['Ion Current of
',num2str(MSInterest), ' m/e'] 'MassperTime'};
    Export_Table = table(exportformat(:,1), exportformat(:,2), exportformat(:,3),
exportformat(:,4),exportformat(:,5),'VariableNames',colnames);
else
colnames = {'TGA time' 'TGA Corrected Mass' 'MassperTime'};
    Export_Table = table(exportformat(:,1),
exportformat(:,2),exportformat(:,3),'VariableNames',colnames);
end
%% Plot results for TGA data and its derivative/rate
plot(table2array(Export_Table(:,"TGA time")),table2array(Export_Table(:,"TGA
Corrected Mass")));
hold on
yyaxis right
plot(table2array(Export_Table(:,"TGA
time")),table2array(Export_Table(:,"MassperTime")));
hold off
%% Export the data into an excel file
     writetable(Export_Table,strcat(savefolder, filename))
%% Delete other variables to have a clear output.
clearvars -except Export_Table
%% functions
% for plotting we can also use addaxis from file exchange
function [ax,hlines] = plotyyy(x1,y1,x2,y2,x3,y3,ylabels)
%PLOTYYY - Extends plotyy to include a third y-axis
%
%Syntax:  [ax,hlines] = plotyyy(x1,y1,x2,y2,x3,y3,ylabels)
%
%Inputs: x1,y1 are the xdata and ydata for the first axes' line
%        x2,y2 are the xdata and ydata for the second axes' line
%        x3,y3 are the xdata and ydata for the third axes' line
%        ylabels is a 3x1 cell array containing the ylabel strings
%
%Outputs: ax -     3x1 double array containing the axes' handles
%         hlines - 3x1 double array containing the lines' handles
%
%Example:
```

```
%x=0:10;
%y1=x;  y2=x.^2;   y3=x.^3;
%ylabels{1}='First y-label';
%ylabels{2}='Second y-label';
%ylabels{3}='Third y-label';
%[ax,hlines] = plotyyy(x,y1,x,y2,x,y3,ylabels);
%legend(hlines, 'y = x','y = x^2','y = x^3',2)
%
%m-files required: none
%Author: Denis Gilbert, Ph.D., physical oceanography
%Maurice Lamontagne Institute
%Dept. of Fisheries and Oceans Canada
%email: gilbertd@dfo-mpo.gc.ca
%Web: http://www.qc.dfo-mpo.gc.ca/iml/
%April 2000; Last revision: 14-Nov-2001
if nargin==6
   %Use empty strings for the ylabels
   ylabels{1}=' '; ylabels{2}=' '; ylabels{3}=' ';
elseif nargin > 7
   error('Too many input arguments')
elseif nargin < 6
   error('Not enough input arguments')
end
figure('units','normalized',...
       'DefaultAxesXMinorTick','on','DefaultAxesYminorTick','on');
%Plot the first two lines with plotyy
[ax,hlines(1),hlines(2)] = plotyy(x1,y1,x2,y2);
cfig = get(gcf,'color');
pos = [0.1  0.1  0.7  0.8];
offset = pos(3)/5.5;
%Reduce width of the two axes generated by plotyy
pos(3) = pos(3) - offset/2;
set(ax,'position',pos);
%Determine the position of the third axes
pos3=[pos(1) pos(2) pos(3)+offset pos(4)];
%Determine the proper x-limits for the third axes
limx1=get(ax(1),'xlim');
limx3=[limx1(1)   limx1(1) + 1.2*(limx1(2)-limx1(1))];
%Bug fix 14 Nov-2001: the 1.2 scale factor in the line above
%was contributed by Mariano Garcia (BorgWarner Morse TEC Inc)
ax(3)=axes('Position',pos3,'box','off',...
   'Color','none','XColor','k','YColor','r',...
   'xtick',[],'xlim',limx3,'yaxislocation','right');
hlines(3) = line(x3,y3,'Color','r','Parent',ax(3));
limy3=get(ax(3),'YLim');
%Hide unwanted portion of the x-axis line that lies
%between the end of the second and third axes
line([limx1(2) limx3(2)],[limy3(1) limy3(1)],...
   'Color',cfig,'Parent',ax(3),'Clipping','off');
axes(ax(2))
%Label all three y-axes
set(get(ax(1),'ylabel'),'string',ylabels{1})
set(get(ax(2),'ylabel'),'string',ylabels{2})
set(get(ax(3),'ylabel'),'string',ylabels{3})
end
```

NMR plotting and Deconvolution Code

```
%% House Keeping
clc;
clear all;
close all;
%% input information (modify every time)
NMRfilename ="C:\Users\lmtre\OneDrive - University of Oklahoma\Catalyst Polymer
Separation\Experimental Results\EXP7 Solvent system\H2O-1Propanol\EXP_7-3-
73_2mg_20230609_01\EXP_7-3-73_2mg-PROTON_02.fid\EXP_7-3-73_2mg-PROTON.csv";
% NMRfilename = "C:\Users\lmtre\OneDrive - University of Oklahoma\Catalyst Polymer
Separation\Experimental Results\EXP7 Solvent system\H2O-
1Propanol\EVOH_20230328_01\EVOH-PROTON_01.fid\EVOH-PROTON_1s_delay.csv";
% NMRfilename  = "C:\Users\lmtre\OneDrive - University of Oklahoma\Catalyst Polymer
Separation\Experimental Results\EXP7 Solvent system\H2O-1Propanol\exp_7-3-
22_beta_19_20230323_01\exp_7-3-22_beta_19-PROTON_02.fid\exp_7-3-22_beta_19-
PROTON.csv";
CNMRfilename  = "C:\Users\lmtre\OneDrive - University of Oklahoma\Catalyst Polymer
Separation\Experimental Results\EXP7 Solvent system\H2O-1Propanol\EXP_7-3-
56_20230524_01\EXP_7-3-56-CARBON_01.fid\EXP_7-3-56-CARBON.csv";
Export_file = 1; % 0 if not export, 1 if you want to export HNMR, 2 if you want to
save HNMR and CNMR
Catalyst = "300 mg Beta19 180C 30min 12.5% H2O"; % name of the catalyst used (no
spaces)
Experiment_Number = "EXP 7-3-73"; %Number of the experiment (no spaces)
name = wildcardPattern("Except","\"); % finding experiment folder from experiment
name
pat = "\" + name + textBoundary; % finding experiment folder from experiment name
path = extractBefore(NMRfilename,pat); % finding experiment folder from experiment
name
savefolder = strcat(path,'\'); % address of folder to save output from directory
name = wildcardPattern("Except","\"); % finding experiment folder from experiment
name
pat = "\" + name + textBoundary; % finding experiment folder from experiment name
path = extractBefore(CNMRfilename,pat); % finding experiment folder from experiment
name
savefolderc = strcat(path,'\');
Deconvolute = 0; % deconvolute last section.
ketonepresentdecov = 0; % adjust when deconvoluting if there is ketone (remove the
gaussian of ketones if not pressent)
typedeconv = 1; % 1 gaussian, 2 Weibull, 3 Voigt
adaptivebaseline = 0; % use adaptive baseline
%% fine tuning integration ranges (may need to modify)
%--------------------------------Proton-----------------------------------------
%  Integration boundaries for OH functional group
shift11OH = 4; % Lower Bound
shift12OH = 4.33; % Upper Bound
shift21OH = 4.41; % Lower Bound
shift22OH = 4.56; % Upper Bound
% Integration boundaries for CH2 in Ether functional group
shift11Prop = 4.33; % Lower Bound
```

```
shift12Prop = 4.385; % Upper Bound
%  Integration boundaries for RCHR functional group
shift11RCHR = 3.47;  % Lower Bound
shift12RCHR = 4; % Upper Bound
%  Integration boundaries for CH2 functional group
shift11CH2 = 1;  % Lower Bound
shift12CH2 = 1.66; % Upper Bound
%  Integration boundaries for CH3 functional group
shift11CH3 = 0.7;  % Lower Bound
shift12CH3 = 0.92; % Upper Bound
% Integration Boundaries for Vynilc CH2 functional group
shift11Vynil = 5.25;  % Lower Bound
shift12Vynil = 5.5; % Upper Bound
% Integration Boundaries for Allylic CH2 functional group
shift11Allyl = 1.8;  % Lower Bound
shift12Allyl = 2.3; % Upper Bound
% Integration Boundaries for DMSO
shift11DMSO = 2.3;  % Lower Bound
shift12DMSO = 2.8; % Upper Bound
% Integration Boundaries for H2O
shift11H2O = 3;  % Lower Bound
shift12H2O = shift11RCHR; % Upper Bound
shift21H2O = 4.6;  % Lower Bound hydrogen bound
shift22H2O = 4.8; % Upper Bound
% Integration Boundaries for Ketone
shift11Ket = 1.8;  % Lower Bound
shift12Ket = 2.3; % Upper Bound
% Integration Boundaries for Ketone
shift11TMS = -0.1;  % Lower Bound
shift12TMS = 0.1; % Upper Bound

%-----------------------------------------Carbon--------------------------------
%  boundaries for OH, Ether, Ester functional group
shift21OHEthEst = 55; % Lower Bound
shift22OHEthEst = 80; % Upper Bound
%  boundaries for C>CH>CH2> CH3 functional group
shift21CH2 = 0;  % Lower Bound
shift22CH2 = 55; % Upper Bound
%  boundaries for C=C functional group
shift21CC = 100;  % Lower Bound
shift22CC = 160; % Upper Bound
%  boundaries for Ester RC=O functional group
shift21Est = 160;  % Lower Bound
shift22Est = 180; % Upper Bound
%  boundaries for Ketone functional group
shift21Ket = 180;  % Lower Bound
shift22Ket = 220; % Upper Bound

%% data processing (do not modify)
%-------------------------------------------------------------------------------
% order of functional gruops
CH3fun = 1; % CH3
CH2fun = 2; % CH2
RCHRfun = 3; % RCHR
OHfun = 4; % OH
```

```
ketonefun = 5; % Vinylic =CH
Propanol = 6; % CH2 next to O in ether
Allylicfun = 6; % Allylic CH2
Vinylicfun = 6; % Vinylic =CH

%-------------------------------------------------------------------------------
%names for exporting table
% colnames = {'R-CH3' '-CH2C-' 'R-CH-R' 'R-OH' 'Allylic' 'Vinylic' 'ketone'}; %
column names with functional groups
colnames = {'R-CH3' '-CH2C-' 'R-CH-R' 'R-OH' 'Ketone' 'Vinylic'}; % column names with
functional groups
rownames = {'Area' 'Number of Protons' 'Area/Number of Protons' '% Normalize Area'};
% row names for each step
%-------------------------------------------------------------------------------
% initializing the matrix that will be our table
NFunGroup = size(colnames);
exportformat = zeros(4,NFunGroup(2));
%-------------------------------------------------------------------------------
% reading the NMR data from the csv file
NMR = readmatrix(NMRfilename);
CNMR = readmatrix(CNMRfilename);
%-------------------------------------------------------------------------------
% finding the areas using the later define function for each functional
% group


Propanol_Area = peakint(NMR, shift11Prop,shift12Prop, adaptivebaseline);

exportformat(1,CH3fun) = peakint(NMR, shift11CH3,shift12CH3,adaptivebaseline);

exportformat(1,CH2fun) = peakint(NMR, shift11CH2,shift12CH2,adaptivebaseline);

exportformat(1,RCHRfun) = peakint(NMR, shift11RCHR,shift12RCHR,adaptivebaseline);

% exportformat(1,Allylicfun) = peakint(NMR,
shift11Allyl,shift12Allyl,adaptivebaseline);

exportformat(1,OHfun) = peakint(NMR,
shift11OH,shift12OH,adaptivebaseline)+peakint(NMR,
shift21OH,shift22OH,adaptivebaseline);

exportformat(1,Vinylicfun) = peakint(NMR,
shift11Vynil,shift12Vynil,adaptivebaseline);

 exportformat(1,ketonefun) = peakint(NMR, shift11Ket,shift12Ket,adaptivebaseline);

 TMSArea = peakint(NMR, shift11TMS,shift12TMS,adaptivebaseline); % Area of TMS

 TMSHCONCENTRATION = 0.6*0.01*88.225*0.648*12; % moles of hydrogen in TMS external
calibration
```

```
%%
================================================================================
% inputing the number of protons depending on the functional group.
% exportformat(2,:) = [3 2 1 1 2 1 2];
exportformat(2,:) =   [3 2 1 1 2 1];
% getting the area per proton by dividing the total area by the number of
% protons
exportformat(3,:) = exportformat(1,:)./exportformat(2,:);
% getting the %mol by normalizing the area previously found
exportformat(4,:) = exportformat(3,:)./sum(exportformat(3,:))*100;
% creating the table to export the data functional groups
% Export_Table_Functional =
table(exportformat(:,CH3fun),exportformat(:,CH2fun),exportformat(:,RCHRfun),exportfor
mat(:,OHfun),exportformat(:,Allylicfun),exportformat(:,Vinylicfun),exportformat(:,ket
onefun),'VariableNames', colnames, 'RowNames', rownames);
Export_Table_Functional =
table(exportformat(:,CH3fun),exportformat(:,CH2fun),exportformat(:,RCHRfun),exportfor
mat(:,OHfun),exportformat(:,ketonefun),exportformat(:,Vinylicfun),'VariableNames',
colnames, 'RowNames', rownames);

%-------------------------------------------------------------------------------
-----
% creating the table to export conversion
conversion = zeros(2,7);
conversion(2,1) = 0.348763813447828;
conversion(2,2) = 50.9937515;
conversion(2,3) =24.04102689;
conversion(2,4) =24.30110468;
conversion(2,5) = 0;
conversion(2,6) = 0;
conversion(2,7) = "";
conversion(2,8) = "";

conversion(1,1) = exportformat(4,CH3fun);
conversion(1,2) =
exportformat(4,CH2fun)+exportformat(4,ketonefun)/2+exportformat(4,Vinylicfun)/2;
conversion(1,3) =
exportformat(4,RCHRfun)+exportformat(4,ketonefun)+exportformat(4,Vinylicfun)/2;
conversion(1,4) = exportformat(4,OHfun);
conversion(1,5) = exportformat(4,ketonefun)/2;
conversion(1,6) = exportformat(4,Vinylicfun);
conversion(1,7) = (conversion(2,4)-conversion(1,4)*(conversion(2,3) /
conversion(1,3)));
conversion(1,8) = (conversion(2,4)-
(conversion(1,4)+conversion(1,5)*2)*(conversion(2,3) / conversion(1,3)));



% conversion(3,1) = "";
% conversion(3,2) = "";
% conversion(3,3) = "";
% conversion(3,4) = "";
% conversion(3,5) = "";
% conversion(3,6) = "";
% conversion(3,7) = (conversion(2,7)-conversion(1,7))/conversion(2,7)*100 ;
```

```
% conversion(3,8) = (conversion(2,8)-conversion(1,8))/conversion(2,8)*100 ;
colnameexp = {'R-CH3' 'CH2' 'RCHR' 'ROH' 'Ketone' 'Vynilic' 'Conversion' 'Mass
Balance'};
rownameexp = {'Raw Area' 'Unreacted Area'};
Export_Table_Conversion =
table(conversion(:,1),conversion(:,2),conversion(:,3),conversion(:,4),conversion(:,5)
,conversion(:,6),conversion(:,7),conversion(:,8),'VariableNames', colnameexp,
'RowNames', rownameexp );

%-------------------------------------------------------------------------------
-------------------
% plot data to make sure everthing is fine HNMR
fig1 = figure(1);
hold on
x = [shift11OH shift12OH shift12OH shift11OH];
y = [0 0 max(NMR(:,2)) max(NMR(:,2))];
fill(x,y,'blue','FaceAlpha',0.3)
text(shift12OH-0.1,max(NMR(:,2))*1.02,'OH')

x = [shift21OH shift22OH shift22OH shift21OH];
y = [0 0 max(NMR(:,2)) max(NMR(:,2))];
fill(x,y,'blue','FaceAlpha',0.3)
text(shift22OH-0.02,max(NMR(:,2))*1.02,'')

x = [shift11CH2 shift12CH2 shift12CH2 shift11CH2];
y = [0 0 max(NMR(:,2)) max(NMR(:,2))];
fill(x,y,'cyan','FaceAlpha',0.3)
text(shift12CH2-0.3,max(NMR(:,2))*1.02,'CH2')

x = [shift11CH3 shift12CH3 shift12CH3 shift11CH3];
y = [0 0 max(NMR(:,2)) max(NMR(:,2))];
fill(x,y,'yellow','FaceAlpha',0.3)
text(shift12CH3-0.05,max(NMR(:,2))*1.02,'CH3')

x = [shift11RCHR shift12RCHR shift12RCHR shift11RCHR];
y = [0 0 max(NMR(:,2)) max(NMR(:,2))];
fill(x,y,'red','FaceAlpha',0.3)
text(shift12RCHR-0.1,max(NMR(:,2))*1.02,'CH')

x = [shift11Allyl shift12Allyl shift12Allyl shift11Allyl];
y = [0 0 max(NMR(:,2)) max(NMR(:,2))];
fill(x,y,[0.4940 0.1840 0.5560] ,'FaceAlpha',0.3)
text(shift12Allyl,max(NMR(:,2))*1.02,'Ketone')

x = [shift11Vynil shift12Vynil shift12Vynil shift11Vynil];
y = [0 0 max(NMR(:,2)) max(NMR(:,2))];
fill(x,y,'green','FaceAlpha',0.3)
text(shift12Vynil,max(NMR(:,2))*1.02,'HC=CH')

x = [shift11H2O shift12H2O shift12H2O shift11H2O];
y = [0 0 max(NMR(:,2)) max(NMR(:,2))];
fill(x,y,'magenta','FaceAlpha',0.3)
text(shift12H2O,max(NMR(:,2))*1.02,'H2O-DMSO')

x = [shift21H2O shift22H2O shift22H2O shift21H2O];
```

```
y = [0 0 max(NMR(:,2)) max(NMR(:,2))];
fill(x,y,'magenta','FaceAlpha',0.3)
text(shift22H2O+0.05,max(NMR(:,2))*1.02,'H2O-OH')

x = [shift11DMSO shift12DMSO shift12DMSO shift11DMSO];
y = [0 0 max(NMR(:,2)) max(NMR(:,2))];
fill(x,y,'black','FaceAlpha',0.3)
text(shift12DMSO,max(NMR(:,2))*1.02,'DMSO')

x = [shift11Prop shift12Prop shift12Prop shift11Prop];
y = [0 0 max(NMR(:,2)) max(NMR(:,2))];
fill(x,y,[0.6 0.8 0.5560],'FaceAlpha',0.3)
text(shift12Prop,max(NMR(:,2))*1.02,'Prop')

axis([0.5 6 0 max(NMR(:,2))*1.05 ])
plot(NMR(:,1),NMR(:,2),'black');
title(['1H NMR' Experiment_Number Catalyst]);
xticks(0:0.25:max(NMR(:,1)));
hold off
set(gca, 'TickDir', 'out', 'xdir', 'reverse')
% set(gcf,'units','normalized','outerposition',[0 0 1 1]);
fig1.WindowState = 'maximized';

%  plot data CNMR (Carbon)
fig2 = figure(2);
hold on
CNMRheight = max(CNMR(:,2))*0.2;
x = [shift21OHEthEst shift22OHEthEst shift22OHEthEst shift21OHEthEst];
y = [0 0 CNMRheight CNMRheight];
fill(x,y,'blue','FaceAlpha',0.3)
text(shift22OHEthEst-2,CNMRheight*0.97,'OH, Ethers, Esters')
x = [shift21CH2 shift22CH2 shift22CH2 shift21CH2];
y = [0 0 CNMRheight CNMRheight];
fill(x,y,'cyan','FaceAlpha',0.3)
text(shift22CH2-20,CNMRheight*0.97,'C>CH>CH2>CH3')
x = [shift21CC shift22CC shift22CC shift21CC];
y = [0 0 CNMRheight CNMRheight];
fill(x,y,'yellow','FaceAlpha',0.3)
text(shift22CC-25,CNMRheight*0.97,'C=C')
x = [shift21Est shift22Est shift22Est shift21Est];
y = [0 0 CNMRheight CNMRheight];
fill(x,y,'red','FaceAlpha',0.3)
text(shift22Est-6,CNMRheight*0.97,'RC=O')
x = [shift21Ket shift22Ket shift22Ket shift21Ket];
y = [0 0 CNMRheight CNMRheight];
fill(x,y,[0.4940 0.1840 0.5560] ,'FaceAlpha',0.3)
text(shift22Ket-15,CNMRheight*0.97,'Ketone')
axis([0 230 0 CNMRheight])
plot(CNMR(:,1),CNMR(:,2),'black');
title(['13C NMR' Experiment_Number Catalyst]);
xticks(0:10:max(CNMR(:,1)));
hold off
set(gca, 'TickDir', 'out', 'xdir', 'reverse')
% set(gcf,'units','normalized','outerposition',[0 0 1 1]);
fig2.WindowState = 'maximized';
```

```
%-------------------------------------------------------------------------------
--------
% export tables
if Export_file == 1 || Export_file ==2
    filenameconversion =
strcat(Catalyst,'_',Experiment_Number,'_conversion','.xlsx'); % name of the file for
conversion
    filenamefunctional =
strcat(Catalyst,'_',Experiment_Number,'_functional','.xlsx'); % name of the file for
functional group

writetable(Export_Table_Functional,strcat(savefolder,filenamefunctional),'WriteRowNam
es',true);
    writetable(Export_Table_Conversion,strcat(savefolder,
filenameconversion),'WriteRowNames',true);
    filenamehnmr = strcat('HNMR_',Experiment_Number);
    print(fig1,strcat(savefolder,filenamehnmr) ,'-dpng','-r300');
    filenamehnmrfig = strcat('HNMR_',Experiment_Number,'.fig');
    savefig(fig1,strcat(savefolder,filenamehnmrfig))
    if Export_file == 2
        filenamecnmr = strcat('CNMR_',Experiment_Number);
        print(fig2,strcat(savefolderc,filenamecnmr) ,'-dpng','-r300');
        filenamecnmrfig = strcat('CNMR_',Experiment_Number,'.fig');
        savefig(fig2,strcat(savefolderc,filenamecnmrfig))
    end
end

%=================================================================================
===========
% Deconvolution
%=================================================================================
===========

if Deconvolute == 1

y = NMR(:,2);
x = NMR(:,1);
tFit = reshape(x, 1, []);
y = reshape(y, 1, []);

if typedeconv == 1 % Gaussian

%     MeanPeakValOH = [ 4.22; 4.23; 4.365; 4.37; 4.39;4.483];% Position of the middle
of the peak
%     MidWidthValOH = [ 0.015;0.03; 0.007;0.007;0.007;0.04]; %The width at the mid of
the peak
%     initialGuessesOH = [MeanPeakValOH, MidWidthValOH];

    MeanPeakValOH = [ 3.575 ;3.82301; 3.8926; 3.93079];% Position of the middle of
the peak 3.98079
    MidWidthValOH = [ 0.0738; 0.06654;0.0543; 0.1587]; %The width at the mid of the
peak 0.15876
    initialGuessesOH = [MeanPeakValOH, MidWidthValOH];

%     MeanPeakValRCHR = [ 3.575; 3.796; 3.8619];% Position of the middle of the peak
```

```
%     MidWidthValRCHR = [ 0.0738; 0.0547; 0.027]; %The width at the mid of the peak
%     initialGuessesRCHR = [MeanPeakValRCHR, MidWidthValRCHR];

    MeanPeakValRCHR = [ 3.33 ];% Position of the middle of the peak
    MidWidthValRCHR = [ 0.0738]; %The width at the mid of the peak
    initialGuessesRCHR = [MeanPeakValRCHR, MidWidthValRCHR];



    MeanPeakValCH2 = [ 1.211; 1.2872; 1.3976];% Position of the middle of the peak
    MidWidthValCH2 = [ 0.07; 0.1; 0.027]; %The width at the mid of the peak
    initialGuessesCH2 = [MeanPeakValCH2, MidWidthValCH2];

    MeanPeakValCH3 = [ 0.7879; 0.8067; 0.8251];% Position of the middle of the peak
    MidWidthValCH3 = [ 0.0046; 0.00758; 0.0046]; %The width at the mid of the peak
    initialGuessesCH3 = [MeanPeakValCH3, MidWidthValCH3];

    MeanPeakValket = [2.15];% Position of the middle of the peak
    MidWidthValket = [0.00758]; %The width at the mid of the peak
    initialGuessesket = [MeanPeakValket, MidWidthValket];

elseif typedeconv ==2 % Weibull
    % mu location parameter / treshold parameter, defines the lowest possible value
in a Weibull distribution (xo)
    % gamma shape parameter, <1 is sharp decrease, 1<x<2.6 Right Skewed, ~3 is
normal, >3.7 left skewed
    % alpha scale parameter, it affects the height of the peak and how sharp it is.
bigger values make it shorter and fatter
    InitialPeak = []; % mu
    ShapeParameter = []; % gamma Shape parameter for normal
    ScaleParameter = []; % alpha scale parameter affects how fat it is
    initialGuesses = [InitialPeak, ShapeParameter, ScaleParameter];

elseif typedeconv ==3 % Voigt
    % gD is the Doppler (Gaussian) width,
    % alpha is theshape constant (ratio of the Lorentzian width gL to the Doppler
width gD.
    % Based on Chong Tao's "Voigt lineshape spectrum simulation", Pos is
    % Position
    MeanPeakValOH = [4.2171; 4.2666; 4.3896; 4.3665; 4.3783;4.4740]; % Position of
the middle of the peak
    MidWidthValOH =[0.0164;0.0369;0.0092;0.0074;0.0030;0.0228]; %gD The width at the
mid of the peak
    ShapeParameterOH = [9.1209e-7;1.0349e-7; 9.9099e-4;7.1466e-6;8.4498e-4;4.325e-4];
% alpha Shape parameter
    initialGuessesOH = [MeanPeakValOH, MidWidthValOH, ShapeParameterOH];

    MeanPeakValRCHR = [ 3.575; 3.796; 3.8619]; % Position of the middle of the peak
    MidWidthValRCHR =[ 0.0738; 0.0547; 0.027]; %gD The width at the mid of the peak
    ShapeParameterRCHR = [0 ; 0; 0]; % alpha Shape parameter
    initialGuessesRCHR = [MeanPeakValRCHR, MidWidthValRCHR, ShapeParameterRCHR];

    MeanPeakValCH2 = [1.211; 1.2872; 1.3976]; % Position of the middle of the peak
    MidWidthValCH2 =[ 0.07; 0.1; 0.027]; %gD The width at the mid of the peak
    ShapeParameterCH2 = [0 ; 0; 0]; % alpha Shape parameter
```

```
    initialGuessesCH2 = [MeanPeakValCH2, MidWidthValCH2, ShapeParameterCH2];

    MeanPeakValCH3 = [0.7879; 0.8067; 0.8251]; % Position of the middle of the peak
    MidWidthValCH3 =[ 0.0046; 0.00758; 0.0046]; %gD The width at the mid of the peak
    ShapeParameterCH3 = [0 ; 0; 0]; % alpha Shape parameter
    initialGuessesCH3 = [MeanPeakValCH3, MidWidthValCH3, ShapeParameterCH3];

    MeanPeakValket = [2.15]; % Position of the middle of the peak
    MidWidthValket =[ 0.00758]; %gD The width at the mid of the peak
    ShapeParameterket = [0]; % alpha Shape parameter
    initialGuessesket = [MeanPeakValket, MidWidthValket, ShapeParameterket];


else % Voigt would be the default
    % gD is the Doppler (Gaussian) width,
    % alpha is theshape constant (ratio of the Lorentzian width gL to the Doppler
width gD.
    % Based on Chong Tao's "Voigt lineshape spectrum simulation", Pos is
    % Position
    MeanPeakValOH = [4.2171; 4.2666; 4.3896; 4.3665; 4.3783;4.4740]; % Position of
the middle of the peak
    MidWidthValOH =[0.0164;0.0369;0.0092;0.0074;0.0030;0.0228]; %gD The width at the
mid of the peak
    ShapeParameterOH = [9.1209e-7;1.0349e-7; 9.9099e-4;7.1466e-6;8.4498e-4;4.325e-4];
% alpha Shape parameter
    initialGuessesOH = [MeanPeakVal, MidWidthVal, ShapeParameter];

    MeanPeakValRCHR = [ 3.575; 3.796; 3.8619]; % Position of the middle of the peak
    MidWidthValRCHR =[ 0.0738; 0.0547; 0.027]; %gD The width at the mid of the peak
    ShapeParameterRCHR = [0 ; 0; 0]; % alpha Shape parameter
    initialGuessesRCHR = [MeanPeakVal, MidWidthVal, ShapeParameter];

    MeanPeakValCH2 = [1.211; 1.2872; 1.3976]; % Position of the middle of the peak
    MidWidthValCH2 =[ 0.07; 0.1; 0.027]; %gD The width at the mid of the peak
    ShapeParameterCH2 = [0 ; 0; 0]; % alpha Shape parameter
    initialGuessesCH2 = [MeanPeakVal, MidWidthVal, ShapeParameter];

    MeanPeakValCH3 = [0.7879; 0.8067; 0.8251]; % Position of the middle of the peak
    MidWidthValCH3 =[ 0.0046; 0.00758; 0.0046]; %gD The width at the mid of the peak
    ShapeParameterCH3 = [0 ; 0; 0]; % alpha Shape parameter
    initialGuessesCH3 = [MeanPeakValCH3, MidWidthValCH3, ShapeParameterCH3];

    MeanPeakValket = [2.15]; % Position of the middle of the peak
    MidWidthValket =[ 0.00758]; %gD The width at the mid of the peak
    ShapeParameterket = [0]; % alpha Shape parameter
    initialGuessesket = [MeanPeakValket, MidWidthValket, ShapeParameterket];

end
global c NumTrials TrialError
parameterOH = deconv(NMR,shift11OH,shift22OH,initialGuessesOH,typedeconv);
AmpOH = c;
c = [];
parameterRCHR = deconv(NMR,shift11RCHR,shift12RCHR,initialGuessesRCHR,typedeconv);
AmpRCHR = c;
c = [];
```

```
parameterCH2 = deconv(NMR,shift11CH2,shift12CH2,initialGuessesCH2,typedeconv);
AmpCH2 = c;
c = [];
parameterCH3 = deconv(NMR,shift11CH3,shift12CH3,initialGuessesCH3,typedeconv);
AmpCH3 = c;
c = [];
if ketonepresentdecov == 1
    parameterket = deconv(NMR,shift11Ket,shift12Ket,initialGuessesket,typedeconv);
    Ampket = c;
    c = [];
    parameter = [parameterCH3 parameterCH2 parameterket parameterRCHR parameterOH];
    c = [AmpCH3; AmpCH2; Ampket; AmpRCHR;AmpOH];
else
    parameter = [parameterCH3 parameterCH2 parameterRCHR parameterOH];
    c = [AmpCH3; AmpCH2; AmpRCHR;AmpOH];
end
%-------------------------------------------------------------------------------
---------------------------

numGaussians = size(c,1);
fontSize = 20;
% Now plot results.
yhat = PlotComponentCurves(x, y, tFit, c, parameter,typedeconv);
% Compute the residuals between the actual y and the estimated y and put that into
the graph's title.
meanResidual = mean(abs(y - yhat));
fprintf('The mean of the absolute value of the residuals is %f.\n', meanResidual);
caption = sprintf('Estimation of %d Gaussian Curves that will fit data.  Mean
Residual = %d.', numGaussians, meanResidual);
title(caption, 'FontSize', fontSize, 'Interpreter', 'none');
drawnow;

% Make table for the fitted, estimated results.
% First make numGaussians row by 3 column matrix: Column 1 = amplitude, column 2 =
mean, column 3 = width.
%     parameter % Print to command window.

if typedeconv == 1 % Gaussian
estimatedMuSigma = reshape(parameter, 2, [])';
% calculate areas
deconvpeaks = zeros(size(x,1),numGaussians);
deconvArea = zeros(1,numGaussians);
      for k = 1 : numGaussians
            % Get each component curve.
            deconvpeaks(:,k) = c(k) .* gaussian(x, estimatedMuSigma(k, 1),
estimatedMuSigma(k, 2));
        deconvArea(k) = peakint([x deconvpeaks(:,k)] ,0,6, 'False');
      end
% gaussianParameters = [c, estimatedMuSigma];
% Now sort parameters in order of increasing mean
% gaussianParameters = sortrows(gaussianParameters, 2);
% Create table of the output parameters and display it below the actual, true
parameters.
```

```
tEstimate = table((1:numGaussians)', c(:), estimatedMuSigma(:, 1),
estimatedMuSigma(:, 2),deconvArea', 'VariableNames', {'Number', 'Amplitude', 'Mean',
'Width','Area'});

elseif typedeconv == 2 % Weibull

estimatedMuSigma = reshape(parameter, 3, [])';
% gaussianParameters = [c, estimatedMuSigma];
% Now sort parameters in order of increasing mean
% gaussianParameters = sortrows(gaussianParameters, 2);
% Create table of the output parameters and display it below the actual, true
parameters.
tEstimate = table((1:numGaussians)', c(:), estimatedMuSigma(:, 1),
estimatedMuSigma(:, 2),estimatedMuSigma(:, 3), 'VariableNames', {'Number',
'Amplitude', 'Mu', 'gamma', 'alpha'});


elseif typedeconv == 3 % Voigt

estimatedMuSigma = reshape(parameter, 3, [])';
% calculate areas
deconvpeaks = zeros(size(x,1),numGaussians);
deconvArea = zeros(1,numGaussians);
      for k = 1 : numGaussians
            % Get each component curve.
            deconvpeaks(:,k) = c(k) .* voigt(x, estimatedMuSigma(k, 1),
estimatedMuSigma(k, 2),estimatedMuSigma(k, 3));
        deconvArea(k) = peakint([x deconvpeaks(:,k)] ,0,6, 'False');
      end
% gaussianParameters = [c, estimatedMuSigma];
% Now sort parameters in order of increasing mean
% gaussianParameters = sortrows(gaussianParameters, 2);
% Create table of the output parameters and display it below the actual, true
parameters.
tEstimate = table((1:numGaussians)', c(:), estimatedMuSigma(:, 1),
estimatedMuSigma(:, 2),estimatedMuSigma(:, 3), deconvArea','VariableNames',
{'Number', 'Amplitude', 'Position', 'gD', 'alpha', 'Area'});

else % Voigt

estimatedMuSigma = reshape(parameter, 3, [])';
% calculate areas
deconvpeaks = zeros(size(x,1),numGaussians);
deconvArea = zeros(1,numGaussians);
      for k = 1 : numGaussians
            % Get each component curve.
            deconvpeaks(:,k) = c(k) .* voigt(x, estimatedMuSigma(k, 1),
estimatedMuSigma(k, 2),estimatedMuSigma(k, 3));
        deconvArea(k) = peakint([x deconvpeaks(:,k)] ,xlbound+0.01,xubound-0.01,
'False');
      end
% gaussianParameters = [c, estimatedMuSigma];
% Now sort parameters in order of increasing mean
% gaussianParameters = sortrows(gaussianParameters, 2);
```

```
% Create table of the output parameters and display it below the actual, true
parameters.
tEstimate = table((1:numGaussians)', c(:), estimatedMuSigma(:, 1),
estimatedMuSigma(:, 2),estimatedMuSigma(:, 3), deconvArea','VariableNames',
{'Number', 'Amplitude', 'Position', 'gD', 'alpha', 'Area'});

end



% Plot the error as a function of trial number.
hFigError = figure();
hFigError.Name = 'Errors';
plot(TrialError, 'b-');
% hFigError.WindowState = 'maximized';
grid on;
xlabel('Trial Number', 'FontSize', fontSize)
ylabel('Error', 'FontSize', fontSize)

caption = sprintf('Errors for all %d trials.', length(TrialError));
title(caption, 'FontSize', fontSize, 'Interpreter', 'none');


end
%-------------------------------------------------------------------------------
-----------------------------------------------
%% Delete other variables to have a clear output.
clearvars -except Export_Table_Functional Export_Table_Conversion


%%%%%%%%%%%%%%%%%%%%%%%%%%%%%%%%%%%%%%%%%%%%%%%%%%%%%%%%%%%%%%%%%%%%%%%%%%%%%%%
%%%%%%%%%%%%%%%%%%%%%%%%%%%%%%%%%%%%%%%%%%%%%%%%%%%%%%%%%%%%%%%%%%%%%%%%%%%%%%%
%-------------------------------------FUNCTIONS---------------------------------
-----------------------------------------------
%%%%%%%%%%%%%%%%%%%%%%%%%%%%%%%%%%%%%%%%%%%%%%%%%%%%%%%%%%%%%%%%%%%%%%%%%%%%%%%
%%%%%%%%%%%%%%%%%%%%%%%%%%%%%%%%%%%%%%%%%%%%%%%%%%%%%%%%%%%%%%%%%%%%%%%%%%%%%%%

%===============================================================================
==============================================
%-------------------------------------Trapezoidal_Integration-------------------
-----------------------------------------------
%===============================================================================
==============================================
% integration function given limit/bouanderies
function peak = peakint(NMR, shift11,shift12,adaptivebaseline)
h =  size(NMR);
ShiftColumn = 1;
for n=1:1:h(1)
if NMR(n,ShiftColumn) < shift11
    if NMR(n+2,ShiftColumn)>shift11
        peak11 = n+1;
    end
end
if NMR(n,ShiftColumn) < shift12
```

```
    if NMR(n+2,ShiftColumn)>shift12
        peak12 = n+1;
    end
end
end
% removing negative baseline
for m = 1:1:h(1)
    if NMR(m,2)<0
        NMR(m,2) = 0;
    end
end
% integrating the peak across the given limit/range (improve baseline to
% adaptive line between lines)
integration1 = 0;
v = baselinevar(NMR,peak11,peak12);
for n=peak11:1:peak12
    if adaptivebaseline == 1
    intemp =  ((NMR(n,2)-baseline(v,n)) + (NMR(n+1,2)-baseline(v,n+1))
)*abs(NMR(n,1)-NMR(n+1,1))/2;
    else
    intemp =  (NMR(n,2) + NMR(n+1,2) )*abs(NMR(n,1)-NMR(n+1,1))/2;
    end
    if intemp<0
    else
    integration1 = integration1 +intemp ;
    end
end
peak = integration1;
end

function line = baselinevar(NMR,peak11,peak12)
v(1) = (NMR(peak12,2)-NMR(peak11,2))/(peak12-peak11); % slope of line
v(2) = NMR(peak11,2)-peak11*v(1); %interception of line
line= v;
end

function line = baseline(v,n)
line = v(1)*n+v(2);
end

function d = deconv(NMR,xlbound,xubound,initialGuesses,typedeconv)
    global c NumTrials TrialError
    NMRtemp = NMR;
    NMRtemp(NMRtemp(:,1)<xlbound | NMRtemp(:,1)>xubound,:) = [];
    y = NMRtemp(:,2);
    x = NMRtemp(:,1);


    % First specify how many Gaussians there will be.
    format long g;
    format compact;



    startingGuesses = reshape(initialGuesses', 1, []);
```

```
    % warning off

    % Initializations
    NumTrials = 0;  % Track trials
    TrialError = 0; % Track errors
    % t and y must be row vectors.
    tFit = reshape(x, 1, []);
    y = reshape(y, 1, []);

    %-------------------------------------------------------------------------
-------------------------------------------------------
    % Perform an iterative fit using the FMINSEARCH function to optimize the height,
width and center of the multiple Gaussians.
    options = optimset('MaxIter',1e100,'TolX', 1e-100, 'MaxFunEvals', 1e100);  %
Determines how close the model must fit the data
    % First, set some options for fminsearch().
    options.TolFun = 1e-100;
    options.TolX = 1e-100;
    options.MaxIter = 1e100;


%%%%%%%%%%%%%%%%%%%%%%%%%%%%%%%%%%%%%%%%%%%%%%%%%%%%%%%%%%%%%%%%%%%%%%%%%%%%%%%%
%%%%%%%%%%
    % HEAVY LIFTING DONE RIGHT HERE:
    % Run optimization
    if typedeconv == 1 % Gaussian
        [parameter, fval, flag, output] = fminsearch(@(lambda)(fitgauss(lambda, tFit,
y)), startingGuesses, options);
    elseif typedeconv == 2 % Weibull
        [parameter, fval, flag, output] = fminsearch(@(lambda)(fitWeibull(lambda,
tFit, y)), startingGuesses, options);
    elseif typedeconv == 3 % Voigt
        [parameter, fval, flag, output] = fminsearch(@(lambda)(fitVoigt(lambda, tFit,
y)), startingGuesses, options);
    else % Voigt
        [parameter, fval, flag, output] = fminsearch(@(lambda)(fitVoigt(lambda, tFit,
y)), startingGuesses, options);
    end

%%%%%%%%%%%%%%%%%%%%%%%%%%%%%%%%%%%%%%%%%%%%%%%%%%%%%%%%%%%%%%%%%%%%%%%%%%%%%%%%
%%%%%%%%%%
    d = parameter;
end

%=========================================================================
=============
%------------------------------Plotting_Functions_Deconv--------------------------
--------------
%=========================================================================
=============
```

```
%-------------------------------------------------------------------------------
-------------
% fit gaussian functions
function yhat = PlotComponentCurves(x, y, t, c, parameter, typedeconv)
try
       fontSize = 20;
       % Get the means and widths.
    if typedeconv == 1 % Gaussian
       means = parameter(1 : 2 : end);
       widths = parameter(2 : 2 : end);
    elseif typedeconv == 2 % Weibull
    mu =parameter(1 : 3 : end);
    gamma = parameter(2 : 3 : end);
    alpha = parameter(3 : 3 : end);
    elseif typedeconv == 3 % Voigt
    pos =parameter(1 : 3 : end);
    gd = parameter(2 : 3 : end);
    alpha = parameter(3 : 3 : end);
    else % Voigt
    pos =parameter(1 : 3 : end);
    gd = parameter(2 : 3 : end);
    alpha = parameter(3 : 3 : end);
    end
       % Now plot results.
       hFig2 = figure;
       hFig2.Name = 'Fitted Component Curves';
       %      plot(x, y, '--', 'LineWidth', 2)
       hold on;
       yhat = zeros(1, length(t));
       numGaussians = length(c);
       legendStrings = cell(numGaussians + 2, 1);
    if typedeconv ==1 % Gaussian
          for k = 1 : numGaussians
                % Get each component curve. weibullfun(x,mu,gamma,alpha)
                thisEstimatedCurve = c(k) .* gaussian(t, means(k), widths(k)) ;
                % Plot component curves.
                plot(x, thisEstimatedCurve, '-', 'LineWidth', 2);
                hold on;
                % Overall curve estimate is the sum of the component curves.
                yhat = yhat + thisEstimatedCurve;
                legendStrings{k} = sprintf('Estimated Gaussian %d', k);
        end
    elseif typedeconv == 2 %Weibull
          for k = 1 : numGaussians
                % Get each component curve. weibullfun(x,mu,gamma,alpha)
                thisEstimatedCurve = c(k) .* weibullfun(t, mu(k),
gamma(k),alpha(k));
                % Plot component curves.
                plot(x, thisEstimatedCurve, '-', 'LineWidth', 2);
                hold on;
                % Overall curve estimate is the sum of the component curves.
                yhat = yhat + thisEstimatedCurve;
                legendStrings{k} = sprintf('Estimated Weibull %d', k);
        end
    elseif typedeconv == 3 % Voigt
```

```
        for k = 1 : numGaussians
                % Get each component curve. voigt(xx,pos,gD,alpha)
                thisEstimatedCurve = c(k) .* voigt(t, pos(k), gd(k),alpha(k));
                % Plot component curves.
                plot(x, thisEstimatedCurve, '-', 'LineWidth', 2);
                hold on;
                % Overall curve estimate is the sum of the component curves.
                yhat = yhat + thisEstimatedCurve;
                legendStrings{k} = sprintf('Estimated Voigt %d', k);
        end
    else % Voigt
        for k = 1 : numGaussians
                % Get each component curve. voigt(xx,pos,gD,alpha)
                thisEstimatedCurve = c(k) .* voigt(t, pos(k), gd(k),alpha(k));
                % Plot component curves.
                plot(x, thisEstimatedCurve, '-', 'LineWidth', 2);
                hold on;
                % Overall curve estimate is the sum of the component curves.
                yhat = yhat + thisEstimatedCurve;
                legendStrings{k} = sprintf('Estimated Voigt %d', k);
        end
    end
      % Plot original summation curve, that is the actual curve.
      plot(x, y, 'r-', 'LineWidth', 1)
      % Plot estimated summation curve, that is the estimate of the curve.
      plot(x, yhat, 'k--', 'LineWidth', 2)
      grid on;
      xlabel('ppm', 'FontSize', fontSize)
      ylabel('', 'FontSize', fontSize)
      caption = sprintf('Estimation of %d Curves that will fit data.',
numGaussians);
      title(caption, 'FontSize', fontSize, 'Interpreter', 'none');
      grid on
      legendStrings{numGaussians+1} = sprintf('Actual original signal');
      legendStrings{numGaussians+2} = sprintf('Sum of all %d Curves', numGaussians);
      legend(legendStrings);
%     xlim(sort([x(1) x(end)]));
    xlim(sort([0 6]));
      hFig2.WindowState = 'maximized';
      drawnow;

catch ME
      % Some error happened if you get here.
      callStackString = GetCallStack(ME);
      errorMessage = sprintf('Error in program %s.\nTraceback (most recent at
top):\n%s\nError Message:\n%s', ...
            mfilename, callStackString, ME.message);
      WarnUser(errorMessage);
end
end % of PlotComponentCurves

%================================================================================
=============
%------------------------------Fitting_Functions_Deconv----------------------------
-------------
```

```
%=========================================================================================
=============
function theError = fitgauss(lambda, t, y)
% Fitting function for multiple overlapping Gaussians, with statements
% added (lines 18 and 19) to slow the progress and plot each step along the
% way, for educational purposes.
% Author: T. C. O'Haver, 2006

global c NumTrials TrialError
try

	A = zeros(length(t), round(length(lambda) / 2));
	for j = 1 : length(lambda) / 2
		A(:,j) = gaussian(t, lambda(2 * j - 1), lambda(2 * j))';
	end

	c = A \ y';
	z = A * c;
	theError = norm(z - y');

	% Penalty so that heights don't become negative.
	if sum(c < 0) > 0
		theError = theError + 1000000;
	end

	NumTrials = NumTrials + 1;
	TrialError(NumTrials) = theError;
catch ME
	% Some error happened if you get here.
	callStackString = GetCallStack(ME);
	errorMessage = sprintf('Error in program %s.\nTraceback (most recent at
top):\n%s\nError Message:\n%s', ...
		mfilename, callStackString, ME.message);
	WarnUser(errorMessage);
end
end % of fitgauss()
%=========================================================================================
=====================================================================
function theError = fitWeibull(lambda, t, y)

global c NumTrials TrialError
try

	A = zeros(length(t), round(length(lambda) / 3));
	for j = 1 : length(lambda) / 3
		A(:,j) = weibullfun(t, lambda(3 * j - 2), lambda(3 * j - 1),lambda(3 *
j))';
	 if lambda(3 * j) <0 % penalty so that lambda does not become negative
	     theError = theError + 1000000;
	 end
	end

	c = A \ y';
	z = A * c;
	theError = norm(z - y');
```

```
	% Penalty so that heights don't become negative.
	if sum(c < 0) > 0
		theError = theError + 1000000;
    end


	NumTrials = NumTrials + 1;
	TrialError(NumTrials) = theError;
catch ME
	% Some error happened if you get here.
	callStackString = GetCallStack(ME);
	errorMessage = sprintf('Error in program %s.\nTraceback (most recent at
top):\n%s\nError Message:\n%s', ...
		mfilename, callStackString, ME.message);
	WarnUser(errorMessage);
end
end % of fitWeibull()
%=============================================================================
=====================================================================
function theError = fitVoigt(lambda, t, y)

global c NumTrials TrialError
try

	A = zeros(length(t), round(length(lambda) / 3));
	for j = 1 : length(lambda) / 3
		A(:,j) = voigt(t, lambda(3 * j - 2), lambda(3 * j - 1),lambda(3 * j))';
	end

	c = A \ y';
	z = A * c;
	theError = norm(z - y');

	% Penalty so that heights don't become negative.
    for j = 1 : length(lambda) / 3
        if lambda(3 * j) <0 % penalty so that lambda does not become negative
            theError = theError + 1000000;
        end
    end
	if sum(c < 0) > 0
		theError = theError + 1000000;
	end

	NumTrials = NumTrials + 1;
	TrialError(NumTrials) = theError;
catch ME
	% Some error happened if you get here.
	callStackString = GetCallStack(ME);
	errorMessage = sprintf('Error in program %s.\nTraceback (most recent at
top):\n%s\nError Message:\n%s', ...
		mfilename, callStackString, ME.message);
	WarnUser(errorMessage);
end
end % of fitVoigt()
```

```
%================================================================================
=============
%------------------------------Model_Functions_Deconv-----------------------------
-----------
%================================================================================
=============

%================================================================================
=====================================================================
function g = gaussian(x, peakPosition, width)
%  gaussian(x,pos,wid) = gaussian peak centered on pos, half-width=wid
%  x may be scalar, vector, or matrix, pos and wid both scalar
%  T. C. O'Haver, 1988
% Examples: gaussian([0 1 2],1,2) gives result [0.5000    1.0000    0.5000]
% plot(gaussian([1:100],50,20)) displays gaussian band centered at 50 with width 20.
g = exp(-((x - peakPosition) ./ (0.60056120439323 .* width)) .^ 2);
end % of gaussian()

%================================================================================
=====================================================================
function wei = weibullfun(x,mu,gamma,alpha)
% mu location parameter / treshold parameter, defines the lowest possible value in a
Weibull distribution (xo)
% gamma shape parameter, <1 is sharp decrease, 1<x<2.6 Right Skewed, ~3 is normal,
>3.7 left skewed
% alpha scale parameter, it affects the height of the peak and how sharp it is.
bigger values make it shorter and fatter
wei = (gamma./alpha).*((x-mu)./alpha).^(gamma-1).*exp(-((x-mu)./alpha).^gamma);
end

%================================================================================
=====================================================================
function g=voigt(xx,pos,gD,alpha)
% Voigt profile function. xx is the independent variable (energy,
% wavelength, etc), gD is the Doppler (Gaussian) width, and alpha is the
% shape constant (ratio of the Lorentzian width gL to the Doppler width gD.
% Based on Chong Tao's "Voigt lineshape spectrum simulation", Pos is
% Position
% File ID: #26707
% alpha=alpha
gL=alpha.*gD;
gV = 0.5346*gL + sqrt(0.2166*gL.^2 + gD.^2);
x = gL/gV;
% sizeabs=size(abs(xx-pos))
% sizegV=size(gV)
y = abs(xx-pos)./gV;
g = 1/(2*gV*(1.065 + 0.447*x + 0.058*x^2))*((1-x)*exp(-0.693.*y.^2) + (x./(1+y.^2)) +
0.016*(1-x)*x*(exp(-0.0841.*y.^2.25)-1./(1 + 0.021.*y.^2.25)));
g=g./max(g);
end

%================================================================================
=============
```

```
%-----------------------------ErrorHandling_Functions_Deconv-----------------------
-------------
%=============================================================================
=============
%=============================================================================
=================================================================
% Gets a string describing the call stack where each line is the filename, function
name, and line number in that file.
% Sample usage
% try
%     % Some code that might throw an error......
% catch ME
%     callStackString = GetCallStack(ME);
%     errorMessage = sprintf('Error in program %s.\nTraceback (most recent at
top):\n%s\nError Message:\n%s', ...
%           mfilename, callStackString, ME.message);
%     WarnUser(errorMessage);
% end
function callStackString = GetCallStack(errorObject)
try
      theStack = errorObject.stack;
      callStackString = '';
      stackLength = length(theStack);
      % Get the date of the main, top level function:
      %     d = dir(theStack(1).file);
      %     fileDateTime = d.date(1:end-3);
      if stackLength <= 3
            % Some problem in the OpeningFcn
            % Only the first item is useful, so just alert on that.
            [folder, baseFileName, ext] = fileparts(theStack(1).file);
            baseFileName = sprintf('%s%s', baseFileName, ext);   % Tack on
extension.
            callStackString = sprintf('%s in file %s, in the function %s, at line
%d\n', callStackString, baseFileName, theStack(1).name, theStack(1).line);
      else
            % Got past the OpeningFcn and had a problem in some other function.
            for k = 1 : length(theStack)-3
                  [folder, baseFileName, ext] = fileparts(theStack(k).file);
                  baseFileName = sprintf('%s%s', baseFileName, ext);   % Tack on
extension.
                  callStackString = sprintf('%s in file %s, in the function %s, at
line %d\n', callStackString, baseFileName, theStack(k).name, theStack(k).line);
            end
      end
catch ME
      errorMessage = sprintf('Error in program %s.\nTraceback (most recent at
top):\nError Message:\n%s', ...
            mfilename, ME.message);
      WarnUser(errorMessage);
end
end % from callStackString

%=============================================================================
====================================
% Pops up a warning message, and prints the error to the command window.
```

```
function WarnUser(warningMessage)
if nargin == 0
	return; % Bail out if they called it without any arguments.
end
try
	fprintf('%s\n', warningMessage);
	uiwait(warndlg(warningMessage));
	% Write the warning message to the log file
	folder = 'C:\Users\Public\Documents\MATLAB Settings';
	if ~exist(folder, 'dir')
		mkdir(folder);
	end
	fullFileName = fullfile(folder, 'Error Log.txt');
	fid = fopen(fullFileName, 'at');
	if fid >= 0
		fprintf(fid, '\nThe error below occurred on %s.\n%s\n', datestr(now),
warningMessage);
		fprintf(fid, '-----------------------------------------------------------
---------------------\n');
		fclose(fid);
	end
catch ME
	message = sprintf('Error in WarnUser():\n%s', ME.message);
	fprintf('%s\n', message);
	uiwait(warndlg(message));
end
end % from WarnUser()
```

References

(1) Chiellini, E.; Corti, A.; D'Antone, S.; Solaro, R. Biodegradation of Poly (Vinyl Alcohol) Based Materials. *Progress in Polymer Science* **2003**, *28* (6), 963–1014. https://doi.org/10.1016/S0079-6700(02)00149-1.

(2) Mokwena, K. K.; Tang, J. Ethylene Vinyl Alcohol: A Review of Barrier Properties for Packaging Shelf Stable Foods. *Critical Reviews in Food Science and Nutrition* **2012**, *52* (7), 640–650. https://doi.org/10.1080/10408398.2010.504903.

(3) Sperling, L. H. *Introduction to Physical Polymer Science*, 4th ed.; Wiley: Hoboken, N.J, 2006.

(4) Mokwena, K. K.; Tang, J. Ethylene Vinyl Alcohol: A Review of Barrier Properties for Packaging Shelf Stable Foods. *Critical Reviews in Food Science and Nutrition* **2012**, *52* (7), 640–650. https://doi.org/10.1080/10408398.2010.504903.

(5) Wang, C.; Hu, K.; Zhao, C.; Zou, Y.; Liu, Y.; Qu, X.; Jiang, D.; Li, Z.; Zhang, M.; Li, Z. Customization of Conductive Elastomer Based on PVA/PEI for Stretchable Sensors. *Small* **2020**, *16* (7), 1904758. https://doi.org/10.1002/smll.201904758.

(6) *Flexible Packaging*. https://www.mcpp-global.com/en/mcpp-asia/applications/segment/flexible-packaging/ (accessed 2023-05-12).

(7) PlasticsEurope; EPRO. Plastics - The Facts 2022, 2022. https://plasticseurope.org/de/wp-content/uploads/sites/3/2022/10/PE-PLASTICS-THE-FACTS_20221017.pdf.

(8) Lambert, S.; Scherer, C.; Wagner, M. Ecotoxicity Testing of Microplastics: Considering the Heterogeneity of Physicochemical Properties. *Integr Environ Assess Manag* **2017**, *13* (3), 470–475. https://doi.org/10.1002/ieam.1901.

(9) Li, L.; Zuo, J.; Duan, X.; Wang, S.; Hu, K.; Chang, R. Impacts and Mitigation Measures of Plastic Waste: A Critical Review. *Environmental Impact Assessment Review* **2021**, *90*, 106642. https://doi.org/10.1016/j.eiar.2021.106642.

(10) Jambeck, J. R.; Geyer, R.; Wilcox, C.; Siegler, T. R.; Perryman, M.; Andrady, A.; Narayan, R.; Law, K. L. Plastic Waste Inputs from Land into the Ocean. *Science* **2015**, *347* (6223), 768–771. https://doi.org/10.1126/science.1260352.

(11) Filatov, V. V.; Zaitseva, N. A.; Larionova, A. A.; Zhenzhebir, V. N.; Polozhentseva, I. V.; Takhumova, O. V.; Kolosova, G. M. State Management of Plastic Production Based on the Implementation of UN Decisions on Environmental Protection. *Ekoloji* **2018**, *27* (106), 635–642.

(12) Hamad, K.; Kaseem, M.; Deri, F. Recycling of Waste from Polymer Materials: An Overview of the Recent Works. *Polymer Degradation and Stability* **2013**, *98* (12), 2801–2812. https://doi.org/10.1016/j.polymdegradstab.2013.09.025.

(13) Gee, I. M.; Heard, B. R.; Webber, M. E.; Miller, S. A. The Future of Food: Environmental Lessons from E-Commerce. *Environ. Sci. Technol.* **2020**, *54* (23), 14776–14784. https://doi.org/10.1021/acs.est.0c01731.

(14) Garcia, J. M.; Robertson, M. L. The Future of Plastics Recycling. *Science* **2017**, *358* (6365), 870–872. https://doi.org/10.1126/science.aaq0324.

(15) Eagan, J. M.; Xu, J.; Di Girolamo, R.; Thurber, C. M.; Macosko, C. W.; LaPointe, A. M.; Bates, F. S.; Coates, G. W. Combining Polyethylene and Polypropylene: Enhanced Performance with

PE/ *i* PP Multiblock Polymers. *Science* **2017**, *355* (6327), 814–816. https://doi.org/10.1126/science.aah5744.
(16) Rahimi, A.; García, J. M. Chemical Recycling of Waste Plastics for New Materials Production. *Nat Rev Chem* **2017**, *1* (6), 0046. https://doi.org/10.1038/s41570-017-0046.
(17) Aguado, R.; Olazar, M.; San José, M. J.; Gaisán, B.; Bilbao, J. Wax Formation in the Pyrolysis of Polyolefins in a Conical Spouted Bed Reactor. *Energy Fuels* **2002**, *16* (6), 1429–1437. https://doi.org/10.1021/ef020043w.
(18) Vollmer, I.; Jenks, M. J. F.; Mayorga González, R.; Meirer, F.; Weckhuysen, B. M. Plastic Waste Conversion over a Refinery Waste Catalyst. *Angew. Chem. Int. Ed.* **2021**, *60* (29), 16101–16108. https://doi.org/10.1002/anie.202104110.
(19) Vasile, C.; Pakdel, H.; Mihai, B.; Onu, P.; Darie, H.; Ciocâlteu, S. Thermal and Catalytic Decomposition of Mixed Plastics. *Journal of Analytical and Applied Pyrolysis* **2001**, *57* (2), 287–303. https://doi.org/10.1016/S0165-2370(00)00151-0.
(20) Celik, G.; Kennedy, R. M.; Hackler, R. A.; Ferrandon, M.; Tennakoon, A.; Patnaik, S.; LaPointe, A. M.; Ammal, S. C.; Heyden, A.; Perras, F. A.; Pruski, M.; Scott, S. L.; Poeppelmeier, K. R.; Sadow, A. D.; Delferro, M. Upcycling Single-Use Polyethylene into High-Quality Liquid Products. *ACS Cent. Sci.* **2019**, *5* (11), 1795–1803. https://doi.org/10.1021/acscentsci.9b00722.
(21) Rorrer, J. E.; Beckham, G. T.; Román-Leshkov, Y. Conversion of Polyolefin Waste to Liquid Alkanes with Ru-Based Catalysts under Mild Conditions. *JACS Au* **2021**, *1* (1), 8–12. https://doi.org/10.1021/jacsau.0c00041.
(22) Marcilla, A.; Gómez, A.; García, Á. N.; Mar Olaya, M. Kinetic Study of the Catalytic Decomposition of Different Commercial Polyethylenes over an MCM-41 Catalyst. *Journal of Analytical and Applied Pyrolysis* **2002**, *64* (1), 85–101. https://doi.org/10.1016/S0165-2370(01)00174-7.
(23) Zhang, W.; Kim, S.; Wahl, L.; Khare, R.; Hale, L.; Hu, J.; Camaioni, D. M.; Gutiérrez, O. Y.; Liu, Y.; Lercher, J. A. Low-Temperature Upcycling of Polyolefins into Liquid Alkanes via Tandem Cracking-Alkylation. *Science* **2023**, *379* (6634), 807–811. https://doi.org/10.1126/science.ade7485.
(24) Yan, G.; Jing, X.; Wen, H.; Xiang, S. Thermal Cracking of Virgin and Waste Plastics of PP and LDPE in a Semibatch Reactor under Atmospheric Pressure. *Energy Fuels* **2015**, *29* (4), 2289–2298. https://doi.org/10.1021/ef502919f.
(25) Walker, T. W.; Frelka, N.; Shen, Z.; Chew, A. K.; Banick, J.; Grey, S.; Kim, M. S.; Dumesic, J. A.; Van Lehn, R. C.; Huber, G. W. Recycling of Multilayer Plastic Packaging Materials by Solvent-Targeted Recovery and Precipitation. *Sci. Adv.* **2020**, *6* (47), eaba7599. https://doi.org/10.1126/sciadv.aba7599.
(26) Ross, J. R. H. Heterogeneous Catalysis – Chemistry in Two Dimensions. In *Heterogeneous Catalysis*; Elsevier, 2012; pp 1–15. https://doi.org/10.1016/B978-0-444-53363-0.10001-5.
(27) Dumesic, J. A.; Huber, G. W.; Boudart, M. Principles of Heterogeneous Catalysis. In *Handbook of Heterogeneous Catalysis*; Ertl, G., Knozinger, H., Schuth, F., Weitkamp, J., Eds.; Wiley-VCH Verlag GmbH & Co. KGaA: Weinheim, Germany, 2008; p hetcat0001. https://doi.org/10.1002/9783527610044.hetcat0001.
(28) Niemantsverdriet, J. W. *Spectroscopy in Catalysis: An Introduction*, 3rd completely rev. and enl. ed.; Wiley-VCH: Weinheim, 2010.

(29) Hagen, J. *Industrial Catalysis: A Practical Approach*, 3rd completely revised and enlarged edition.; Wiley-VCH: Weinheim, 2015.
(30) *Contemporary Catalysis*; Elsevier, 2019. https://doi.org/10.1016/C2014-0-00159-1.
(31) Cruciani, G. Zeolites upon Heating: Factors Governing Their Thermal Stability and Structural Changes. *Journal of Physics and Chemistry of Solids* **2006**, *67* (9–10), 1973–1994. https://doi.org/10.1016/j.jpcs.2006.05.057.
(32) Gounder, R.; Iglesia, E. The Catalytic Diversity of Zeolites: Confinement and Solvation Effects within Voids of Molecular Dimensions. *Chem. Commun.* **2013**, *49* (34), 3491. https://doi.org/10.1039/c3cc40731d.
(33) Klein, D. R. *Organic Chemistry*, Third edition.; John Wiley & Sons, Inc: Hoboken, 2017.
(34) De, S. Production of Long-Chain Hydrocarbon Biofuels from Biomass-Derived Platform Chemicals: Catalytic Approaches and Challenges. In *Hydrocarbon Biorefinery*; Elsevier, 2022; pp 327–354. https://doi.org/10.1016/B978-0-12-823306-1.00001-7.
(35) Chen, S. S.; Maneerung, T.; Tsang, D. C. W.; Ok, Y. S.; Wang, C.-H. Valorization of Biomass to Hydroxymethylfurfural, Levulinic Acid, and Fatty Acid Methyl Ester by Heterogeneous Catalysts. *Chemical Engineering Journal* **2017**, *328*, 246–273. https://doi.org/10.1016/j.cej.2017.07.020.
(36) Ennaert, T.; Van Aelst, J.; Dijkmans, J.; De Clercq, R.; Schutyser, W.; Dusselier, M.; Verboekend, D.; Sels, B. F. Potential and Challenges of Zeolite Chemistry in the Catalytic Conversion of Biomass. *Chem. Soc. Rev.* **2016**, *45* (3), 584–611. https://doi.org/10.1039/C5CS00859J.
(37) Zhang, L.; Chen, K.; Chen, B.; White, J. L.; Resasco, D. E. Factors That Determine Zeolite Stability in Hot Liquid Water. *J. Am. Chem. Soc.* **2015**, *137* (36), 11810–11819. https://doi.org/10.1021/jacs.5b07398.
(38) Lutz, W. Zeolite Y: Synthesis, Modification, and Properties—A Case Revisited. *Advances in Materials Science and Engineering* **2014**, *2014*, 1–20. https://doi.org/10.1155/2014/724248.
(39) Lutz, W.; Gessner, W.; Bertram, R.; Pitsch, I.; Fricke, R. Hydrothermally Resistant High-Silica Y Zeolites Stabilized by Covering with Non-Framework Aluminum Species. *Microporous Materials* **1997**, *12* (1–3), 131–139. https://doi.org/10.1016/S0927-6513(97)00070-9.
(40) Lutz, W.; Rüscher, C. H.; Heidemann, D. Determination of the Framework and Non-Framework [SiO2] and [AlO2] Species of Steamed and Leached Faujasite Type Zeolites: Calibration of IR, NMR, and XRD Data by Chemical Methods. *Microporous and Mesoporous Materials* **2002**, *55* (2), 193–202. https://doi.org/10.1016/S1387-1811(02)00403-1.
(41) Lutz, W.; Rüscher, C. H.; Gesing, Th. M.; Stöcker, M.; Vasenkov, S.; Freude, D.; Gläser, R.; Berger, C. Investigations of the Mechanism of Dealumination of Zeolite y by Steam: Tuned Mesopore Formation versus the Si/Al Ratio. In *Studies in Surface Science and Catalysis*; Elsevier, 2004; Vol. 154, pp 1411–1417. https://doi.org/10.1016/S0167-2991(04)80658-X.
(42) Zapata, P. A.; Faria, J.; Ruiz, M. P.; Jentoft, R. E.; Resasco, D. E. Hydrophobic Zeolites for Biofuel Upgrading Reactions at the Liquid–Liquid Interface in Water/Oil Emulsions. *J. Am. Chem. Soc.* **2012**, *134* (20), 8570–8578. https://doi.org/10.1021/ja3015082.
(43) Resasco, D. E.; Crossley, S. P.; Wang, B.; White, J. L. Interaction of Water with Zeolites: A Review. *Catalysis Reviews* **2021**, *63* (2), 302–362. https://doi.org/10.1080/01614940.2021.1948301.

(44) Li, G.; Wang, B.; Resasco, D. E. Water-Mediated Heterogeneously Catalyzed Reactions. *ACS Catal.* **2020**, *10* (2), 1294–1309. https://doi.org/10.1021/acscatal.9b04637.
(45) Chen, K.; Damron, J.; Pearson, C.; Resasco, D.; Zhang, L.; White, J. L. Zeolite Catalysis: Water Can Dramatically Increase or Suppress Alkane C–H Bond Activation. *ACS Catal.* **2014**, *4* (9), 3039–3044. https://doi.org/10.1021/cs500858d.
(46) Lee, K.; Jing, Y.; Wang, Y.; Yan, N. A Unified View on Catalytic Conversion of Biomass and Waste Plastics. *Nat Rev Chem* **2022**, *6* (9), 635–652. https://doi.org/10.1038/s41570-022-00411-8.
(47) Jin, S.; McKenna, G. B. Effect of Nanoconfinement on Polymer Chain Dynamics. *Macromolecules* **2020**, *53* (22), 10212–10216. https://doi.org/10.1021/acs.macromol.0c00365.
(48) Tennakoon, A.; Wu, X.; Paterson, A. L.; Patnaik, S.; Pei, Y.; LaPointe, A. M.; Ammal, S. C.; Hackler, R. A.; Heyden, A.; Slowing, I. I.; Coates, G. W.; Delferro, M.; Peters, B.; Huang, W.; Sadow, A. D.; Perras, F. A. Catalytic Upcycling of High-Density Polyethylene via a Processive Mechanism. *Nat Catal* **2020**, *3* (11), 893–901. https://doi.org/10.1038/s41929-020-00519-4.
(49) Elias, L.; Fenouillot, F.; Majesté, J.-C.; Martin, G.; Cassagnau, P. Migration of Nanosilica Particles in Polymer Blends. *J. Polym. Sci. B Polym. Phys.* **2008**, *46* (18), 1976–1983. https://doi.org/10.1002/polb.21534.
(50) Anders, H.; Zimmermann, H. A Comparison of the Thermal Degradation Behaviours of Poly(Vinyl Acetate), Poly(Vinyl Alcohol) and Poly(Vinyl Chloride). *Polymer Degradation and Stability* **1987**, *18* (2), 111–122. https://doi.org/10.1016/0141-3910(87)90024-3.
(51) Peng, Z.; Kong, L. X. A Thermal Degradation Mechanism of Polyvinyl Alcohol/Silica Nanocomposites. *Polymer Degradation and Stability* **2007**, *92* (6), 1061–1071. https://doi.org/10.1016/j.polymdegradstab.2007.02.012.
(52) Maruyama, K.; Takeuchi, K.; Tanizaki, Y. Activation Parameters for Degradation of Polyenes Produced in Heated Poly(Vinyl Alcohol) Film. *Polymer* **1989**, *30* (3), 476–479. https://doi.org/10.1016/0032-3861(89)90017-7.
(53) Lagaron, J. M.; Giménez, E.; Saura, J. J. Degradation of High Barrier Ethylene–Vinyl Alcohol Copolymer under Mild Thermal-Oxidative Conditions Studied by Thermal Analysis and Infrared Spectroscopy. *Polymer International* **2001**, *50* (6), 635–642. https://doi.org/10.1002/pi.674.
(54) Thomas, P. S.; Guerbois, J.-P.; Russell, G. F.; Briscoe, B. J. FTIR Study of the Thermal Degradation of Poly(Vinyl Alcohol). *Journal of Thermal Analysis and Calorimetry* **2001**, *64* (2), 501–508. https://doi.org/10.1023/A:1011578514047.
(55) Zhou, X.-Y.; Jia, D.-M.; Cui, Y.-F.; Xie, D. Kinetics Analysis of Thermal Degradation Reaction of PVA and PVA/Starch Blends. *Journal of Reinforced Plastics and Composites* **2009**, *28* (22), 2771–2780. https://doi.org/10.1177/0731684408093872.
(56) Hayashi, T.; Kinashi, K.; Sakai, W.; Tsutsumi, N.; Fujii, A.; Inada, S.; Yamamoto, H. Spin-Trapping Analysis for Thermal Degradation of Poly(Vinyl Alcohol). *Polymer* **2021**, *217*, 123416. https://doi.org/10.1016/j.polymer.2021.123416.
(57) Holland, B. J.; Hay, J. N. The Thermal Degradation of Poly(Vinyl Alcohol). *Polymer* **2001**, *42* (16), 6775–6783. https://doi.org/10.1016/S0032-3861(01)00166-5.

(58) Gilman, J. W.; VanderHart, D. L.; Kashiwagi, T. Thermal Decomposition Chemistry of Poly(Vinyl Alcohol). In *Fire and Polymers II*; ACS Symposium Series; American Chemical Society, 1995; Vol. 599, pp 161–185. https://doi.org/10.1021/bk-1995-0599.ch011.
(59) Tsuchiya, Y.; Sumi, K. Thermal Decomposition Products of Poly(Vinyl Alcohol). *Journal of Polymer Science Part A-1: Polymer Chemistry* **1969**, *7* (11), 3151–3158. https://doi.org/10.1002/pol.1969.150071111.
(60) Shie, J.-L.; Chen, Y.-H.; Chang, C.-Y.; Lin, J.-P.; Lee, D.-J.; Wu, C.-H. Thermal Pyrolysis of Poly(Vinyl Alcohol) and Its Major Products. *Energy Fuels* **2002**, *16* (1), 109–118. https://doi.org/10.1021/ef010082s.
(61) Ghorbanpour, A.; Gumidyala, A.; Grabow, L. C.; Crossley, S. P.; Rimer, J. D. Epitaxial Growth of ZSM-5@Silicalite-1: A Core–Shell Zeolite Designed with Passivated Surface Acidity. *ACS Nano* **2015**, *9* (4), 4006–4016. https://doi.org/10.1021/acsnano.5b01308.
(62) Jerdy, A. C.; Trevisi, L.; Monwar, M.; González-Borja, M. Á.; Abbott, R.; Lobban, L.; Crossley, S. Deconvoluting the Roles of Polyolefin Branching and Unsaturation on Depolymerization Reactions over Acid Catalysts. *Applied Catalysis B: Environmental* **2023**, *337*, 122986. https://doi.org/10.1016/j.apcatb.2023.122986.
(63) Tittensor, J. G.; Gorte, R. J.; Chapman, D. M. Isopropylamine Adsorption for the Characterization of Acid Sites in Silica-Alumina Catalysts. *Journal of Catalysis* **1992**, *138* (2), 714–720. https://doi.org/10.1016/0021-9517(92)90318-C.
(64) Gorte, R. J.; Crossley, S. P. A Perspective on Catalysis in Solid Acids. *Journal of Catalysis* **2019**, *375*, 524–530. https://doi.org/10.1016/j.jcat.2019.07.015.
(65) Peterson, G. I.; Ko, W.; Hwang, Y.-J.; Choi, T.-L. Mechanochemical Degradation of Amorphous Polymers with Ball-Mill Grinding: Influence of the Glass Transition Temperature. *Macromolecules* **2020**, *53* (18), 7795–7802. https://doi.org/10.1021/acs.macromol.0c01510.
(66) Bui, D.-P.; Gomez, A.; Alalq, I.; Trevisi, L.; Jerdy, A.; Chau, H.; Lobban, L.; Crossley, S. Selective Deoxygenation of Polar Polymers Using Metal Supported on TiO2 Nanotubes.
(67) Fogler, H. S. *Elements of Chemical Reaction Engineering*, Fifth edition.; Prentice Hall: Boston, 2016.
(68) Suárez, N.; Pérez-Pariente, J.; Mondragón, F.; Moreno, A. Generation of Hierarchical Porosity in Beta Zeolite by Post-Synthesis Treatment with the Cetyltrimethylammonium Cationic Surfactant under Alkaline Conditions. *Microporous and Mesoporous Materials* **2019**, *280*, 144–150. https://doi.org/10.1016/j.micromeso.2019.02.001.
(69) Sanhoob, M. A.; Khalil, U.; Shafei, E. N.; Choi, K.-H.; Yokoi, T.; Muraza, O. Steam Cracking of Green Diesel (C12) to BTX and Olefins over Silane-Treated Hierarchical BEA. *Fuel* **2020**, *263*, 116624. https://doi.org/10.1016/j.fuel.2019.116624.
(70) Grilc, M.; Likozar, B.; Levec, J. Simultaneous Liquefaction and Hydrodeoxygenation of Lignocellulosic Biomass over NiMo/Al2O3, Pd/Al2O3, and Zeolite Y Catalysts in Hydrogen Donor Solvents. *ChemCatChem* **2016**, *8* (1), 180–191. https://doi.org/10.1002/cctc.201500840.
(71) Wang, Y.-Y.; Đăng, T. H.; Chen, B.-H.; Lee, D.-J. Transesterification of Triolein to Biodiesel Using Sodium-Loaded Catalysts Prepared from Zeolites. *Ind. Eng. Chem. Res.* **2012**, *51* (30), 9959–9965. https://doi.org/10.1021/ie202782q.

(72) Souza, M. S.; Aguieiras, E. C. G.; da Silva, M. A. P.; Langone, M. A. P. Biodiesel Synthesis via Esterification of Feedstock with High Content of Free Fatty Acids. *Appl Biochem Biotechnol* **2009**, *154* (1), 74–88. https://doi.org/10.1007/s12010-008-8444-4.

(73) Zhang, R.; Xu, S.; Raja, D.; Khusni, N. B.; Liu, J.; Zhang, J.; Abdulridha, S.; Xiang, H.; Jiang, S.; Guan, Y.; Jiao, Y.; Fan, X. On the Effect of Mesoporosity of FAU Y Zeolites in the Liquid-Phase Catalysis. *Microporous and Mesoporous Materials* **2019**, *278*, 297–306. https://doi.org/10.1016/j.micromeso.2018.12.003.

(74) Blay, V.; Miguel, P. J.; Corma, A. Theta-1 Zeolite Catalyst for Increasing the Yield of Propene When Cracking Olefins and Its Potential Integration with an Olefin Metathesis Unit. *Catal. Sci. Technol.* **2017**, *7* (24), 5847–5859. https://doi.org/10.1039/C7CY01502J.

(75) Callister, W. D.; Rethwisch, D. G. *Materials Science and Engineering: An Introduction*, 9th edition.; Wiley: Hoboken, NJ, 2014.

(76) Mishin, I. V.; Levin, I. S.; Kustov, L. M. Unit Cell Volume as a Measure of the Framework Composition of ZSM-5 Type Zeolites. *Crystal Growth & Design* **2023**, *23* (6), 4074–4081. https://doi.org/10.1021/acs.cgd.2c01478.

(77) Rouquerol, J.; Llewellyn, P.; Sing, K. 12 - Adsorption by Clays, Pillared Clays, Zeolites and Aluminophosphates. In *Adsorption by Powders and Porous Solids (Second Edition)*; Rouquerol, F., Rouquerol, J., Sing, K. S. W., Llewellyn, P., Maurin, G., Eds.; Academic Press: Oxford, 2014; pp 467–527. https://doi.org/10.1016/B978-0-08-097035-6.00012-7.

(78) Newsam, J. M.; Treacy, M. M. J.; Koetsier, W. T.; De Gruyter, C. B. Structural Characterization of Zeolite Beta. *Proceedings of the Royal Society of London. Series A, Mathematical and Physical Sciences* **1988**, *420* (1859), 375–405.

(79) Madon, R. J.; Boudart, M. Experimental Criterion for the Absence of Artifacts in the Measurement of Rates of Heterogeneous Catalytic Reactions. *Ind. Eng. Chem. Fund.* **1982**, *21* (4), 438–447. https://doi.org/10.1021/i100008a022.

(80) Korbag, I.; Mohamed Saleh, S. Studies on the Formation of Intermolecular Interactions and Structural Characterization of Polyvinyl Alcohol/Lignin Film. *International Journal of Environmental Studies* **2016**, *73* (2), 226–235. https://doi.org/10.1080/00207233.2016.1143700.

(81) Gottlieb, H. E.; Kotlyar, V.; Nudelman, A. NMR Chemical Shifts of Common Laboratory Solvents as Trace Impurities. *J. Org. Chem.* **1997**, *62* (21), 7512–7515. https://doi.org/10.1021/jo971176v.

(82) Babij, N. R.; McCusker, E. O.; Whiteker, G. T.; Canturk, B.; Choy, N.; Creemer, L. C.; Amicis, C. V. D.; Hewlett, N. M.; Johnson, P. L.; Knobelsdorf, J. A.; Li, F.; Lorsbach, B. A.; Nugent, B. M.; Ryan, S. J.; Smith, M. R.; Yang, Q. NMR Chemical Shifts of Trace Impurities: Industrially Preferred Solvents Used in Process and Green Chemistry. *Org. Process Res. Dev.* **2016**, *20* (3), 661–667. https://doi.org/10.1021/acs.oprd.5b00417.

(83) Salimon, J.; Salih, N.; Abdullah, B. M. Production of Chemoenzymatic Catalyzed Monoepoxide Biolubricant: Optimization and Physicochemical Characteristics. *Journal of Biomedicine and Biotechnology* **2012**, *2012*, 1–11. https://doi.org/10.1155/2012/693848.

(84) *1-Propanol(71-23-8) 1H NMR spectrum*. https://www.chemicalbook.com/SpectrumEN_71-23-8_1HNMR.htm (accessed 2023-07-13).

(85) Hansen, C. M. *Hansen Solubility Parameters: A User's Handbook*, 2nd ed.; CRC Press: Boca Raton, 2007.

(86) Chew, A. K.; Walker, T. W.; Shen, Z.; Demir, B.; Witteman, L.; Euclide, J.; Huber, G. W.; Dumesic, J. A.; Van Lehn, R. C. Effect of Mixed-Solvent Environments on the Selectivity of Acid-Catalyzed Dehydration Reactions. *ACS Catal.* **2020**, *10* (3), 1679–1691. https://doi.org/10.1021/acscatal.9b03460.
(87) Pacetti, S. D. Method of Purifying Ethylene Vinyl Alcohol Copolymers for Use with Implantable Medical Devices. US8183337B1, May 22, 2012. https://patents.google.com/patent/US8183337B1/en (accessed 2023-06-09).